Chemo-selective Proteomics for Discovery of Polymicrobial Interactions

Thesis by
Grace Z. Wang

In Partial Fulfillment of the Requirements for the
degree of
Doctor of Philosophy in Chemistry

CALIFORNIA INSTITUTE OF TECHNOLOGY
Pasadena, California
2024
Defended March 28th, 2024

Grace Zimu Wang

0000-0002-0938-304X

Dedicated to Professor Emily R. Derbyshire,

for inspiring my journey in scientific discovery;

and to Maria Salomea Skłodowska-Curie,

for blazing a trail in science that inspires every woman who follows.

Acknowledgments

First and foremost, I wish to express my profound gratitude to my undergraduate thesis advisor, Professor Emily Derbyshire, for inspiring me to go into science, for believing in me and my potential, and for being the very first advocate in my life, who supported me through my formative years and helped me learn to advocate for myself. During the end of my PhD career, I often recalled that day 10 years ago, when I sat across from Emily in her office and asked her to give me my first research job. Even though I have always had a strong intellectual curiosity surrounding the natural sciences, especially in chemistry and microbiology, I had never seen the inside of a research lab. I grew up in an environment where women are told we are not good enough to do many things, one of them being science. Seated across from Emily, I didn't have anything to speak or show for myself, but only to ask earnestly for her to take a chance on me. I was incredibly lucky that Emily extended the opportunity to join her lab, which started my decade-long academic research journey.

I would like to deeply thank my graduate thesis advisor, Professor David Tirrell, whose leadership and mentorship exemplify the highest standards in scientific rigor and human conduct. I was fortunate to have overlapped with many highly talented individuals who trained in the Tirrell lab, each a beacon of inspiration in their own right—Professor Seunghyun Sim, Dr. Samuel Ho, and Professor Josh Baccile, to name a few. In addition, as Dave's last few students, Sophie Miller and I forged an indelible bond through many shared struggles and tears. Her unwavering resilience in the face of hardships and steadfast determination to persevere despite many obstacles are extremely inspiring to me.

I am also deeply indebted to the generosity of Professor Megan Bergkessel (University of Dundee), Professor Melanie Spero (University of Oregon), and Professor Chelsey VanDrisse (University of Georgia). I was fortunate to have overlapped with these scholars during their postdoctoral careers in the Newman Lab at Caltech, and they were extremely gracious in helping me get started on navigating the intricacies of complex microbial systems. I am also grateful to my thesis committee members, Professor Mikhail Shapiro, Professor Dianne Newman, and Professor Linda Hsieh-Wilson.

Lastly, it takes a village to do science. I would like to acknowledge the core facilities and external collaborators who took part in completing the research stories in this thesis.

Table of Contents

Abstract

The future of microbiome research lies in our ability to engineer polymicrobial interactions toward improved host health outcomes, which requires a fundamental molecular understanding of how microbial species sense and respond to ecological competition. Chronic respiratory infection by polymicrobial communities is the leading cause of mortality and morbidity in people living with cystic fibrosis (CF). My thesis work adapts chemo-selective proteomics to dissect molecular mechanisms that drive interspecies dynamics between two notorious opportunistic pathogens dominating chronic CF infection, *Pseudomonas aeruginosa* and *Staphylococcus aureus*.

In Chapter 1, I introduce **b**io**o**rthogonal **n**on**c**anonical **a**mino acid **t**agging (BONCAT)-based comparative proteomics, focusing on time-resolved, cell-specific, and cellular state-selective proteomic applications in the dissection of complex microbial systems. In Chapter 2, I discuss a new usage of time-resolved BONCAT to monitor immediate competition-sensing responses in interbacterial warfare. While coinfection by the Gram-negative *Pseudomonas aeruginosa* and the Gram-positive *Staphylococcus aureus* is associated with poor patient outcomes, the interspecies interactions responsible for such decline remain unknown. We discovered that *P. aeruginosa* senses *S. aureus* secreted cytotoxic peptides from a distance and preempts potential competition through activation of type six secretion system (T6SS). *P. aeruginosa* enhances such competition-sensing-induced antagonism through concomitant attraction toward *S. aureus* peptides, effectively reducing cellular distances between neighboring species and providing a competitive advantage. In Chapter 3, I discuss a new usage of cell-selective BONCAT to target protein synthesis analysis of the low-abundance organism, *S. aureus*, in a coculture environment predominated by *P. aeruginosa*. *P. aeruginosa* robustly outcompetes *S. aureus,* and conventional shotgun proteomics, which is biased toward high-abundance proteins on principle, could only identify and quantify less than 5% of total protein synthesis by *S. aureus* in coculture. We demonstrate that chemical enrichment affords a more than 12-fold increase in total protein abundances synthesized by *S. aureus*. About 50% of protein "hits" with statistically significant changes in expression were not detected in pre-enrichment lysates, highlighting BONCAT as a powerful strategy that facilitates high-resolution proteomic analysis of low-abundance organisms in polymicrobial communities.

Nomenclature

aaRS. Aminoacyl-tRNA synthetase

ACN. Acetonitrile

Aha. Azidohomoalanine

Anl. Azidonorleucine

ASM. Artificial sputum medium

attTn7. Tn7 attachment site

Azf. 4-azido-L-phenylalanine

BONCAT. Bioorthogonal noncanonical amino acid tagging

CDS. Coding sequence

CF. Cystic fibrosis

CFU. Colony-forming units

DBCO. Aza-dibenzocyclooctyne

DMSO. Dimethyl sulfoxide

DTT. Dithiothreitol

FDR. False discovery rate

Gm^R. Gentamicin resistant

GSEA. Gene set enrichment analysis

HPLC. High-performance liquid chromatography

Hpg. Homopropargylglycine

KDE. kernel density estimation

KEGG. Kyoto Encyclopedia of Genes and Genomes

LB. Luria broth

LFQ. Label-free quantitation

Limma. Linear models for microarray data

MRSA. Methicillin-resistant *Staphylococcus aureus*

MSSA. Methicillin-sensitive *Staphylococcus aureus*

MSA. Mannitol salt agar

MS. Mass spectrometry

NcAA. Noncanonical amino acid

PBS. Phosphate-buffered saline

PCA. Principal component analysis

PCR. Polymerase chain reaction

PIA. Pseudomonas isolation agar

Pra. Propargylglycine

PSM. Phenol-soluble modulin (peptides)

SDS. Sodium dodecyl sulfate

SILAC. Stable isotope labeling by amino acids

TAMRA. Tetramethylrhodamine

THPTA. Tris(3-hydroxypropyltriazolylmethyl)amine

T6SS. Type six secretion system

TMT. Tandem Mass Tags

UniProt. The universal protein knowledgebase

TSB. Tryptic soy broth

Chapter 1. Chemo-selective Proteomics for Functional Interrogation of Microbial Systems

Abstract

Over the past two decades, the field of bioorthogonal chemistry has transitioned from emerging to an established cornerstone of scientific inquiry. Here, I delve into the synergy between chemo-selective proteomic technologies based on noncanonical amino acids and another rapidly transforming research area—the human-associated microbiome. This introduction chapter discusses examples of applications of BioOrthogonal noncanonical Amino Acid Tagging (BONCAT) and comments on possibilities for novel applications on the horizon, focusing on the utilities of BONCAT in the functional proteomic analysis of microbial systems relevant to human health.

This chapter is part of a perspective article to be submitted as:
Wang G.Z., Bergkessel M., VanDrisse C.M., Chemo-selective Proteomics for Functional Interrogation of Microbial Systems.

Introduction

Meta- and multi-omics technologies are the present and future of microbiome research. The complexity of polymicrobial and host-microbial interactions requires *in vitro* and *in vivo* functional dissection at the gene and protein expression level.

Currently, the field witnesses a substantial amount of metagenomic studies and a growing abundance of meta-transcriptomic research, juxtaposed with a noticeable dearth of metaproteomic data. A search for Pubmed articles containing the query word "metagenomic" and its variant forms in the title and abstract yielded >29,000 results; >2200 results were found for "meta-transcriptomic" and variants, but only <1000 results for "metaproteomic" and variants. This asymmetry highlights a critical gap in our understanding of multifaceted microbial communities. In particular, proteins are the ultimate functional molecules in a biological system, and protein expression analysis is essential for a comprehensive characterization of host-microbial cellular physiology.

Functional proteomic applications trail behind genomics and transcriptomics due to fundamental limitations in mass spectrometry (MS)-based proteomics analysis. The dynamic range of protein abundance in biological samples far exceeds that of nucleic acids, but the sensitivity of detection and quantification of proteins via MS cannot match those of DNA and RNA molecules. Further, the complexity of protein-protein interactions and the diversity of protein post-translational modifications (PTMs) present significant challenges for functional proteomics in multi-component biological systems.

Chemo-selective proteomics offers creative technologies to counter these limitations and enables high-resolution proteomic analysis in complex microbial systems. Here, I discuss several comparative proteomics strategies using **b**io**o**rthogonal **n**on**c**anonical **a**mino acid **t**agging (BONCAT). I provide existing examples of BONCAT-based applications and further comment on possibilities on the horizon for novel applications using bioorthogonal chemical approaches in combination with tandem mass spectrometry-based analysis.

The tenets of bioorthogonal chemistry lie in the fundamental principle of applying chemical tools in a biological system without interfering with its natural components. Under this idea, click chemistry is often utilized to allow for the in-situ conjugation of bioorthogonal probes in complex biological systems. For a comprehensive review of click chemistry-based bioconjugation reactions and commonly used bioorthogonal probes, see[1–3].

The dynamic flux of protein synthesis within a complex microbial community, where microorganisms interact and adapt in response to the host environment and ecological competition, is directly linked to the functional landscape of the system. The ability to monitor protein synthesis with temporal resolution, species selectivity, and directed targeting of heterogenous subpopulations can enable molecular dissection of cellular activities underlying microbial growth and pathogenesis.

Time-resolved BONCAT comparative proteomics

BONCAT[4–6] capitalizes on the incorporation of non-canonical amino acids (ncAAs) decorated with desired functional moieties into natural or synthetic cellular translational machinery (**Fig. 1.1**). Proteins metabolically labeled by ncAAs can be physically separated from the unlabeled pool via chemical enrichment for downstream identification and analysis.

One obvious advantage of this approach is the ability to perform temporally resolved proteomics without radioactive or isotopic labeling. By simply administering micro- to milli-molar concentrations of ncAAs during defined timeframes, nascent protein synthesis is effectively "marked" for subsequent chemical reactions to distinguish it from the rest of the population (**Fig. 1.2a**).

Time-resolved BONCAT has been applied in microbial systems to study quorum-sensing associated proteomic expression profile in *Vibrio Harveyi*[7], reveal proteomic signatures of slow-growing opportunistic pathogen *Pseudomonas aeruginosa*[8], and investigate newly synthesized proteins in the parasite *Leishmania mexicana* during starvation[9]. In Chapter 2, I discuss a new usage of BONCAT to study immediate competition-sensing responses in interbacterial warfare[10]. In the aforementioned examples, temporally-resolved comparative proteomics performed using BONCAT led to the discovery of previously undescribed links between functional protein families[7,10], the identification of a previously unknown transcriptional factor[8], and the discovery of protein hits that can serve as potential drug targets for treating pathogen infection[9]. The labeling time windows in these studies range from 10 minutes to 16 hours, highlighting the precise temporal resolution achieved and the high versatility of BONCAT to adapt to both short-term and long-term timeframes of interest.

Further, ncAAs recognized by the natural translational machinery in microbes can be used to identify and profile subpopulations of microbes that are actively synthesizing proteins in a microbiome (**Fig.1a**). BONCAT ncAAs have been demonstrated to be metabolically incorporated by clinically or environmentally isolated samples, where host-adapted microbes typically exhibit dormant or low metabolic activity. For example,

azidohomoalanine (Aha, **Fig. 1a**) was added to clinical sputum samples collected from cystic fibrosis (CF) patients, which revealed translationally active subpopulations[11]. Homopropargylglycine (Hpg), another ncAA recognized by the endogenous methionyl-tRNA synthetase (MetRS) in microbes, has been used to label marine microbes[12,13], including in slow-growing archaeal–bacterial consortia[14]. This provides a general strategy to identify and profile metabolically active commensals or harmful pathogens isolated from clinical samples of the human-associated microbiome, such as those in the gut, vaginal, or skin microbiota.

It is worth noting that even though ncAAs such as Aha and Hpg compete with methionine as substrates for the MetRS, administering Aha and Hpg at low concentrations (<9mM Aha and < 90μM Hpg) does not significantly perturb metabolic activities or induce cellular toxicity[15,16]. In addition, even though reducing methionine concentration in the medium can boost ncAA labeling (for example, a 30:1 ratio of Met: Aha has been reported to produce optimal labeling[17]), methionine depletion is unnecessary for incorporation.

Cell-selective BONCAT comparative proteomics

Numerous studies adapted BONCAT to study mammalian systems *in vivo*[18–21]. In comparison, cell-selective BONCAT remains underutilized in microbial systems, where it offers unique advantages in the analysis of host-pathogen or polymicrobial systems with dynamic interspecies interactions. Precise targeting of protein synthesis analysis within a microbial community can provide insights into crucial cellular processes during pathogen invasion of host cells and adaptations in host infections. In a polymicrobial community, the ability to track protein synthesis by a particular species helps dissect complex interactions, such as the molecular mechanisms underlying symbiotic or competitive relationships.

Cell specificity can be achieved by engineering a strain of interest to express a mutant aminoacyl-tRNA synthetase (aaRS) that, when paired with its ncAA partner, can selectively label the strain of interest in a mixed-species community (**Fig. 2**).

Several studies have engineered intracellular pathogens to express a mutant aaRS, and successfully demonstrated selective labeling of proteins produced by *Salmonella typhimurium* [22], *Toxoplasma gondii* [23], *Staphylococcus aureus* [24] and *Mycobacterium tuberculosis* [25] in a host environment. Additionally, with this strategy, proteins secreted by pathogens that enter host cells during infection can be tracked because they are tagged by ncAAs, which presents a unique approach to discovering and analyzing virulence factors and their subsequent localization in host cells. For instance, Mahdavi et al. labeled *Yersinia enterocolitica* during

infection of host cells, and selective lysis of host cells revealed groups of *Yersinia* outer proteins (YOPs) injected into HeLa cells by the *Y. enterocolitica* type III secretion system (T3SS)[26].

In these systems, conventional shotgun proteomics on harvested lysates consisting of host and microbial cells will identify predominantly host proteins due to the bias towards abundances intrinsic to MS-based proteomics. BONCAT enrichment can significantly boost signals from microbial peptides to provide a high-resolution analysis of pathogen protein synthesis. In Chapter 3, I discuss a new usage of BONCAT to target proteomic analysis to a low-abundance microorganism in a polymicrobial system using a cell-selective approach.

Introducing multiple ncAA and mutant aaRS pairs into the system can achieve simultaneous labeling and analysis of several species within a polymicrobial community[27] (**Fig. 1.1b**, **Fig.1. 2b**). For example, one microbe expressing mutant PheRS can selectively charge azido-phenylalanine (Azf, decorated with an azide handle), and a separate species expressing the engineered PraRS can selectively charge propargylglycine (Pra, decorated with an alkyne handle). To enable multiplexed labeling, varieties of ncAAs decorated with non-overlapping, orthogonal chemical handles are needed. For this purpose, there is always a reason to expand the BONCAT ncAA tool kit further (**Fig. 1.1**).

Cellular state-selective or subpopulation-targeting BONCAT comparative proteomics

The ability to selectively target specific microbial cells or subpopulations for protein synthesis monitoring provides tools for a deeper understanding of microbial community heterogeneity and functional specialization.

High heterogeneity exists in complex microbial communities, such as the bacterial biofilm. In sessile populations, extracellular matrix (ECM) secreted by bacteria tightly wraps around layers upon layers of cellular aggregates[28], which in turn limit penetration of nutrients into the inner subpopulation of the biofilm and create a stratified distribution of species such as oxygen, antibiotics, and iron[29,30]. Placing the expression of a mutant aaRS under the control of defined promoters allows for selective labeling of subpopulations according to cellular states (**Fig. 1.2b**). Previously, this was done to characterize antibiotic-resistant[31] or iron-starved subpopulations[32] in *Pseudomonas aeruginosa* biofilm.

When combined with synthetic biology strategies, state-selective BONCAT labeling can be further exploited to be activated by multiple stimuli. This has been successfully demonstrated by coupling the expression of the aaRS to more than one regulatory stimulus, such as an AND gate logic[33] or a split intein system[34] (**Fig. 1.2c**). Previously, a split-intein[35] mutant aaRS approach was applied in the multicellular organism *Caenorhabditis elegans* to limit labeling to amphid sensory neurons spatiotemporally[34]. While such dual-stimuli mutant aaRS strategy has not been applied in microbial systems, it presents a unique opportunity to design tightly controlled ncAA incorporation under specific cues. For example, a microbe can be engineered to activate only the expression of mutant aaRS in the presence of a host-derived signal as well as a species-specific metabolite from another microbe. Such dynamic control of protein synthesis monitoring can serve as a versatile tool for investigating diverse aspects of host-microbiome interactions to accommodate environmental triggers such as drug treatment, inflammatory signals, or disease-related metabolites.

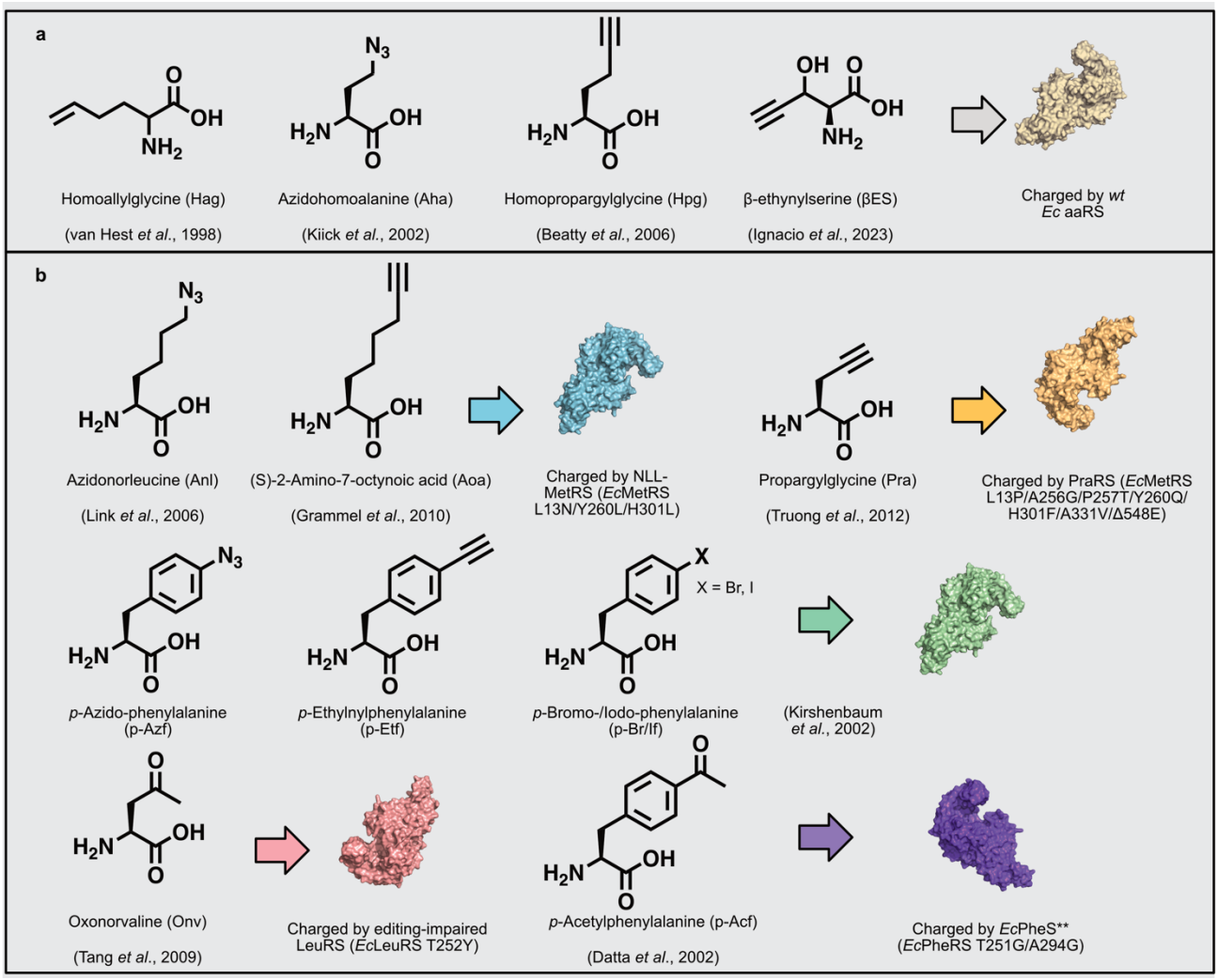

Figure 1.1 BONCAT ncAA tool kit. Amino acids are separated into two groups: ncAAs that can be recognized and incorporated into the proteome by the endogenous translational machinery (**a**) and ncAAs that require engineered mutant aaRS for their incorporation (**b**). Azide or alkyne functionalized proteins can react through azide-alkyne click chemistry-based conjugation[36]. Aryl-halide functionalized proteins can react via a modified Suzuki-Miyaura cross-coupling reaction[37]. Ketone-modified proteins react with hydrazide, another orthogonal bioconjugation strategy. The referenced primary literature is as follows: Hag [38]; Aha [39]; Hpg [40]; βES [41]; Anl[42]; Aoa[22]; Pra[27]; p-Azf. p-Etf, p-Brf/If[43]; Onv[44]; p-Acf[45].

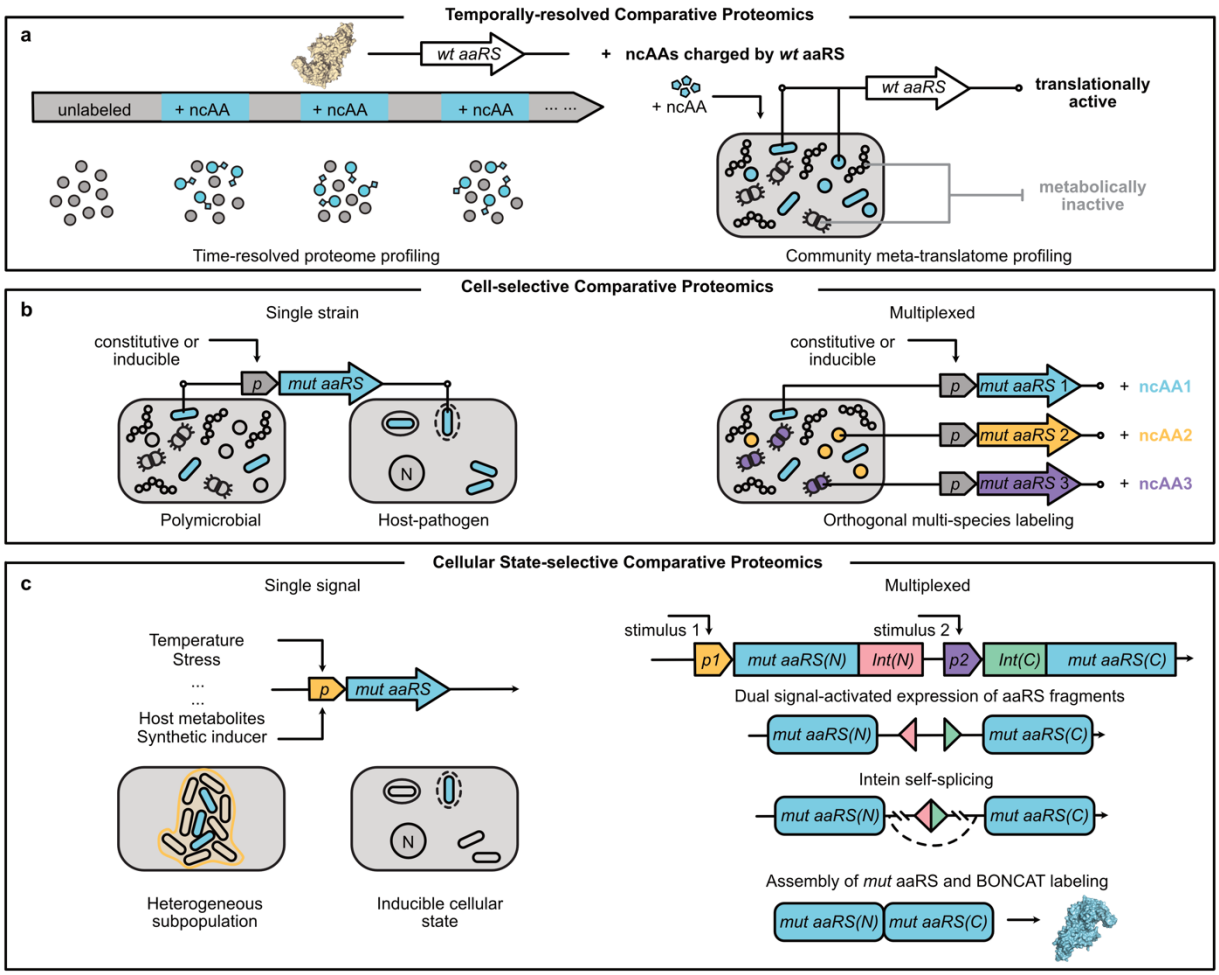

Figure 1.2. Scheme of BONCAT comparative proteomics. a. Temporally-resolved comparative proteomics using BONCAT ncAAs recognized by the endogenous translational machinery in microbes. **b.** Cell-selective BONCAT comparative proteomics and **c.** Cellular state-selective BONCAT comparative proteomics using engineered ncAA-mutant aaRS pairs.

References

1. Scinto, S. L. *et al.* Bioorthogonal chemistry. *Nat. Rev. Methods Prim.* **1**, 30 (2021).
2. Finn, M. G., Kolb, H. C. & Sharpless, K. B. Click chemistry connections for functional discovery. *Nat. Synth.* **1**, 8–10 (2022).
3. Best, M. D. Click Chemistry and Bioorthogonal Reactions: Unprecedented Selectivity in the Labeling of Biological Molecules. *Biochemistry* **48**, 6571–6584 (2009).
4. Landgraf, P., Antileo, E. R., Schuman, E. M. & Dieterich, D. C. BONCAT: metabolic labeling, click chemistry, and affinity purification of newly synthesized proteomes. *Methods Mol. Biol.* **1266**, 199–215 (2015).
5. Dieterich, D. C., Link, A. J., Graumann, J., Tirrell, D. A. & Schuman, E. M. Selective identification of newly synthesized proteins in mammalian cells using bioorthogonal noncanonical amino acid tagging (BONCAT). *Proc. Natl. Acad. Sci.* **103**, 9482 LP – 9487 (2006).
6. Stone, S. E., Glenn, W. S., Hamblin, G. D. & Tirrell, D. A. Cell-selective proteomics for biological discovery. *Curr. Opin. Chem. Biol.* **36**, 50–57 (2017).
7. Bagert, J. D. *et al.* Time-resolved proteomic analysis of quorum sensing in *Vibrio harveyi*. *Chem. Sci.* **7**, 1797–1806 (2016).
8. Babin, B. M. *et al.* SutA is a bacterial transcription factor expressed during slow growth in Pseudomonas aeruginosa. *Proc. Natl. Acad. Sci. U. S. A.* **113**, E597-605 (2016).
9. Kalesh, K. & Denny, P. W. A BONCAT-iTRAQ method enables temporally resolved quantitative profiling of newly synthesised proteins in Leishmania mexicana parasites during starvation. *PLoS Negl. Trop. Dis.* **13**, e0007651 (2019).
10. Wang, G. Z. *et al.* Staphylococcal secreted cytotoxins are competition sensing signals for Pseudomonas aeruginosa. *bioRxiv* 2023.01.29.526047 (2023). doi:10.1101/2023.01.29.526047
11. Valentini, T. D. *et al.* Bioorthogonal non-canonical amino acid tagging reveals translationally active subpopulations of the cystic fibrosis lung microbiota. *Nat. Commun.* **11**, 2287 (2020).
12. Leizeaga, A., Estrany, M., Forn, I. & Sebastián, M. Using Click-Chemistry for Visualizing in Situ Changes of Translational Activity in Planktonic Marine Bacteria. *Front. Microbiol.* **8**, (2017).
13. Samo, T. J., Smriga, S., Malfatti, F., Sherwood, B. P. & Azam, F. Broad distribution and high proportion of protein synthesis active marine bacteria revealed by click chemistry at the single cell level . *Frontiers in Marine Science* **1**, (2014).
14. Hatzenpichler, R. *et al.* Visualizing in situ translational activity for identifying and sorting slow-growing archaeal–bacterial consortia. *Proc. Natl. Acad. Sci.* **113**, E4069–E4078 (2016).
15. Landor, L. A. I., Bratbak, G., Larsen, A., Tjendra, J. & Våge, S. Differential toxicity of bioorthogonal non-canonical amino acids (BONCAT) in Escherichia coli. *J. Microbiol. Methods* **206**, 106679 (2023).
16. Steward, K. F. *et al.* Metabolic Implications of Using BioOrthogonal Non-Canonical Amino Acid Tagging (BONCAT) for Tracking Protein Synthesis. *Front. Microbiol.* **11**, 197 (2020).

17. Bagert, J. D. *et al.* Quantitative, time-resolved proteomic analysis by combining bioorthogonal noncanonical amino acid tagging and pulsed stable isotope labeling by amino acids in cell culture. *Mol. Cell. Proteomics* **13**, 1352–1358 (2014).

18. Liu, Y. *et al.* Application of bio-orthogonal proteome labeling to cell transplantation and heterochronic parabiosis. *Nat. Commun.* **8**, 643 (2017).

19. Evans, H. T., Bodea, L.-G. & Götz, J. Cell-specific non-canonical amino acid labelling identifies changes in the de novo proteome during memory formation. *Elife* **9**, e52990 (2020).

20. Schanzenbächer, C. T., Sambandan, S., Langer, J. D. & Schuman, E. M. Nascent Proteome Remodeling following Homeostatic Scaling at Hippocampal Synapses. *Neuron* **92**, 358–371 (2016).

21. Alvarez-Castelao, B., Schanzenbächer, C. T., Langer, J. D. & Schuman, E. M. Cell-type-specific metabolic labeling, detection and identification of nascent proteomes in vivo. *Nat. Protoc.* **14**, 556–575 (2019).

22. Grammel, M., Zhang, M. M. & Hang, H. C. Orthogonal Alkynyl Amino Acid Reporter for Selective Labeling of Bacterial Proteomes during Infection. *Angew. Chemie Int. Ed.* **49**, 5970–5974 (2010).

23. Wier G.M., McGreevy E.M., Brown M.J., B. J. P. New Method for the Orthogonal Labeling and Purification of Toxoplasma gondii Proteins While Inside the Host Cell. *MBio* **6**, 10.1128/mbio.01628-14 (2015).

24. Stone, S. E. Cell-Selective Chemoproteomics for Biological Discovery. (California Institue of Technology, 2017). doi:10.7907/Z9V122ZF

25. Chande, A. G. *et al.* Selective enrichment of mycobacterial proteins from infected host macrophages. *Sci. Rep.* **5**, 13430 (2015).

26. Mahdavi, A. *et al.* Identification of secreted bacterial proteins by noncanonical amino acid tagging. *Proc. Natl. Acad. Sci. U. S. A.* **111**, 433–438 (2014).

27. Truong, F., Yoo, T. H., Lampo, T. J. & Tirrell, D. A. Two-Strain, Cell-Selective Protein Labeling in Mixed Bacterial Cultures. *J. Am. Chem. Soc.* **134**, 8551–8556 (2012).

28. Okegbe, C. *et al.* Electron-shuttling antibiotics structure bacterial communities by modulating cellular levels of c-di-GMP. *Proc. Natl. Acad. Sci. U. S. A.* **114**, E5236–E5245 (2017).

29. Nguyen, D. *et al.* Active Starvation Responses Mediate Antibiotic Tolerance in Biofilms and Nutrient-Limited Bacteria. *Science (80-.).* **334**, 982 LP – 986 (2011).

30. Drenkard, E. & Ausubel, F. M. Pseudomonas biofilm formation and antibiotic resistance are linked to phenotypic variation. *Nature* **416**, 740–743 (2002).

31. Babin, B. M. *et al.* Selective Proteomic Analysis of Antibiotic-Tolerant Cellular Subpopulations in Pseudomonas aeruginosa Biofilms. *MBio* **8**, e01593-17 (2017).

32. Liu, X. Cell-Selective Proteomic Profiling in Complex Biological Systems. (California Institute of Technology, 2020). doi:10.7907/p18t-5j69

33. Mahdavi, A. *et al.* Engineered Aminoacyl-tRNA Synthetase for Cell-Selective Analysis of Mammalian Protein Synthesis. *J. Am. Chem. Soc.* **138**, 4278–4281 (2016).

34. Yuet, K. P. Tools For Spatiotemporally Specific Proteomic Analysis In Multicellular Organisms.

(California Institute of Technology, 2016). doi:10.7907/Z9VD6WDH

35. Wang, H., Wang, L., Zhong, B. & Dai, Z. Protein Splicing of Inteins: A Powerful Tool in Synthetic Biology . *Frontiers in Bioengineering and Biotechnology* **10**, (2022).

36. Presolski, S. I., Hong, V. P. & Finn, M. G. Copper-Catalyzed Azide-Alkyne Click Chemistry for Bioconjugation. *Curr. Protoc. Chem. Biol.* **3**, 153–162 (2011).

37. Chalker, J. M., Wood, C. S. C. & Davis, B. G. A convenient catalyst for aqueous and protein Suzuki-Miyaura cross-coupling. *J. Am. Chem. Soc.* **131**, 16346–16347 (2009).

38. van Hest, J. C. M. & Tirrell, D. A. Efficient introduction of alkene functionality into proteins in vivo. *FEBS Lett.* **428**, 68–70 (1998).

39. Kiick, K. L., Saxon, E., Tirrell, D. A. & Bertozzi, C. R. Incorporation of azides into recombinant proteins for chemoselective modification by the Staudinger ligation. *Proc. Natl. Acad. Sci. U. S. A.* **99**, 19–24 (2002).

40. Beatty, K. E. *et al.* Fluorescence visualization of newly synthesized proteins in mammalian cells. *Angew. Chem. Int. Ed. Engl.* **45**, 7364–7367 (2006).

41. Ignacio, B. J. *et al.* THRONCAT: metabolic labeling of newly synthesized proteins using a bioorthogonal threonine analog. *Nat. Commun.* **14**, 3367 (2023).

42. Link, A. J., Vink, M. K. S., Agard, N. J., Prescher, J. A., Bertozzi, C. R., & Tirrell, D. A. Discovery of aminoacyl-tRNA synthetase activity through cell-surface display of noncanonical amino acids. *Proc. Natl. Acad. Sci. U. S. A.*, ***103***(27), 10180–10185 (2006).

43. Kirshenbaum, K., Carrico, I. S. & Tirrell, D. A. Biosynthesis of Proteins Incorporating a Versatile Set of Phenylalanine Analogues. *ChemBioChem* **3**, 235–237 (2002).

44. Tang, Y., Wang, P., Van Deventer, J. A., Link, A. J. & Tirrell, D. A. Introduction of an Aliphatic Ketone into Recombinant Proteins in a Bacterial Strain that Overexpresses an Editing-Impaired Leucyl-tRNA Synthetase. *ChemBioChem* **10**, 2188–2190 (2009).

45. Datta, D., Wang, P., Carrico, I. S., Mayo, S. L. & Tirrell, D. A. A Designed Phenylalanyl-tRNA Synthetase Variant Allows Efficient in Vivo Incorporation of Aryl Ketone Functionality into Proteins. *J. Am. Chem. Soc.* **124**, 5652–5653 (2002).

Chapter 2. Time-resolved BONCAT Reveals Immediate Competition Sensing Responses in Interbacterial Warfare

ABSTRACT

Coinfection with two notorious opportunistic pathogens, the Gram-negative *Pseudomonas aeruginosa* and Gram-positive *Staphylococcus aureus*, dominates chronic pulmonary infections. While coinfection is associated with poor patient outcomes, the interspecies interactions responsible for such decline remain unknown. Here, we dissected molecular mechanisms of interspecies sensing between *P. aeruginosa* and *S. aureus*. We discovered that *P. aeruginosa* senses *S. aureus* secreted peptides and, counterintuitively, moves towards these toxins. *P. aeruginosa* tolerates such a strategy through "competition sensing," whereby it preempts imminent danger/competition by arming cells with type six secretion system (T6SS) and iron acquisition systems. Competition sensing was activated under various environmental conditions, including during coinfection of bronchial epithelia, in which T6SS islands targeting human cells were upregulated. Intriguingly, while T6SS is predominantly described as weaponry targeting Gram-negative and eukaryotic cells, we find that T6SS may also contribute to full *P. aeruginosa* competition with *S. aureus*, a previously undescribed role for T6SS. This study reveals critical insight into both interspecies competition and how antagonism may cause collateral damage to the host environment.

This chapter is a manuscript in revision as:
Wang G.Z., Warren E.A., Haas A.L., Peña, A.S., Kiedrowski M.R., Lomenick B., Chou T.F., Bomberger J.M., Tirrell D.A., Limoli D.H. *Staphylococcal* Secreted Cytotoxins are Competition Sensing Signals for *Pseudomonas aeruginosa*.

Introduction

The future of microbiome research lies in our ability to manipulate polymicrobial interactions toward improved human health outcomes, which requires a fundamental molecular understanding of how microbial species sense and respond to ecological competition. Chronic respiratory infections in people with cystic fibrosis (CF) consist of diverse and heterogeneous microbial communities[1]. Nonetheless, *Pseudomonas aeruginosa* and *Staphylococcus aureus* are the most prevalent[2,3]. Critically, coinfection with these pathogens correlates with worsened clinical outcomes and altered antibiotic efficacy[2-4], urging the need for molecular dissection of their interspecies crosstalk.

We previously reported that *P. aeruginosa* is attracted to *S. aureus* resulting in invasion of *S. aureus* colonies[5]; however, what, if any, selective benefit *P. aeruginosa* achieves by adopting this behavior remains unknown. A potential role for such a strategy may be to bridge cellular distances for contact-dependent mechanisms of antagonism. The type six secretion system (T6SS), widely found in Gram-negative bacteria, such as *P. aeruginosa*, equips cells with a versatile nanomachinery that functions as an interspecies weapon capable of targeting both eukaryotic and prokaryotic cells[6-8]. *P. aeruginosa* typically maintains low basal T6SS activity but is capable of rapid reciprocal firing following T6SS attack by other Gram-negative species[9,10]. However, whether an analogous response may occur in response to Gram-positive competitors lacking T6SS remains unknown. A greater fundamental understanding of interspecies sensing and resulting competition, particularly between Gram-negative and Gram-positive pathogens common during coinfection, is necessary to develop interventions directed at interspecies interactions.

Here, we report the discovery that *P. aeruginosa* activates T6SS after an encounter with the Gram-positive pathogen *S. aureus*. We present a "competition sensing" model uncovered by a combination of genetics, microscopy and multi-omics approaches whereby secreted *Staphylococcal* peptides are key interspecies signals that trigger *P. aeruginosa* antagonism. *P. aeruginosa* was found to sense *S. aureus* via secreted peptides (phenol soluble modulins, PSMs) at a distance, subsequently increasing type IV pili-mediated directional motility and activating antagonism. Although PSMs are potent *Staphylococcal* toxins, *S. aureus* deficient in PSMs exhibited enhanced survival during competition with *P. aeruginosa*. We also examined coinfection on fully differentiated CF-derived bronchial epithelia—the gold standard model of *in vivo* CF airway infection—and found *P. aeruginosa* T6SS activity was significantly increased, including host-targeting T6SS islands. Finally, to gain insight into how competition sensing is activated in *P. aeruginosa*, we measured

T6SS translation and activity in the absence of the major regulators of T6SS (Gac/Rsm and threonine phosphorylation pathway, TPP). T6SS could be further activated in response to PSMs in Δ*retS* (Gac/Rsm) or Δ*pppA* (TPP) *P. aeruginosa*, where T6SS is constitutively high, suggesting competition sensing may be activated through an additional pathway. Overall, these results broaden our mechanistic understanding of interspecies antagonism between distantly related species, reveal interspecies pathways that might be targeted therapeutically, and lend insight into the mechanism of increased patient decline during coinfection with *P. aeruginosa* and *S. aureus*.

Results and Discussion

PSMα peptides are necessary and sufficient for *P. aeruginosa* attraction toward *S. aureus*

We previously reported that *P. aeruginosa* travels up a gradient of *S. aureus* secreted factors using type IV pilus (TFP)-dependent motility[5]. The *S. aureus* attractants identified are secreted *S. aureus* peptides, referred to as phenol soluble modulins (PSMs). *S. aureus* produces five alpha peptides: PSMα1-4 and PSMδ (δ-toxin) and two β-peptides: PSMβ1 and 2 (**Supplementary Fig. 2.1**). Here, we first asked if *P. aeruginosa* possesses specificity in attraction towards individual peptides in a macroscopic TFP chemotaxis assay (**Fig. 2.1a**). PSM α-peptides were examined for initial characterization given that the α-peptides have known roles in neutrophil chemoattraction[11] and cytotoxicity to mammalian host cells[12]. *P. aeruginosa* traveled further towards an increasing gradient of WT *S. aureus* supernatant (**Fig. 2.1b**), whereas directional motility towards supernatant derived from a double *psm*α1-4 and *psm*δ mutant (Δ*psm*α1-4 δATG-ATT; start codon of *psm*δ mutated to preserve expression of RNAIII, referred to as Δ*psm*αδ, **Supplementary Fig. 2.1**) was eliminated, suggesting that at least one α-peptide is necessary for attracting *P. aeruginosa* (**Fig. 2.1b, c**). The magnitude of *P. aeruginosa* attraction towards Δ*psm*α was between WT *S. aureus* and the double Δ*psm*αδ mutant, suggesting PSMδ, along with the other α peptides, is necessary for *P. aeruginosa* directional motility. We then determined if PSMs are sufficient to attract *P. aeruginosa* and the specificity of individual PSM peptides' contributions. Pure synthetic PSMα3 and δ-toxin strongly attracted *P. aeruginosa* in a dose-dependent manner (**Fig. 2.1d**). These data demonstrate that PSMδ and PSMα3 are necessary and sufficient for *S. aureus* to attract *P. aeruginosa*.

P. aeruginosa is often described to outcompete *S. aureus in vitro*[13–16]. We previously reported that *P. aeruginosa* attraction to *S. aureus* on surfaces provides *P. aeruginosa* a competitive advantage[5]. Curiously, however, a moderate increase in *S. aureus* survival was also observed here for PSM-deficient *S. aureus*

cocultured with *P. aeruginosa* in shaking liquid culture, where TFP mediated directional motility is not expected to occur (**Fig. 2.1e**). Addition of PSM peptides to coculture with the Δ*psm*αδ mutant restored *S. aureus* survival to the reduced level seen with WT strains, raising the possibility that there exist unknown PSM-dependent competition mechanisms between *P. aeruginosa* and *S. aureus*. These factors further led us to investigate the roles of PSMs in mediating *P. aeruginosa* responses to *S. aureus*, and the cellular events occurring after *P. aeruginosa* cells are recruited to the site of *S. aureus*.

P. aeruginosa undergoes immediate, systematic proteome remodeling in response to PSM peptide pulse-in and coculture with *S. aureus*

To gain insight into the effects PSMs have on *P. aeruginosa* cellular functions, we took advantage of the precise temporal resolution afforded by BioOrthogonal Non-Canonical Amino acid Tagging (BONCAT)[17] to monitor *P. aeruginosa* immediate protein synthesis in response either to direct addition of PSMs or to coculture with *S. aureus* cells (**Fig. 2.2a**). *P. aeruginosa* cells constitutively expressing an engineered mutant methionyl-tRNA synthetase (NLL-MetRS) allow for selective metabolic labeling of newly synthesized proteins by the azide-bearing methionine (Met) analog: azidonorleucine (Anl) (**Supplementary Fig. 2.2**). Downstream chemical enrichment[18] of labeled proteins enables targeted analysis of nascent *P. aeruginosa* protein synthesis during the Anl labeling period.

We identified 3,348 and 3,256 total proteins newly synthesized by *P. aeruginosa* during the 30-min labeling period immediately following PSM pulse-in and coculture with *S. aureus*, respectively (**Fig. 2.2b, c**), and quantified differentially expressed proteins in each condition. We found 60 *P. aeruginosa* proteins with statistically significant and greater than 2-fold increase and 98 proteins with greater than 2-fold decrease in abundances in response to PSM pulse-in. For coculture with *S. aureus* compared to monoculture, we found 178 proteins with significant increase (>2-fold) in abundances and 124 with significant decrease (>2-fold) in abundances (**Supplementary Table 2.2**). Candidates were then grouped by their annotated functional categories, which include the following: T6SS, pyoverdine biosynthesis, cyclic di-GMP sensing/regulating enzymes, chemotaxis/motility, cellular response to envelope stress, and DNA damage/stress response (**Fig. 2.2d, e**). Strikingly, PSMs alone are sufficient to promote the synthesis of proteins in each category.

P. aeruginosa activates T6SS in response to PSMs and *S. aureus* cells

Notably, proteins involved in T6SS are over-represented among the total significantly up-regulated hits in *P. aeruginosa* global proteomic response to PSM pulse-in and *S. aureus* coculture (**Fig. 2.3, Supplementary**

Fig. 2.3). *P. aeruginosa* T6SS is a speargun-shaped secretory apparatus that injects toxic cargo into prey cells. We detected significantly increased synthesis of various components of the T6SS structural architecture, including core, accessory, bacteriophage-like subunits, and membrane-associated components[19,20] (**Fig. 2.3a-c**), suggesting the T6SS apparatus is being systematically assembled during the 30-min labeling period following the introduction of PSMs or *S. aureus*. In particular, the increased expression levels of two proteins—the hemolysin coregulated protein (Hcp, T6SS "tube") and the valine-glycine repeat protein G (VgrG, T6SS "tip")—indicate potential for functional activity of the T6SS[6,7,20]. Their relative fold-changes are the highest among other T6SS proteins that showed significantly changed abundances in response to coculture with *S. aureus* (**Fig. 2.3a**). Additionally, proteins encoded by all three known *P. aeruginosa* T6SS loci, denoted H1-T6SS (PA00-), H2-T6SS (PA16-) and H3-T6SS (PA23-)[5,19,20] were increased (**Fig. 2.3a, c**). Previous literature suggests that H1-T6SS is antibacterial and is activated in a "tit-for-tat" pattern following exogenous T6SS+ attacks, while H2- and H3-T6SS both exhibit anti-eukaryotic activity[21]. Interestingly, H3-T6SS was observed to be mildly induced and only in response to coculture with *S. aureus* cells, rather than the addition of PSMs. These results support a model where *P. aeruginosa* up-regulates T6SS after encountering *S. aureus* via sensing of *Staphylococcal* secreted PSMs, and that other *Staphylococcal* factors in addition to PSMs may induce *P. aeruginosa* T6SS assembly and firing.

We next ranked the nascent *P. aeruginosa* proteome by individual protein raw abundances quantified by label-free quantitation (LFQ) via mass spectrometry (**Supplementary Fig. 2.4**) to examine the cellular allocation of protein synthesis resources following PSM pulse-in and *S. aureus* coculture challenge. Remarkably, several T6SS proteins appeared in the top quartile with significantly elevated average abundances in PSM-treated and *S. aureus* coculture samples compared to untreated/monoculture controls, further indicating T6SS antagonism is prioritized by *P. aeruginosa* in responding to interspecies stress. Interestingly, even under non-induced conditions, T6SS proteins were relatively abundant, suggesting proteins necessary for T6SS are continually synthesized, perhaps in preparation for competitor attacks.

We next sought to determine if increased T6SS protein expression in response to *S. aureus* translates to increased T6SS activity. Although T6SS apparatus assembly does not necessarily indicate firing of T6SS effectors, the AAA+ ATPase ClpV1 (PA0090/TssH) is often used to monitor T6SS activity[22-24]. Since localization and ATP hydrolysis activity of ClpV1 drive T6SS sheath contraction and propulsion of effectors, we reasoned that significantly increased ClpV1 protein expression could lead to increased T6SS firing, followed by rounds of ClpV1 assembly and recycling of the H1-T6SS components. Therefore, to examine *P.*

aeruginosa H1-T6SS activity, single-cell microscopy using a fluorescent reporter of ClpV1 activity was employed (ClpV1-GFPmut3[9]) (**Fig. 2.3d**). PSM-treated cells exhibited both significantly increased ClpV1-GFPmut3 puncta formation (**Fig. 2.3e**) as well as overall fluorescence intensity (**Fig. 2.3f**) per cellular total area, supporting the proteomics data that expression of H1-T6SS is increased upon *P. aeruginosa* exposure to PSMs and suggesting that PSMs induce *P. aeruginosa* deployment of H1-T6SS.

***Staphylococcal* secreted PSM peptides increase siderophore biosynthesis**

We also observed that the T6SS induction in *P. aeruginosa* is accompanied by systematic upregulation of the pyoverdine biosynthesis cluster (**Supplementary Fig. 2.3**), which produces a siderophore that binds to extracellular Fe^{3+} with high affinity[25,26]. Iron starvation is a major stress response pathway evolutionarily conserved in bacteria. Proteins encoded by five pyoverdine operons (**Supplementary Fig. 2.5a**) entirely covering the complex cellular biosynthesis machinery for the pyoverdine siderophore were found to be significantly up-regulated in response to PSM pulse-in or *S. aureus* coculture—including the extracytoplasmic function iron starvation σ factor PvdS, which positively regulates pyoverdine biosynthesis and secretion[27], and PvdR, which controls transport of pyoverdine out of the cell[28], suggesting that siderophores are being increasingly synthesized and dispatched out of the cell during the 30-min labeling period. Thus, we simultaneously monitored pyoverdine production and induction of gene expression using a fluorescent reporter P'*pvdG-mScarlet*[29] (**Supplementary Fig. 2.5b, c**). Consistent with the proteomic results, we observed significantly increased pyoverdine production by *P. aeruginosa* following PSMs treatment, as well as significant induction of *pvdG* promoter activity, suggesting increased transcription of *pvdG*, which encodes a thioesterase essential for the biosynthesis of pyoverdine in *P. aeruginosa*.

Pathogens face intense competition for iron with host and other microbial species due to the essentiality of iron as a nutrition source, and siderophore production is often reported to be involved in exploitive interspecies competition[13,30,31]. Interestingly, a recent study reported upregulation of siderophore biosynthesis in *P. aeruginosa* when treated with *Staphylococcal* culture supernatant[29], though the molecular signals responsible for the observed upregulation remained elusive. Here, we show that *Staphylococcal* secreted PSM peptides alone can trigger increased pyoverdine biosynthesis and export, further suggesting that PSMs play important roles in mediating interspecies competition between *P. aeruginosa* and *S. aureus*.

Significantly increased *P. aeruginosa* T6SS activity in coculture with *S. aureus* on CF patient-derived bronchial epithelial cells

Previous studies reported that Hcp1 is detected at high levels in chronic CF sputum[6], and H2-, H3-T6SS promote *P. aeruginosa* invasion of epithelial cells[8,32], suggesting that differential regulation of any of the three T6SS loci in polymicrobial infections may have implications for the host. Prompted by the potential roles for all three T6SS loci in *P. aeruginosa* in CF pathogenicity, we further investigated *P. aeruginosa* and *S. aureus* interactions in a host-derived environment to explore interspecies virulence factor crosstalk in a clinically relevant context.

For this purpose, we utilized the healthcare-associated methicillin-resistant *Staphylococcus aureus* (HA-MRSA) strain USA100, a highly antibiotic-resistant clinical isolate and a leading cause of invasive infections by MRSA[33,34], and *P. aeruginosa* strain PAO1, a laboratory derivative more closely related than PA14 to most clinical isolates of CF[35]. We performed RNA-sequencing to examine *P. aeruginosa* transcriptomic changes that contribute to interspecies interactions in a coinfection model with *S. aureus* using polarized, fully differentiated CF bronchial epithelial cells (CFBE41o-, **Fig. 2.4a**). This model closely mimics the CF host environment by recapitulating approximately 84% of *P. aeruginosa* gene expression in human expectorated CF sputum, outperforming both laboratory media and the acute mouse pneumonia model of infection[36].

We identified 1,325 differentially expressed genes during coculture with *S. aureus* (fold change >2 or <-2, P<0.05). Of these, we detected increased transcription of T6SS genes from all three T6SS clusters (**Fig. 2.5b, c**). Transcription of *hcp*, *vgrG*, and *tssBC* sheath genes was significantly increased, suggesting that the T6SS apparatus has the potential to be functional. In addition, we observed significantly increased transcription of several effector genes including *tse1* (*PA1844*), a peptidoglycan amidase[37], *pldB* (*PA5089*), a phospholipase[38], and *tseF* (*PA2374*), a known facilitator of iron uptake in *P. aeruginosa*[39]. These results further support that *P. aeruginosa* T6SS induction by *S. aureus* is sustained in a host-derived environment.

***P. aeruginosa* T6SS induction by PSMs does not require the Gac/Rsm regulator RetS or threonine phosphorylation pathway phosphatase PppA**

We next probed the molecular mechanism of PSM-induced T6SS activation. The activity of T6SS in *P. aeruginosa* is controlled at multiple levels. Post-transcriptionally, the global activation of antibiotic and cyanide synthesis/regulator of secondary metabolism (Gac/Rsm) pathway regulates the expression of all three T6SS loci[10,40]. Here, a histidine sensor kinase (GacS) responds to an unknown signal to activate the

response regulator GacA. Phosphorylation of GacA, through a complex regulatory cascade, ultimately leads to translational activation of its targets, including T6SS[41]. Translational repression of T6SS can occur through inhibition of GacS, via binding by its cognate sensor kinase, RetS. Prior studies demonstrate the Gac/Rsm pathway mediates activation of H1-T6SS in response to lysed kin cells (*P. aeruginosa* response to antagonism, PARA)[10].

Post-translational activation of H1-T6SS is regulated by the threonine phosphorylation pathway (TPP), whereby phosphorylation of Fha1 initiates apparatus assembly and effector secretion[22]. Dephosphorylation of Fha1 by the phosphatase PppA returns the system to its baseline state[23]. Previous literature suggests that TagQRST-PpkA-Fha1-PppA of the TPP pathway mediates *P. aeruginosa* "tit-for-tat" counterattack antagonism[9] and H1 activation by exogenous mediators of membrane stress (i.e., polymyxin B)[42]. We therefore sought to investigate whether PSMs activation of T6SS is dependent on key components in Gac/Rsm or TPP pathways.

First, we investigated a role for the Gac/Rsm pathway by monitoring induction of the T6SS sheath proteins (TssB) in H1, H2, & H3 native, chromosomal fusions to GFP in WT *P. aeruginosa* and a Δ*retS* mutant. As expected, in WT *P. aeruginosa* cells, the addition of both polymyxin B and PSMs increased the expression of TssB1. In polymyxin B-treated cells, TssB1 expression peaked around 2 hours and remained high for the duration of the experiment (6 hours). Induction of TssB1-GFP fluorescence by PSMs also peaked after 2h but appeared to be more transient (**Fig. 2.5a**). Given the inhibitory role for RetS, a Δ*retS* mutant would be expected to exhibit constitutively high levels of TssB. Our data are consistent with this prediction, whereby TssB1 expression was approximately five-fold higher at time zero with vehicle alone (*note differences in y-axes*, **Fig. 2.5b**). Importantly, while activation was slightly delayed, likely due to the already high TssB1 translation in Δ*retS*, the addition of both polymyxin B and 4 μg/mL of PSMs also increased TssB1 expression, suggesting that *P. aeruginosa* response to PSMs is independent of Gac/Rsm regulation, like that previously observed for membrane stress. However, we were surprised to see 8 μg/mL of PSMs significantly increased TssB1 expression above vehicle treatment by an even larger magnitude and sustained for a longer duration than that observed for WT. When comparing the growth rate of the Δ*retS* mutant upon polymyxin B and PSM treatment, we noticed that loss of RetS modestly sensitized *P. aeruginosa* to both polymyxin B and PSMs, in comparison to WT (**Supplementary Fig. 2.7a**). While enhanced sensitivity to these agents may explain the larger response in Δ*retS*, such exaggerated activation of TssB1 was not seen during treatment with polymyxin B, suggesting the regulatory responses between PSMs and polymyxin B may differ. We observed generally

similar patterns for TssB2, although translation was lower compared to TssB1 overall (**Fig. 2.5b**, **Supplementary Fig. 2.7b, c)**. For TssB3, translational activation was below the level of detection for all conditions examined, consistent with global proteomic analyses. Overall, these data demonstrate that PSMs activate the translation of H1- and H2-T6SS in the absence of regulation by RetS.

To examine the role of the post-translational TPP pathway, we again employed a ClpV1-GFP translational reporter and examined PSM-induced ClpV1-GFP puncta formation in a *P. aeruginosa* Δ*pppA* mutant via microscopy. We observed significantly increased puncta formation in both PSM- and polymyxin B-treated cells compared to vehicle control (**Fig. 2.5c**). These results suggest that the TPP pathway phosphatase PppA is dispensable in PSM- and polymyxin B-induced T6SS activation. While the Gac/Rsm pathway post-transcriptionally orchestrates the assembly of *P. aeruginosa* H1-T6SS[40], the TPP pathway post-translationally controls the firing of T6SS effectors[22]. Our results further support a model where Gac/Rsm and TPP pathways converge to regulate the expression and activity of *P. aeruginosa* T6SS.

Since the response of *P. aeruginosa* to PSMs exhibited some similarities, yet also a differential response from the pore-forming toxin polymyxin B, we sought to further determine how *P. aeruginosa* responds to these two T6SS-activating compounds. While PSMs generally exhibit low activity towards bacterial membranes[43], we asked whether PSMs could permeabilize the *P. aeruginosa* membrane, cause kin cell lysis, and/or cause envelope stress in *P. aeruginosa*. Live imaging of *P. aeruginosa* with propidium iodide +/- PSMs did not show evidence of kin lysis, inner membrane permeability or altered *P. aeruginosa* growth rate (**Supplementary Fig. 2.8a**). In comparison, polymyxin B significantly inhibited *P. aeruginosa* growth and induced a moderate uptake of propidium iodide (**Supplementary Fig. 2.8b**). Further analysis of outer membrane permeability by uptake of 1-N-phenylnaphthylamine (NPN) also did not reveal significant permeabilization by PSMs, while polymyxin B significantly induced outer membrane permeability (**Supplementary Fig. 2.8c**).

Given these differences in membrane activity between polymyxin B and PSMs, we revisited T6SS activation by polymyxin B with the ClpV1 fluorescent reporter[9] under the current study conditions for comparison. Polymyxin B-treated cells displayed distinct ClpV1 puncta induction but yielded low mean fluorescence intensity per cell (**Supplementary Fig. 2.8d, e**), further suggesting potential molecular differences between mechanisms of T6SS induction by polymyxin B versus PSM treatment. Polymyxin B can be inserted into the

membrane, causing cell lysis by creating pores in the envelope[44]. In contrast, PSMs are cationic, amphipathic small helical peptides with membrane perturbing and cell surface-adhering properties[45].

While we were unable to detect significant membrane-damaging activity by PSMs, we hypothesize that non-lethal membrane perturbations may explain PSM-induced T6SS activation in *P. aeruginosa*. Several factors contributed to this hypothesis: first, global differential proteomic profiling revealed significant and systematically decreased production of electron transport chain (ETC) enzymes in response to PSM pulse-in and coculture with *S. aureus* (**Supplementary Fig. 2.3, 8f-g**), a characterized cellular response to envelope stress evolutionarily conserved in *E. coli* and other Gram-negative bacteria[46,47]. In addition, while we did not detect increased protein synthesis of classic regulators of membrane stress, such as σ^E and CpxAR[48], we observed significant up-regulation of a subset of proteins involved in membrane stress responses, most notably protein encoded by *PA3731*, a close homolog of the phage shock protein PspA in *E. coli* and member of a family of proteins characterized to play crucial roles in the cellular response to and protection against envelope stress in *E. coli* and other Gram-negative species[49]. These findings suggest a possible link between PSM-induced *P. aeruginosa* T6SS firing and transient perturbations of cellular envelope stress.

A potential role for *P. aeruginosa* T6SS in competition against *S. aureus*

A wealth of existing literature shows that T6SS-delivered effectors target and kill Gram-negative bacteria[9,10,21]. However, T6SS-mediated killing of Gram-positive species has only been demonstrated recently[50-52].

To examine if T6SS provides *P. aeruginosa* a competitive advantage in coculture with *S. aureus*, we constructed clean deletions of each T6SS sheath gene, Δ*tssB1* (ΔH1-T6SS), Δ*tssB2* (ΔH2-T6SS), Δ*tssB3* (ΔH3-T6SS) and a triple T6SS mutant with all three T6SS loci disrupted (Δ*tssB1-3*). We first validated that the triple T6SS mutant is defective in T6SS-mediated competition in coculture with T6SS+ *V. cholerae* (**Supplementary Fig. 2.9a**). While *V. cholerae* cells survived significantly more in coculture with *P. aeruginosa* Δ*tssB1-3* than with the wild type, complementation with an arabinose-induced vector expressing *tssB1-3* restored killing of *V. cholerae* to the level seen in coculture with the WT. We note complementation with P*araBAD-tssB1-3* in the absence of arabinose, due to the previously described non-induced expression of this promoter[53].

Next, we utilized these mutants to examine if there is a role for T6SS under the conditions utilized to examine both competition and T6SS expression thus far (shaking liquid). WT *S. aureus* cells exhibited a moderate increase in survival when in coculture with the triple T6SS mutant of *P. aeruginosa* compared to coculture with the WT (**Fig. 2.6**), suggesting a role for one or more T6SS islands in competition with *S. aureus* under these conditions. Further, similar to the observation in Figure 1, the Δ*psm*αδ mutant exhibited increased survival with WT *P. aeruginosa*. Yet, when *P. aeruginosa* Δ*tssB1-3* is cocultured with *S. aureus* Δ*psm*αδ, the outcome of *S. aureus* survival is similar to that in coculture with *P. aeruginosa* WT. These observations suggest that PSM-induced T6SS activation may contribute to *P. aeruginosa* competitive fitness against *S. aureus*.

To determine which T6SS loci specifically contribute to *S. aureus* antagonism, we measured *S. aureus* survival in coculture with single T6SS mutants. Interestingly, deletion of *tssB1*, *tssB2* or *tssB3* alone did not significantly rescue *S. aureus* survival in coculture (**Supplementary Fig. 2.9b**). These results indicate that there is a minor contribution of two or more of the three T6SS islands in *P. aeruginosa* competition against *S. aureus*.

To further interrogate *P. aeruginosa* T6SS-dependent competition, we sought to enhance T6SS-dependent killing through previously described methods, including coculture on the surface of a nitrocellulose membrane to enhance cellular contact and surface sensing, and deletion of *retS* to increase T6SS constitutive expression. However, neither method significantly increased killing of *S. aureus* (**Supplementary Fig. 2.10a**), suggesting that increased *P. aeruginosa* T6SS expression alone may not be sufficient to enhance competition. To specifically test a role for T6SS under these conditions, we constructed a *P. aeruginosa* triple T6SS mutant (Δ*tssB1-3*) in the Δ*retS* mutant background (Δ*retS*Δ*tssB1-3*, quadruple deletion). We did not observe significant differences in *S. aureus* survival after 6 hours or 8 hours of coculture with the *P. aeruginosa* quadruple Δ*retS*Δ*tssB1-3* mutant compared to the single Δ*retS* mutant (**Supplementary Fig. 2.10b**), suggesting that T6SS is not necessary for *P. aeruginosa* competition under the conditions examined here. Based on previously described functions for T6SS, to observe a greater contribution by T6SS in liquid versus solid is quite surprising. Thus, future efforts will be dedicated to dissecting the different T6SS-mediated phenotypes under various conditions. Overall, these data support a model whereby *P. aeruginosa* senses *S. aureus* peptides from a distance and activates competitive pathways that provide a competitive advantage.

The "competition-sensing" hypothesis states that bacteria adapt evolutionarily conserved stress response pathways to directly detect and respond to ecological competition[54]. The results presented here provide empirical evidence for this hypothesis, which predicts increased bacterial toxin production in response to stress caused by competitors. We propose a model in accordance, whereby *P. aeruginosa* senses secreted competitor signals and swiftly responds by moving towards the signals and activating antagonistic responses (**Fig. 2.7**). Activation of membrane stress and iron starvation responses observed in *P. aeruginosa* further supports that "competition sensing" is manifested in several stress response pathways.

P. aeruginosa is attracted to diverse bacterial species and moves towards the site of competition[5]; thus, a close analogy can be drawn between *P. aeruginosa* and the notorious predacious bacterium, *Myxococcus xanthus*, characterized to coordinate group responses to invade and lyse prey[55]. *P. aeruginosa* displays incipient multicellularity via complex collective behaviors, including ones of a predatory nature as described here. We propose that upon sensing interspecies signals, *P. aeruginosa* cells move to "trap" a *S. aureus* colony, further enabling contact-dependent invasion and/or local concentration of secreted antimicrobials.

One potential mechanistic model of competition sensing is that *P. aeruginosa* closely monitors cell envelope integrity to detect environmental and/or interspecies insults. While PSMs do not affect the *P. aeruginosa* membrane sufficiently to allow permeabilization, even transient envelope stress may induce T6SS assembly and firing. We recently reported that a methyl-accepting chemotaxis inducer PilJ (PA0411) in the Pil-Chp pathway is necessary for *P. aeruginosa* sensing of PSM peptides[56]. Whether PilJ binds to PSMs directly or is activated indirectly, perhaps by sensing transient membrane stress, is unknown and an area of current investigation by our group. Interestingly, it has been recently reported that *P. aeruginosa* chemotaxes towards, instead of away from, antibiotics and releases bacteriocins before dying[57]. While PSMs did not reduce *P. aeruginosa* viability, we found induction of two pyocins in *P. aeruginosa* in response to both PSM pulse-in and coculture with *S. aureus*, potentially supporting a similar "suicidal chemotaxis" model. PSMs alone are sufficient to trigger TFP-mediated motility, synthesis and transport of siderophores, activation of T6SS antagonism and envelope stress responses, suggesting that PSMs are important interspecies signals that help *P. aeruginosa* sense and respond to imminent danger/competition. Interestingly, T6SS, pyoverdine production, chemotaxis and cellular response to envelope stress in *P. aeruginosa* are all known to be regulated by cyclic di-GMP[33, 58–61]. We propose herein that secondary messenger signaling networks mediate "competition sensing" and global bacterial responses to interspecies insults. In support of this hypothesis, we observed up-regulation of multiple cyclic di-GMP

metabolizing enzymes, suggesting several cyclic di-GMP mediated signaling networks are activated and are involved in *P. aeruginosa* response to PSMs and *S. aureus* (**Supplementary Fig. 2.11**).

While deletion of *retS* did not limit *P. aeruginosa* competition sensing, proteomic analysis detected significantly increased abundance of PA1611, a known inhibitor of RetS and regulator of the Gac/Rsm pathway[59], both in response to PSM treatment and *S. aureus* coculture. Consistent with deletion studies, we did not observe a change in RetS abundance in either proteomic or RNA-seq analyses. Thus, it is formally possible that PSMs activate competition sensing through Gac/Rsm, potentially through PA1611, though independent of RetS. Consistent with this model, we detected systematic repression of T3SS and simultaneously increased T6SS activity during coinfection with *S. aureus* (**Supplementary Fig. 2.12**), which supports previous reports that *P. aeruginosa* T6SS and T3SS are inversely regulated via RetS[41]. Intriguingly, the Gac/Rsm pathway and cyclic di-GMP signaling networks both regulate T6SS and iron uptake[41,61]. Future work will be dedicated to studying overlap in signal transduction pathways and potential coordination of interspecies phenotypes reported in this study, including *P. aeruginosa* TFP-mediated directional motility, downstream antagonistic attacks and exploitive iron scavenging.

Interestingly, we observed inverse regulation of siderophore biosynthesis in coculture with *S. aureus* using global proteomics analysis performed *in vitro* versus transcriptomic analysis performed in a host environment. *P. aeruginosa* down-regulates pyoverdine biosynthesis during coinfection with *S. aureus* on CF-derived bronchial epithelial cells (**Supplementary Fig. 2.12**). We attribute this to the differences in temporal resolution of the experiments—while chemo-selective proteomic analysis captured immediate "competition sensing" responses, global RNA-sequencing investigated long-term coinfection phenotypes. These results highlight *P. aeruginosa* versatile genetic plasticity in regulating iron scavenging behaviors during short-term versus long-term competition and underline the importance of studying and comparing polymicrobial interactions both *in vitro* and *in vivo*.

Numerous studies have reported that *P. aeruginosa* secretes diverse secondary metabolites known to be toxic to *S. aureus*[14,15], but our study is the first to reveal a role for a contact-dependent interspecies weaponry, the T6SS, in *P. aeruginosa*-*S. aureus* interactions. Nonetheless, when embarking on this study, we presumed that *P. aeruginosa* T6SS would neither be activated by nor effective in competition with *S. aureus*. Several reasons contributed to this initial assumption. First, Gram-positive bacteria lack a conjugative pilus, and therefore cannot provoke *P. aeruginosa* reciprocal firing. Further, the Gram-positive cell wall constitutes

a thicker peptidoglycan (PG) layer in comparison to that of Gram-negative species, which was thought to prohibit penetration by the T6SS apparatus and effective delivery of toxic effectors. Recent studies by other groups demonstrating that the T6SS-delivered effectors of *Acinetobacter baumannii*[50,51] and *Acidovorax citrulli*[52] can kill Gram-positive species challenge these assumptions. Furthermore, it has been reported that the T6SS apparatus of *Serratia marcescens*[62] and *Klebsiella pneumoniae*[63] can penetrate the fungal cell wall, which is thicker than the Gram-positive cell wall. The discovery here that *P. aeruginosa* T6SS is induced by a Gram-positive pathogen further expands the role of T6SS during infection, opening a wealth of new opportunities to study, inhibit, or co-opt interspecies competition.

How does *P. aeruginosa* T6SS mediate competition with *S. aureus*? Intriguingly, proteomic, transcriptional, and mutational analyses suggest that multiple T6SS loci may have roles in enhancing the competitive fitness of *P. aeruginosa* during coculture with *S. aureus*. Future work will be dedicated to defining the scope and specificity of functionality for *P. aeruginosa* antagonism against *S. aureus* mediated by T6SS effectors. Moreover, the global proteomics study was only performed on the *P. aeruginosa* intracellular lysate fraction, which did not include most secreted protein effectors found in the extracellular fraction; thus, it is possible *S. aureus* induces the secretion of T6SS effectors not identified here. A recent study demonstrated that Tse4, a T6SS muramidase effector of *A. baumannii*, exhibits promiscuous PG-degrading activity and kills Gram-positive species, including *S. aureus*[50]. While previous literature indicated T6SS-exported muramidases generally cannot effectively lyse Gram-positive cells[64], the possibility remains that certain PG-targeting T6SS effectors can impact cellular functions of Gram-positive bacteria, not limited to causing cellular death or lysis. Beyond cell wall degrading toxins, developing evidence that suggests the T6SS apparatus can inject and deliver effectors into the Gram-positive cell wall[50-52] points to the emerging possibility that diverse T6SS effectors could have bacteriostatic and bactericidal potential towards both Gram-negative and Gram-positive bacteria. For instance, studies analyzing differential regulation for *S. aureus* in coculture with *P. aeruginosa* consistently reported up-regulation of SOS response and oxidative stress response pathways[15,30], but it remained unclear how *P. aeruginosa* triggers these responses in *S. aureus*. It is therefore curious to speculate that these effects could be due to previously unknown attacks by *P. aeruginosa* antibacterial T6SS nuclease toxins[65] and NAD(P)+ glycohydrolase effectors[66].

Cumulatively, our findings provide a new model of T6SS-mediated interspecies interactions for Gram-negative and Gram-positive species. Our results revealed complex polymicrobial virulence factors crosstalk and highlighted the importance of leveraging a comprehensive molecular understanding of polymicrobial

competition while studying the host-pathogen interface. Considering both *Staphylococcal* PSMs and *P. aeruginosa* T6SS have well-characterized functions in modulating host immune responses, their interactivity uncovered by our study could have detrimental implications on the host.

References

1. O'Sullivan, B. P. & Freedman, S. D. Cystic fibrosis. *Lancet (London, England)* **373**, 1891–1904 (2009).
2. Fischer, A. J. *et al*. Sustained coinfections with *Staphylococcus aureus* and *Pseudomonas aeruginosa* in cystic fibrosis. *Am. J. Respir. Crit. Care Med*. **203**, 328–338 (2021).
3. Limoli, D. H. *et al*. *Staphylococcus aureus* and *Pseudomonas aeruginosa* coinfection is associated with cystic fibrosis-related diabetes and poor clinical outcomes. *Eur. J. Clin. Microbiol. Infect. Dis*. **35**, 947–953 (2016).
4. Hubert, D. *et al*. Association between *Staphylococcus aureus* alone or combined with *Pseudomonas aeruginosa* and the clinical condition of patients with cystic fibrosis. *J. Cyst. Fibros. Off. J. Eur. Cyst. Fibros. Soc*. **12**, 497–503 (2013).
5. Limoli, D. H. *et al*. Interspecies interactions induce exploratory motility in *Pseudomonas aeruginosa*. *elife* **8**, (2019).
6. Mougous, J. D. *et al*. A virulence locus of *Pseudomonas aeruginosa* encodes a protein secretion apparatus. *Science* **312**, 1526–1530 (2006).
7. Hood, R. D. *et al*. A type VI secretion system of *Pseudomonas aeruginosa* targets a toxin to bacteria. *Cell Host Microbe* **7**(1), 25-37 (**2010**).
8. Sana, T. G. *et al*. The second type VI secretion system of *Pseudomonas aeruginosa* strain PAO1 is regulated by quorum sensing and Fur and modulates internalization in epithelial cells. *J. Biol. Chem*. **287**, 27095–27105 (2012).
9. Basler, M., Ho, B. T. & Mekalanos, J. J. Tit-for-tat: Type VI secretion system counterattack during bacterial cell-cell interactions. *Cell* **152**, 884–894 (2013).
10. LeRoux, M. *et al*. Kin cell lysis is a danger signal that activates antibacterial pathways of *Pseudomonas aeruginosa*. *elife* **4**, e05701 (2015).
11. Peschel, A. & Otto, M. Phenol-soluble modulins and *Staphylococcal* infection. *Nat. Rev. Microbiol*. **11**, 667–673 (2013).
12. Surewaard, B. G. J. *et al*. *Staphylococcal* alpha-phenol soluble modulins contribute to neutrophil lysis after phagocytosis. *Cell. Microbiol*. **15**, 1427–1437 (2013).

13. Mashburn, L. M., Jett, A. M., Akins, D. R. & Whiteley, M. *Staphylococcus aureus* serves as an iron source for *Pseudomonas aeruginosa* during *in vivo* coculture. *J. Bacteriol.* **187**, 554–566 (2005).
14. Hoffman, L. R. *et al.* Selection for *Staphylococcus aureus* small-colony variants due to growth in the presence of *Pseudomonas aeruginosa*. *Proc. Natl. Acad. Sci.* **103**, 19890 LP – 19895 (2006).
15. Filkins, L. M. *et al.* Coculture of *Staphylococcus aureus* with *Pseudomonas aeruginosa* drives *S. aureus* towards fermentative metabolism and reduced viability in a cystic fibrosis model. *J. Bacteriol.* **197**, 2252 LP – 2264 (2015).
16. Limoli, D. H. *et al.* *Pseudomonas aeruginosa* alginate overproduction promotes coexistence with *Staphylococcus aureus* in a model of cystic fibrosis respiratory infection. *mBio* **8**, (2017).
17. Dieterich, D. C., Link, A. J., Graumann, J., Tirrell, D. A. & Schuman, E. M. Selective identification of newly synthesized proteins in mammalian cells using bioorthogonal noncanonical amino acid tagging (BONCAT). *Proc. Natl. Acad. Sci.* **103**, 9482 LP – 9487 (2006).
18. Landgraf, P., Antileo, E. R., Schuman, E. M. & Dieterich, D. C. BONCAT: metabolic labeling, click chemistry, and affinity purification of newly synthesized proteomes. *Methods Mol. Biol.* **1266**, 199–215 (2015).
19. Silverman, J. M., Brunet, Y. R., Cascales, E. & Mougous, J. D. Structure and regulation of the type VI secretion system. *Annu. Rev. Microbiol.* **66**, 453–472 (2012).
20. Chen, L., Zou, Y., She, P. & Wu, Y. Composition, function, and regulation of T6SS in *Pseudomonas aeruginosa*. *Microbiol. Res.* **172**, 19–25 (2015).
21. Russell, A. B., Peterson, S. B. & Mougous, J. D. Type VI secretion system effectors: poisons with a purpose. *Nat. Rev. Microbiol.* **12**, 137–148 (2014).
22. Mougous, J. D., Gifford, C. A., Ramsdell, T. L. & Mekalanos, J. J. Threonine phosphorylation post-translationally regulates protein secretion in *Pseudomonas aeruginosa*. *Nat. Cell Biol.* **9**, 797–803 (2007).
23. Silverman, J. M. *et al.* Separate inputs modulate phosphorylation-dependent and -independent type VI secretion activation. *Mol. Microbiol.* **82**, 1277–1290 (2011).
24. Silverman, J. M. *et al.* Haemolysin coregulated protein is an exported receptor and chaperone of type VI secretion substrates. *Mol. Cell* **51**, 584–593 (2013).
25. Braud, A., Hoegy, F., Jezequel, K., Lebeau, T. & Schalk, I. J. New insights into the metal specificity of the *Pseudomonas aeruginosa* pyoverdine-iron uptake pathway. *Environ. Microbiol.* **11**, 1079–1091 (2009).

26. Ehud, B., L., V. M. & Peter, G. E. Iron and *Pseudomonas aeruginosa* biofilm formation. *Proc. Natl. Acad. Sci.* **102**, 11076–11081 (2005).
27. Leoni, L., Orsi, N., de Lorenzo, V. & Visca, P. Functional analysis of PvdS, an iron starvation sigma factor of *Pseudomonas aeruginosa*. *J. Bacteriol.* **182**, 1481–1491 (2000).
28. Wandersman, C. & Delepelaire, P. Bacterial iron sources: from siderophores to hemophores. *Annu. Rev. Microbiol.* **58**, 611–647 (2004).
29. Zarrella, T. M. & Khare, A. Systematic identification of molecular mediators of interspecies sensing in a community of two frequently coinfecting bacterial pathogens. *PLoS Biol.* **20**, e3001679 (2022).
30. Tognon, M., Köhler, T., Luscher, A. & van Delden, C. Transcriptional profiling of *Pseudomonas aeruginosa* and *Staphylococcus aureus* during *in vitro* coculture. *BMC Genomics* **20**, 30 (2019).
31. Leinweber, A., Weigert, M. & Kümmerli, R. The bacterium *Pseudomonas aeruginosa* senses and gradually responds to interspecific competition for iron. *Evolution (N. Y).* **72**, 1515–1528 (2018).
32. Chugani, S. & Greenberg, E. P. The influence of human respiratory epithelia on *Pseudomonas aeruginosa* gene expression. *Microb. Pathog.* **42**, 29–35 (2007).
33. King, J. M., Kulhankova, K., Stach, C. S., Vu, B. G. & Salgado-Pabón, W. Phenotypes and virulence among *Staphylococcus aureus* USA100, USA200, USA300, USA400, and USA600 clonal lineages. *mSphere* **1**, (2016).
34. Grundstad, M. L. *et al.* Quorum sensing, virulence, and antibiotic resistance of USA100 methicillin-resistant *Staphylococcus aureus* isolates. *mSphere* **4**, (2019).
35. Armbruster, C. R. *et al.* Adaptation and genomic erosion in fragmented *Pseudomonas aeruginosa* populations in the sinuses of people with cystic fibrosis. *Cell Rep.* **37**, 109829 (2021).
36. Cornforth, D. M., Diggle, F. L., Melvin, J. A., Bomberger, J. M. & Whiteley, M. Quantitative framework for model evaluation in microbiology research using *Pseudomonas aeruginosa* and cystic fibrosis infection as a test case. *mBio* **11**, (2020).
37. Russell, A. B. *et al.* Type VI secretion delivers bacteriolytic effectors to target cells. *Nature* **475**, 343–347 (2011).
38. Wettstadt, S., Wood, T. E., Fecht, S. & Filloux, A. Delivery of the *Pseudomonas aeruginosa* phospholipase effectors PldA and PldB in a VgrG- and H2-T6SS-dependent manner. *Front. Microbiol.* **10**, 1718 (2019).
39. Lin, J. *et al.* A *Pseudomonas* T6SS effector recruits PQS-containing outer membrane vesicles for iron acquisition. *Nat. Commun.* **8**, 14888 (2017).

40. Allsopp, L. P. *et al.* RsmA and AmrZ orchestrate the assembly of all three type VI secretion systems in *Pseudomonas aeruginosa*. *Proc. Natl. Acad. Sci.* **114**, 7707 LP – 7712 (2017).
41. Moscoso, J. A., Mikkelsen, H., Heeb, S., Williams, P. & Filloux, A. The *Pseudomonas aeruginosa* sensor RetS switches type III and type VI secretion via c-di-GMP signaling. *Environ. Microbiol.* **13**, 3128–3138 (2011).
42. Stolle, A.-S., Meader, B. T., Toska, J. & Mekalanos, J. J. Endogenous membrane stress induces T6SS activity in *Pseudomonas aeruginosa*. *Proc. Natl. Acad. Sci. U. S. A.* **118**, (2021).
43. Cheung, G. Y. C., Joo, H.-S., Chatterjee, S. S. & Otto, M. Phenol-soluble modulins—critical determinants of *Staphylococcal* virulence. *FEMS Microbiol. Rev.* **38**, 698–719 (2014).
44. Ulhuq, F. R. & Mariano, G. Bacterial pore-forming toxins. *Microbiology* **168**, (2022).
45. Kizaki, H. *et al.* Cell-surface phenol soluble modulins regulate *Staphylococcus aureus* colony spreading. *PLoS One* **11**, e0164523 (2016).
46. Tsviklist, V., Guest, R. L. & Raivio, T. L. The Cpx stress response regulates turnover of respiratory chain proteins at the inner membrane of *Escherichia coli*. *Frontiers in Microbiology* **12**, (2022).
47. Guest, R. L., Wang, J., Wong, J. L. & Raivio, T. L. A bacterial stress response regulates respiratory protein complexes to control envelope stress adaptation. *J. Bacteriol.* **199**, (2017).
48. Raivio, T. L., Leblanc, S. K. D. & Price, N. L. The *Escherichia coli* Cpx envelope stress response regulates genes of diverse function that impact antibiotic resistance and membrane integrity. *J. Bacteriol.* **195**, 2755–2767 (2013).
49. Brissette, J. L., Russel, M., Weiner, L. & Model, P. Phage shock protein, a stress protein of *Escherichia coli*. *Proc. Natl. Acad. Sci.* **87**, 862–866 (1990).
50. Nguyen-Hung, L., Victor, P., Juvenal, L., Felipe, C. & F., F. M. Killing of Gram-negative and Gram-positive bacteria by a bifunctional cell wall-targeting T6SS effector. *Proc. Natl. Acad. Sci.* **118**, e2106555118 (2021).
51. Luo, J., Chu, X., Jie, J., Sun, Y., Guan, Q., *et al.* *Acinetobacter baumannii* kills fungi via a type VI DNase effector. *mBio*. **14**:e03420–03422 (2023).
52. Pei, T., Kan, Y., Wang, Z., Tang, M., Li, H., Yan, S., Cui, Y., Zheng, H., Luo, H., Liang, X. & Dong, T. Delivery of an Rhs-family nuclease effector reveals direct penetration of the gram-positive cell envelope by a type VI secretion system in *Acidovorax citrulli*. *mLife* 1:66–78 (2022).
53. Meisner, J., & Goldberg, J. B. The *Escherichia coli* rhaSR-PrhaBAD Inducible Promoter System Allows Tightly Controlled Gene Expression over a Wide Range in *Pseudomonas aeruginosa*. *Appl. Envir. Microbiol.*, ***82***(22), 6715–6727 (2016).

54. Cornforth, D. M. & Foster, K. R. Competition sensing: the social side of bacterial stress responses. *Nat. Rev. Microbiol.* **11**, 285–293 (2013).
55. Keane, R. & Berleman, J. The predatory life cycle of *Myxococcus xanthus*. *Microbiology* **162**, 1–11 (2016).
56. Yarrington, K. D., Shendruk, T. N. & Limoli, D. H. Twitching cells use a chemoreceptor to detect bacterial competitors. *bioRxiv* 2022.11.28.518211 (2022).
57. Oliveira, N. M. *et al.* Suicidal chemotaxis in bacteria. *Nat. Commun*. **13**, 7608 (2022).
58. Ha, D.G. & O'Toole, G. A. c-di-GMP and its effects on biofilm formation and dispersion: a *Pseudomonas aeruginosa* review. *Microbiol. Spectr.* **3**, MB-0003-2014 (2015).
59. O'Neal, L. *et al.* The Wsp system of *Pseudomonas aeruginosa* links surface sensing and cell envelope stress. *Proc. Natl. Acad. Sci.* **119**, e2117633119 (2022).
60. Chen, Y. *et al.* Multiple diguanylate cyclase-coordinated regulation of pyoverdine synthesis in *Pseudomonas aeruginosa*. *Environ. Microbiol. Rep.* **7**, 498–507 (2015).
61. Frangipani, E. *et al.* The Gac/Rsm and cyclic-di-GMP signaling networks coordinately regulate iron uptake in *Pseudomonas aeruginosa*. *Environ. Microbiol.* **16**, 676–688 (2014).
62. Trunk, K. *et al.* The type VI secretion system deploys antifungal effectors against microbial competitors. *Nat. Microbiol.* **3**, 920–931 (2018).
63. Storey, D. *et al. Klebsiella Pneumoniae* Type VI Secretion System-Mediated Microbial Competition Is PhoPQ Controlled and Reactive Oxygen Species Dependent. *Plos Pathog.* ***16***(3), e1007969 (2020).
64. Chou, S. *et al.* Structure of a peptidoglycan amidase effector targeted to Gram-negative bacteria by the type VI secretion system. *Cell Rep.* **1**, 656–664 (2012).
65. Pissaridou, P. *et al.* The *Pseudomonas aeruginosa* T6SS-VgrG1b spike is topped by a PAAR protein eliciting DNA damage to bacterial competitors. *Proc. Natl. Acad. Sci. U. S. A.* **115**, 12519–12524 (2018).
66. Whitney, J. C. *et al.* An interbacterial NAD(P)(+) glycohydrolase toxin requires elongation factor Tu for delivery to target cells. *Cell.* **163**, 607–619 (2015).

Figures

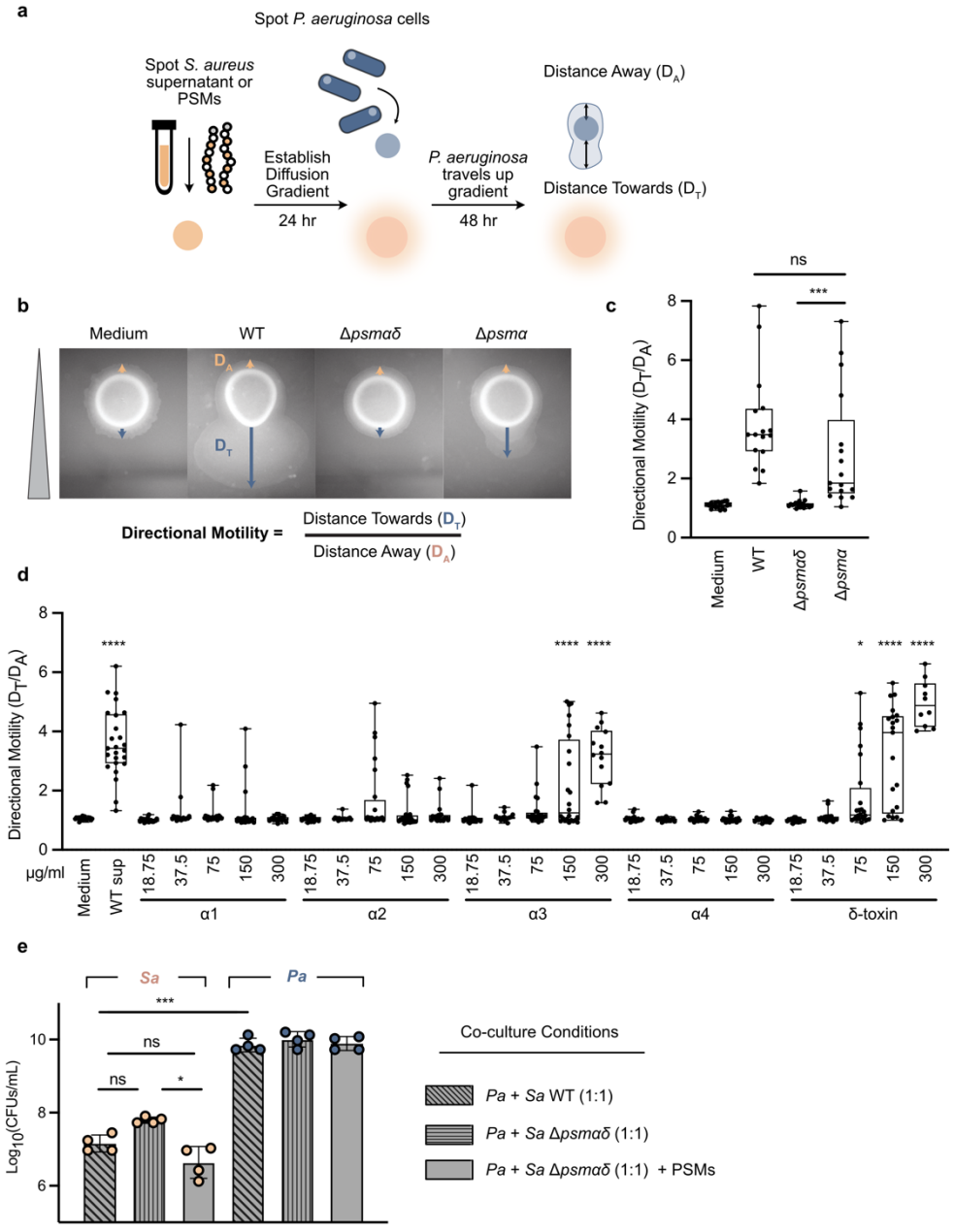

Figure 2.1. PSMα peptides are necessary and sufficient for *P. aeruginosa* attraction towards *S. aureus*. **a.** Schematic of macroscopic TFP-mediated chemotaxis assays to monitor directional *P. aeruginosa* motility up a pre-established gradient of cell-free *S. aureus* supernatant. Directional motility was calculated as ratio of the motility distance towards (D_T) over distance away (D_A) from *S. aureus* supernatant spots. **b.** Representative images of *P. aeruginosa* WT in the presence of a gradient of *S. aureus* growth medium or supernatant derived from the indicated strains (Δ*psmα* and Δ*psmαδ*). Quantification of directional motility

towards a gradient of *S. aureus* supernatant (**c**) or synthetic PSM peptides (**d**) with the median, interquartile range, maximum and minimum indicated for three independent experiments performed in triplicate. Statistical significance was determined by one-way ANOVA followed by Dunnett's multiple comparisons test. ns, not significant; *, $P \leq 0.05$; ***, $P \leq 0.001$; ****, $P \leq 0.0001$. **e.** CFU enumeration for indicated *P. aeruginosa* and *S. aureus* strains in coculture for 24 hours. Data represent four independent biological replicates with the mean and standard deviation indicated. Statistical significance was determined by one-way ANOVA followed by Tukey's multiple comparisons test. ns, not significant; *, $P \leq 0.05$; ***, $P \leq 0.001$.

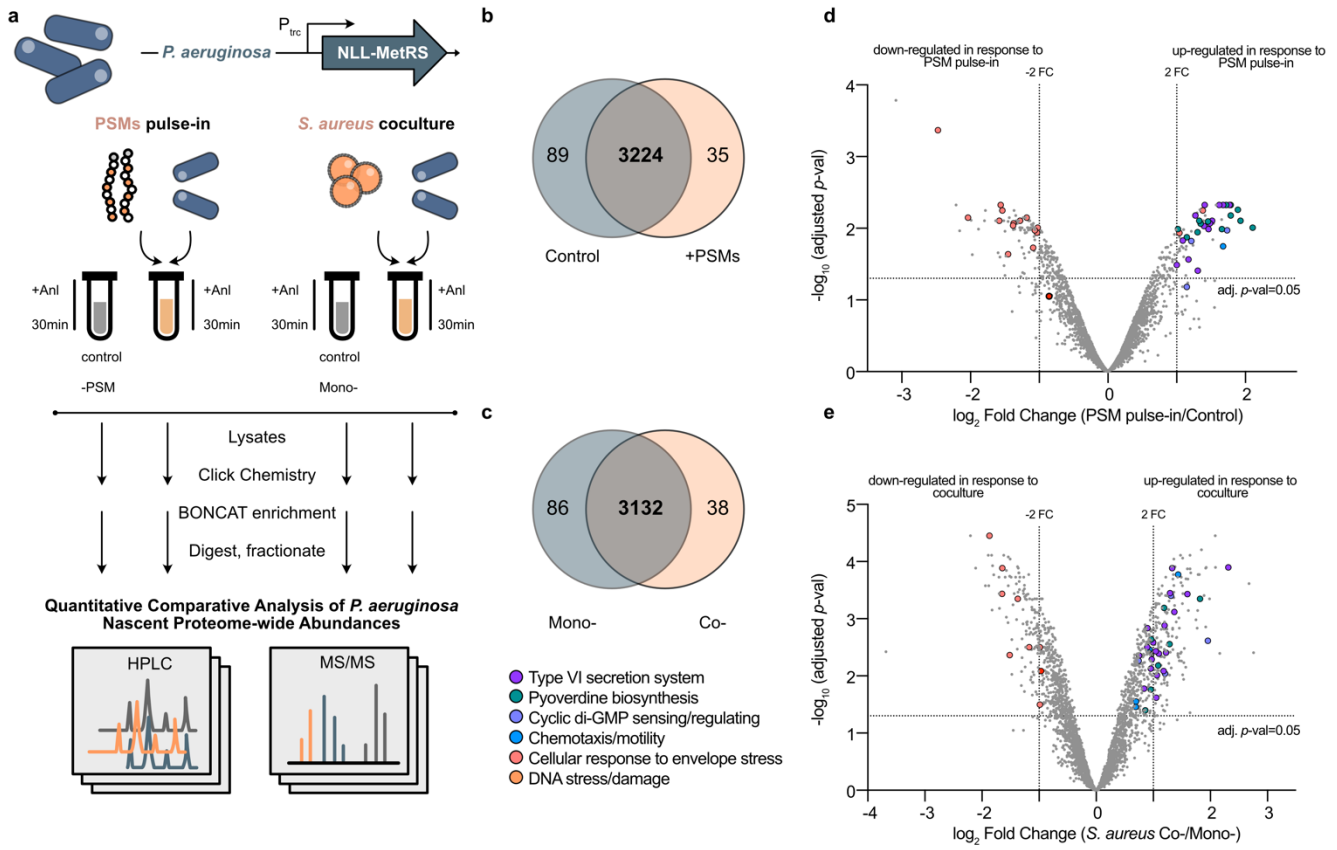

Figure 2.2. Time-resolved proteome mapping reveals *P. aeruginosa* immediate global responses to PSM peptides pulse-in and coculture with *S. aureus* cells.

P. aeruginosa cells were engineered to express a mutant tRNA synthetase that allows for metabolic labeling of newly synthesized proteins by a non-canonical amino acid azidonorleucine (Anl). **a.** Schematic depiction of BONCAT experimental workflow. *P. aeruginosa* protein synthesis immediately following treatment of PSM pulse-in or coculture with *S. aureus* cells is labeled with Anl for 30 min, selectively enriched, and analyzed to compare global nascent proteome abundances with that of untreated control. **b.** Venn diagram showing total proteins quantified for differential expression (overlap) and proteins uniquely identified in +/- PSM pulse-in (**b**) or +/- *S. aureus* coculture (**c**). Volcano plots summarizing the global proteomic comparisons for +/- PSM pulse-in conditions (**d)** and *S. aureus* coculture vs. monoculture conditions (**e**). Protein expression fold-changes between sample groups were calculated via label-free quantification. “Hits” that showed statistically significant changes (Benjamini–Hochberg false-discovery rate adjusted, $P < 0.05$) in abundances in response to PSM pulse-in and *S. aureus* coculture include proteins involved in: type VI secretion system, pyoverdine biosynthesis, c-di-GMP regulation, chemotaxis, motility and cellular responses to envelope stress. n=3 biological replicates for PSM pulse-in proteomics analysis and n=4 for *S. aureus* coculture proteomics analysis.

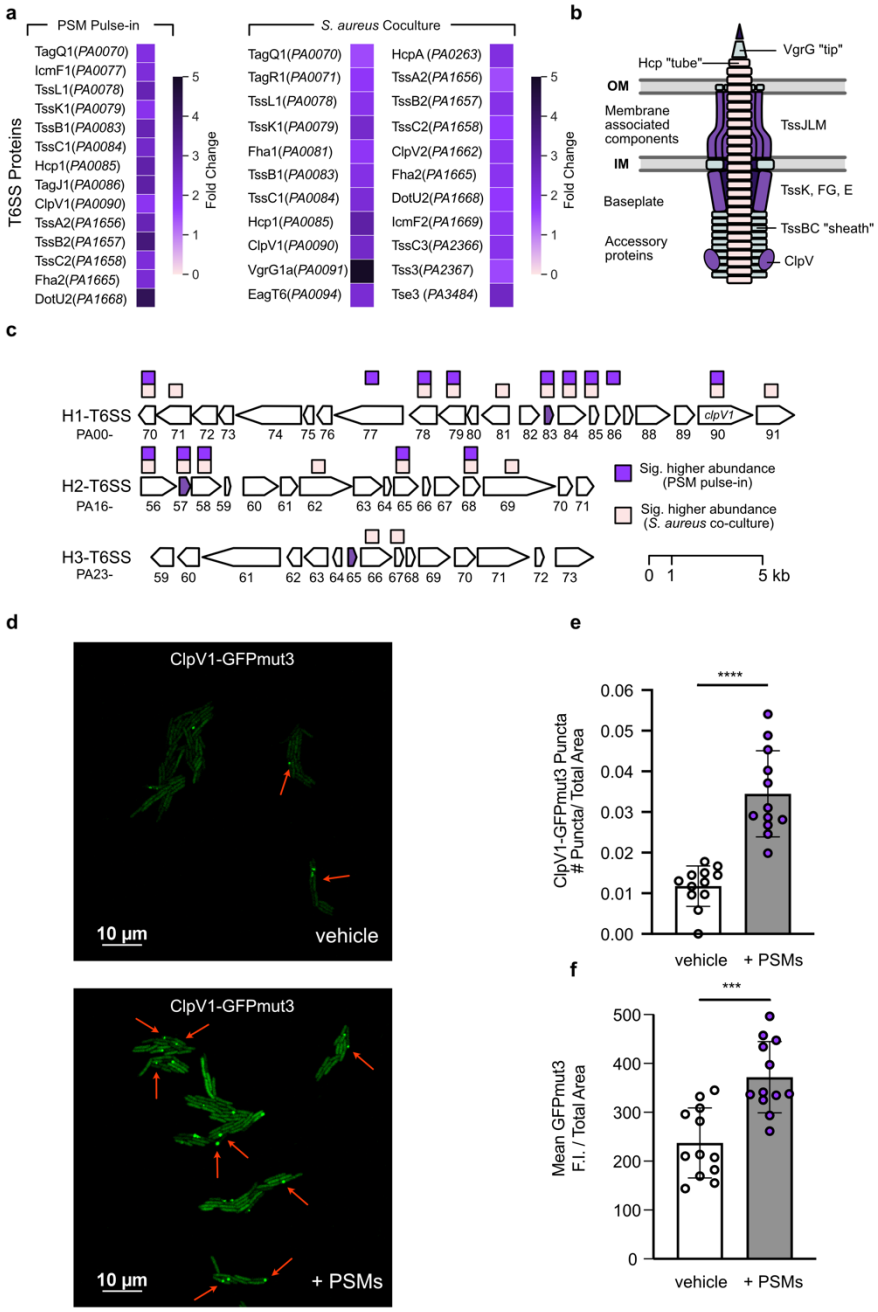

Figure 2.3. PSMs are interspecies signals that trigger *P. aeruginosa* T6SS antagonism.

a. *P. aeruginosa* induction of T6SS-related protein expression in response to PSM pulse-in and coculture with *S. aureus* cells. T6SS proteins with significantly up-regulated fold-changes in response to PSM pulse-in or *S. aureus* coculture are summarized in associated heatmaps. **b.** Illustration of the structural architecture of the T6SS apparatus. **c.** Schematic depiction of the *P. aeruginosa* T6SS genetic loci and the 3 T6SS clusters in *P. aeruginosa* (H1-, H2- and H3-T6SS). Squares represent significantly up-regulated in response to PSM

pulse-in (purple) or *S. aureus* coculture (peach). Specific names are indicated for *P. aeruginosa* T6SS genes that are further examined in subsequent figures (t*ssB1*, t*ssB2* and *tssB3* are colored purple). **d.** Representative microscopy images of *P. aeruginosa* ClpV1-GFPmut3 fluorescence with vehicle control (water, top) and with synthetic PSM treatment (8 μg/mL, bottom). Examples of ClpV1 fluorescent puncta formation are highlighted with arrows (red). For additional microscopy images, see **Supplementary Fig. 6**. Quantification of number of ClpV1-GFPmut3 fluorescent puncta per cellular total area is shown with the mean and standard deviation indicated in (**e**) and mean GFPmut3 fluorescence intensity (F.I.) per cellular total area in (**f**). Data represent a total of three biological replicates with four technical replicates (FOVs) per condition, per biological replicate, analyzed. Statistical significance was determined by unpaired *t*-test: ***, $P = 0.0001$; ****, $P \leq 0.0001$.

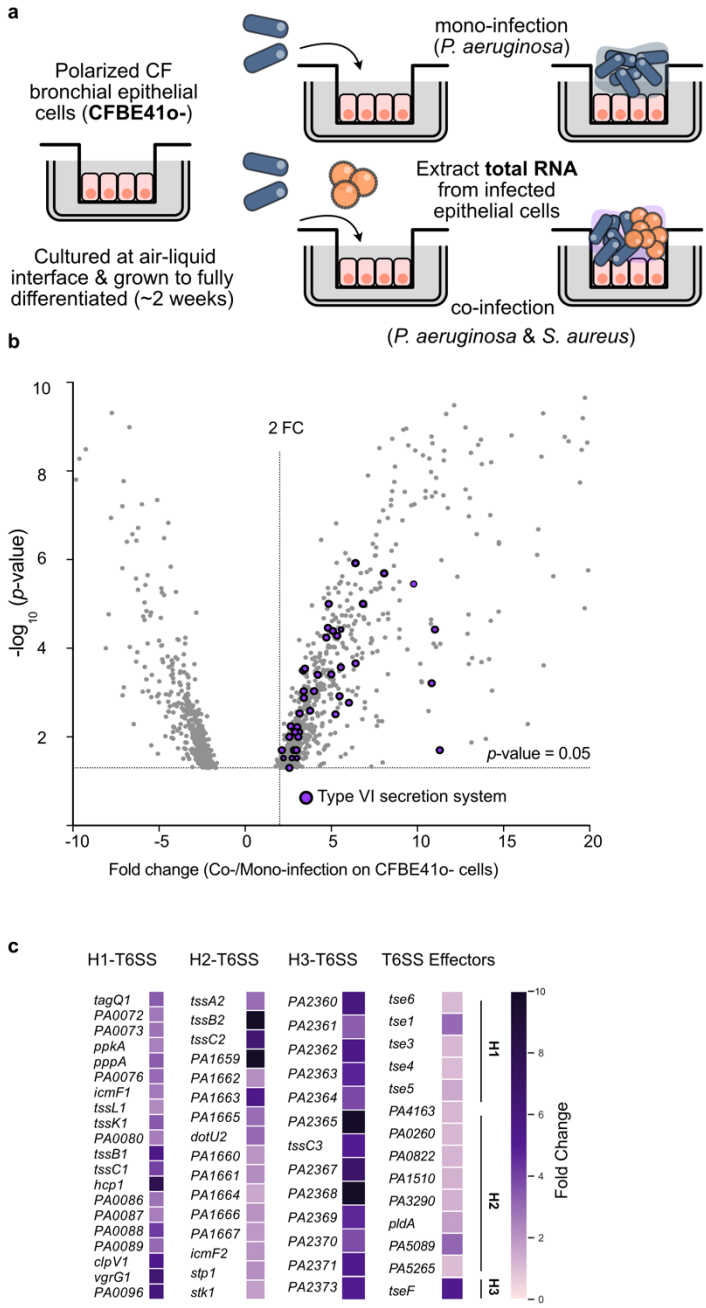

Figure 2.4. *P. aeruginosa* T6SS activity is significantly increased during coculture with *S. aureus* on CF patient-derived bronchial epithelial cells.

a. Schematic of dual-species RNA-seq approach. CF bronchial epithelial cells (CFBE41o-) were seeded at an air-liquid interface and allowed to differentiate fully. Polarized cells were infected apically with *P. aeruginosa* alone or cocultured with *S. aureus* for 6 hours before total RNA was collected and RNA sequencing performed. **b**. Volcano plot summarizing differentially expressed *P. aeruginosa* genes in coculture with *S. aureus* as compared to *P. aeruginosa* mono-infection. T6SS-related genes quantified to be

statistically significantly up-regulated are highlighted as purple dots. **c.** Heatmaps summarizing significant differential fold changes of T6SS genes grouped by the three T6SS clusters. Data represent the mean fold change from two independent, biological replicates.

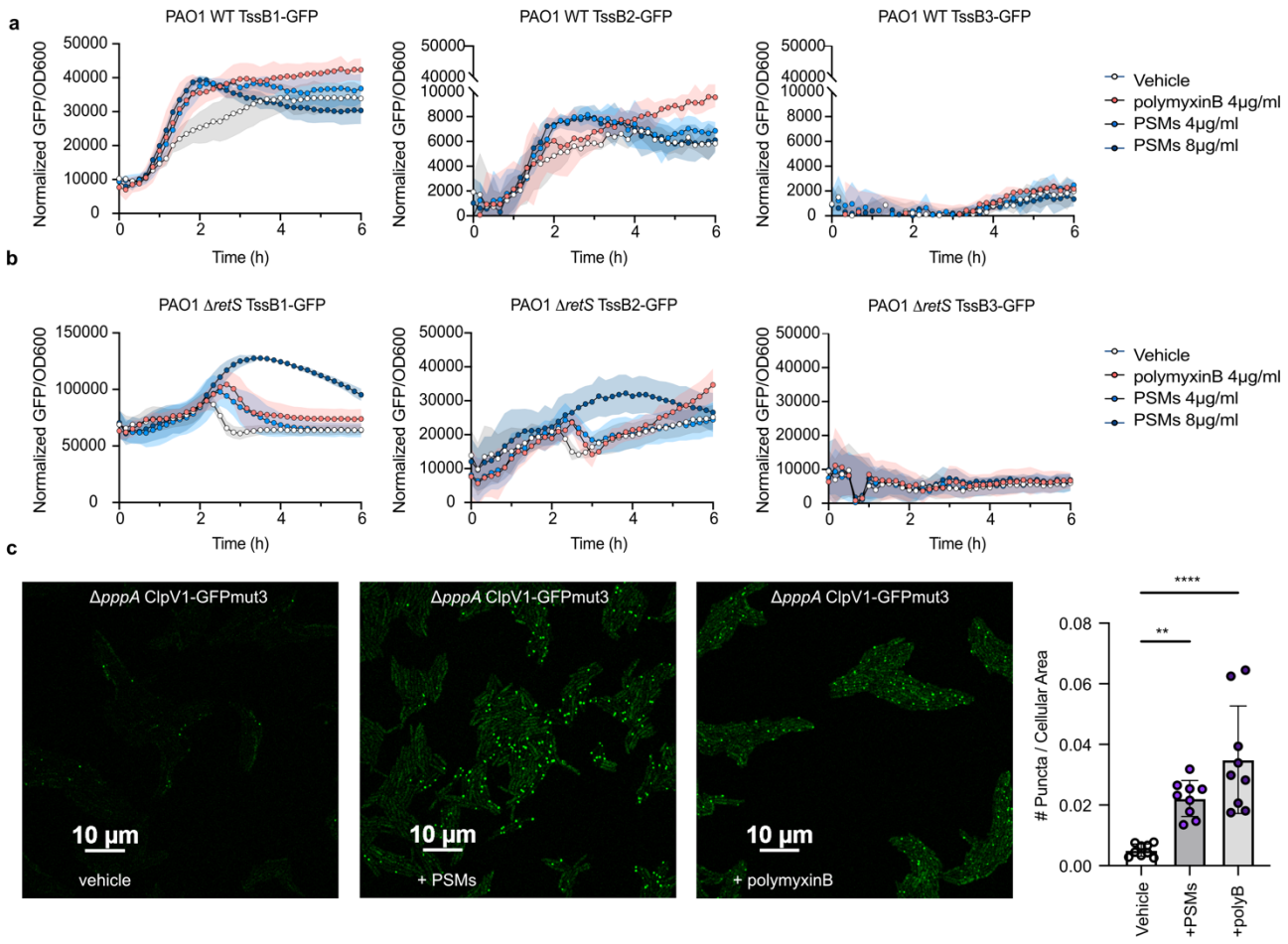

Figure 2.5. ***P. aeruginosa*** **T6SS induction by PSMs does not require the Gac/Rsm regulator RetS or threonine phosphorylation pathway phosphatase PppA.**

TssB1, TssB2, or TssB3 fusions to GFP in *P. aeruginosa* WT (**a**) or Δ*retS* (**b**) treated with vehicle control (water), polymyxin B (4 µg/mL), or PSMs (4 µg/mL and 8 µg/mL). For each condition, fluorescence intensity was normalized by subtracting GFP/OD_{600} ratios of empty vector controls from GFP/OD_{600} ratios of reporter strains. For statistical analysis, see **Supplementary Fig. 7. c.** Representative microscopy images of *P. aeruginosa* Δ*pppA* ClpV1-GFPmut3 fluorescence with vehicle control (water) and synthetic PSMs treatment (8 µg/mL) and polymyxin B (4 µg/mL). For additional microscopy images, see **Supplementary Fig. 6.** Quantification of number of ClpV1-GFPmut3 fluorescent puncta per cellular total area in *P. aeruginosa* Δ*pppA* is shown on the right. Data represent a total of three biological replicates with three technical replicates (FOVs) per condition, per biological replicate, analyzed with the mean and standard deviation indicated. Statistical significance was determined by one-way ANOVA followed by Dunnett's Multiple Comparison Test. **, $P < 0.01$; ****, $P < 0.0001$.

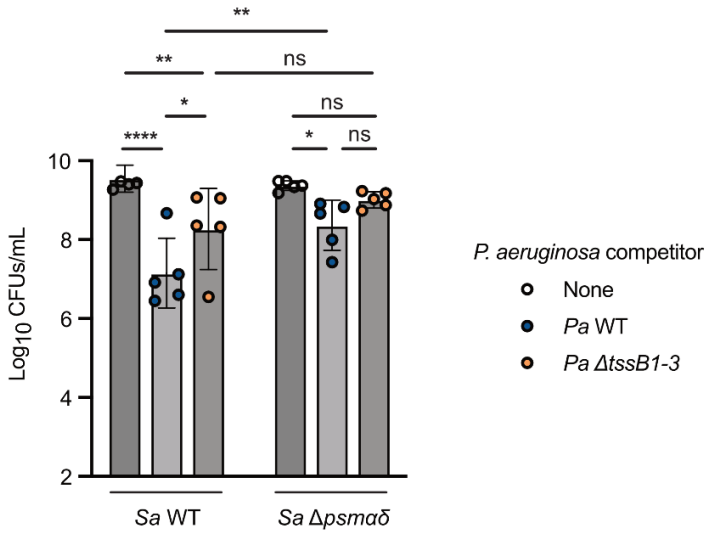

Figure 2.6. *P. aeruginosa* T6SS may contribute to competitive fitness in coculture with *S. aureus*. CFU enumeration of *S. aureus* in coculture for 24 hours in M14 broth with *P. aeruginosa* for indicated mutant strains (same conditions as in **Fig. 1e**.) *P. aeruginosa* and *S. aureus* CFU were enumerated through differential plating. Data represent five independent biological replicates in technical triplicate with the mean and standard deviation indicated. Statistical significance was determined by two-way ANOVA using uncorrected Fisher's least significance difference (LSD) test. ns, not significant; *, $P \leq 0.05$; **; $P \leq 0.01$; ****; $P \leq 0.0001$.

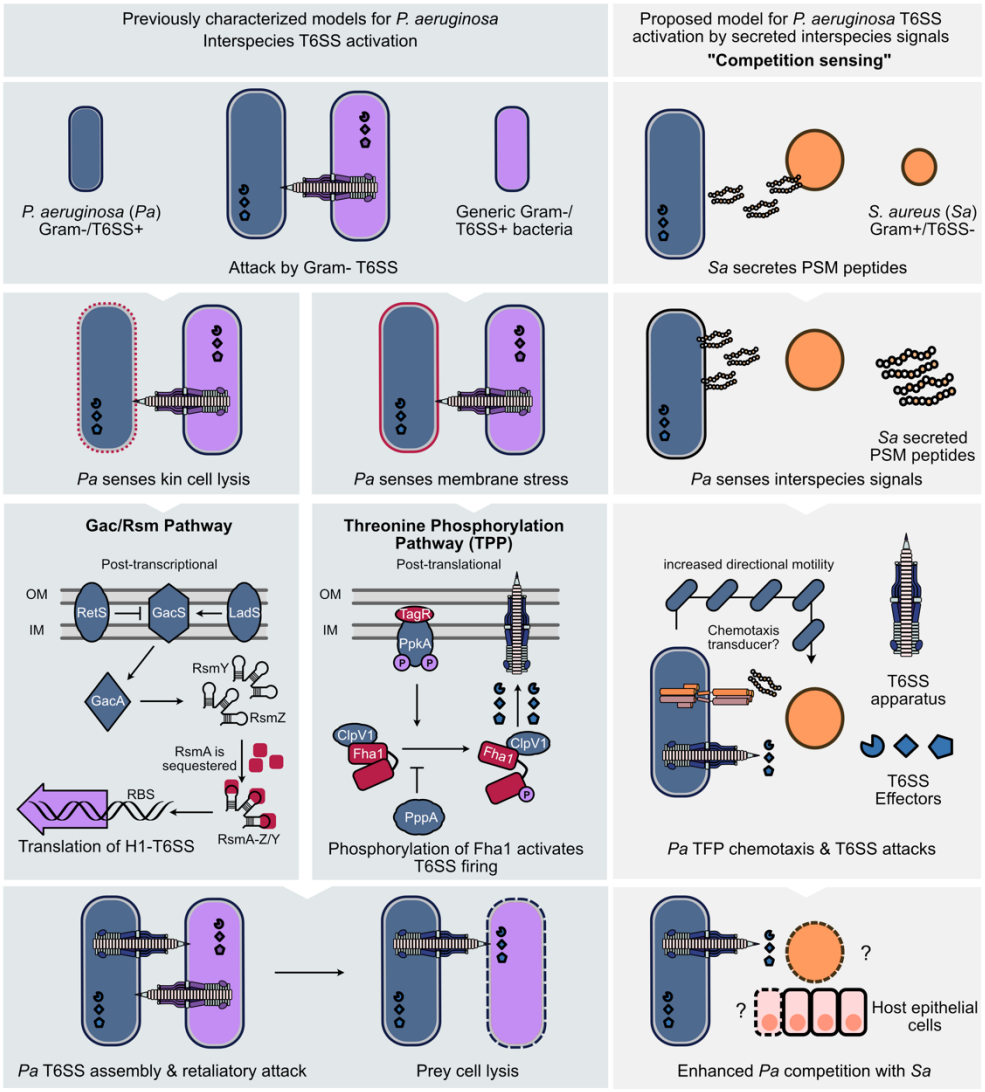

Figure 2.7. Proposed model for *P. aeruginosa* T6SS activation by *S. aureus* secreted interspecies signals.

P. aeruginosa has been characterized to activate its T6SS following interspecies attacks by other T6SS+ Gram-negative species (left). Several mechanisms of *P. aeruginosa* T6SS activation have been described previously. *P. aeruginosa* can sense lysed kin cells following exogenous T6SS attacks and activate T6SS post-transcriptionally via the Gac/Rsm pathway[10]. In "tit-for-tat", *P. aeruginosa* senses membrane stress following T6SS provocation and launches retaliatory T6SS attacks via post-translational activation of the Threonine phosphorylation pathway (TPP), which often results in the lysis and death of the competitor[9]. In addition, a T6SS accessory protein TagF post-translationally represses H1-T6SS independently of the TPP[23] (not depicted in figure). In "competition sensing" (right panel), *P. aeruginosa* detects *Staphylococcal*

secreted PSM peptides (potentially through transient membrane stress), subsequently travels towards *S. aureus* with increased directional motility and simultaneously activates T6SS firing. *P. aeruginosa* T6SS activation is sustained during coinfection with *S. aureus* and results in enhanced competitive fitness against *S. aureus*. Effectors may be delivered by T6SS apparatus or secreted extracellularly and have bactericidal or static action towards *S. aureus*. Increased *P. aeruginosa* T6SS activity, particularly of the H2- and H3-T6SS, during coinfection, may have detrimental consequences on host epithelial cells and contribute to worsened CF patient clinical outcome.

Supplementary Information

Materials and Methods

Bacterial strains, plasmids and culture conditions

P. aeruginosa and *Escherichia coli* were routinely cultured in lysogeny broth (LB; 1% tryptone, 0.5% yeast extract, 1% sodium chloride) and *S. aureus* in tryptic soy broth (TSB, Becton Dickenson), unless otherwise indicated, with aeration at 37ºC. Antibiotics were added, when appropriate: carbenicillin (Cb) at 250 µg/mL for *P. aeruginosa* and gentamycin (Gm) at 30 µg/mL for *P. aeruginosa* and 15 µg/mL for *Escherichia coli*. All strains used in this study can be found in **Table 1**.

Generating *P. aeruginosa* mutants

Markerless deletion mutations were constructed in PAO1 to inactivate each of the *P. aeruginosa* T6SS loci. Deletions were introduced using two-step allelic exchange, as previously described for *P. aeruginosa*[1]. Briefly, 500 bp upstream and downstream regions of the *tssB* gene from each T6SS loci (H1-H3-T6SS) were amplified to construct a contiguous mutant allele by SOE-PCR. The deletion allele was inserted into the donor vector pENTRPEX18Gm by Gateway cloning, transformed into *E. coli* S17.1, and introduced to *P. aeruginosa* through conjugation using a mating filter apparatus. Deletion mutants were first confirmed by PCR and followed by whole genome sequencing and *breseq* analysis to ensure no secondary mutations arose. To generate *retS* and *pppA* deletion strains and TssB-GFP reporter strains, pEXG2 plasmids carrying the respective allelic exchange constructs were electroporated into *E. coli* S17 and were then conjugated into PAO1 as previously described[1]. Mutations were confirmed by PCR and Sanger sequencing. All oligonucleotides used to generate *P. aeruginosa* mutants can be found in **Table 1**. The *tssB1-3* complementation vector was generated by Gibson assembly using SacI/XbaI-linearized pJN105 and synthetic DNA fragment gene blocks containing sequential *tssB1*, *tssB2*, and *tssB3* genes with their respective native ribosome binding sites, and the plasmid was then electroporated into *P. aeruginosa*.

Construction of *S. aureus psm*α1-4 markerless deletion

Genomic DNA of *S. aureus* strains was isolated using the Puregene cell kit, including a lysis step with lysostaphin (100 ng/µL). For a marker less deletion of the *psm*α1-4 operon, regions flanking the operon were amplified from MRSA USA300 LAC (AH1263), using primers KAS214/KAS215 and KAS216/KAS217 (**Table 1**). The amplified products were column purified, digested with *PstI*/*KpnI* and *PstI*/*SalI* and ligated into pJB38, digested with *KpnI* and *SalI*, to generate pKAS40 (**Table 1**). The plasmid was electroporated into *E. coli*

DC10B, sequenced with primer KAS169/KAS170 (**Table 1**) and subsequently electroporated into MRSA USA300 LAC, as previously described[2,3] Deletions were generated as described in[4] and the mutant was confirmed by PCR and sequencing with primers listed in **Table 1**. Sequencing was performed at the Molecular Biology Service Center at the University of Colorado Anschutz Medical Campus.

Macroscopic coculture twitching chemotaxis assay

Motility experiments were performed as previously described[5–7]. Buffered agar plates (10 mM Tris, pH 7.6; 8 mM MgSO4; 1 mM NaPO4, pH 7.6; and 1.5% agar) were poured and allowed to solidify for 1 hour prior to incubation for 16 hours at 37°C and 22% humidity. After solidifying, 4 µL of either growth medium (TSB) or cell-free supernatant derived from an overnight culture of USA300 *S. aureus* at OD_{600} 5.0 and filter sterilized with a 0.22 µm filter were spotted on the surface of the plate and allowed to diffuse for 24 hours at 37°C and 22% humidity to establish a gradient. *P. aeruginosa* PA14 cultures were incubated overnight in TSB with aeration at 37°C, subcultured 1:100 in TSB the following morning, then standardized to OD_{600} 12.0 in 100 µL of 1 mM MOPS buffer supplemented with 8 mM $MgSO_4$ prior to inoculating 1 µL on the surface of the plate at five mm from the center of the gradient. Plates were incubated in a single layer, agar-side down, for 24 hours at 37°C with 22% humidity, followed by an additional 16 hours at room temperature prior to imaging the motility response of *P. aeruginosa*. Images were captured using a Zeiss stereoscope with Zeiss Axiocam 506 camera and directional motility ratios were calculated in Fiji before graphing and performing statistical analysis in GraphPad Prism.

Bacterial competition assay

Liquid competition. *P. aeruginosa* (PA14, PAO1, PAO1 Δ*tssB1*, Δ*tssB2*, Δ*tssB3*, and Δ*tssB1-3*) and *S. aureus* (USA300 WT and Δ*psm*α1-4 δATG-ATT) overnight cultures were diluted to OD_{600} = 0.1 in fresh M14 medium (M9 salts supplemented with 10 mM glucose, 10 mg/mL casamino acids, 1 mM $MgSO_4$, 2 µg/mL thiamine (vitamin B1), 2 µg/mL niacin (vitamin B3), 2 µg/mL calcium pantothenate (vitamin B5), 0.1 µg/mL biotin (vitamin B9)), mixed at 1:1 ratio by species in 5 mL of M14 and grown for 24 hours at 37°C shaking. PSMα1 and PSMα3 (Genscript, 5 µg/mL each) were added to the medium at time of inoculation of coculture. Harvested cocultures were serially diluted and plated on *Pseudomonas* isolation agar (PIA) for selective isolation of *P. aeruginosa* and Mannitol Salt Agar for selective isolation of *S. aureus*.

Solid competition. *P. aeruginosa* (PA14, PAO1, Δ*tssB1*, Δ*tssB2*, Δ*tssB3*, Δ*tssB1-3*, and Δ*tssB1-3* Δ*retS*) and *S. aureus* (USA300 WT and Δ*psm*α1-4 δATG-ATT) overnight cultures were subcultured in fresh M14 (*S. aureus-P. aeruginosa*) and LB (*V. cholerae-P. aeruginosa*) and grown to OD_{600} = 0.8. Cells were then mixed in

a 1:1 or 10:1 ratio of attacker:prey and 10 µL were spotted onto nitrocellulose membranes atop agar plates with either M14 or LB media. Plates were incubated for 3 - 20 hours at 37ºC, cells were collected from filters and resuspended in 500 µL of PBS, vortexed for 30 seconds, serially diluted, and plated on PIA, MSA, or LB + 50 µg/mL polymyxin B (*V. cholerae* selection) for enumeration of CFU.

BONCAT labeling of *P. aeruginosa*

For PSM pulse-in and *S. aureus* coculture proteomics experiments, *P. aeruginosa* PA14 NLL-MetRS cells were grown to OD_{600}~2 in defined M14 medium. For PSM pulse-in, PSMα1 and PSMα3 (Genscript, 0.2 µg/mL each) were added to *P. aeruginosa* cells; for cocultures, *P. aeruginosa* (PA14 NLL-MetRS) and *S. aureus* (USA300_FPR3757) cells were mixed at 1:1 ratio. Labeling was initiated by the addition of 1 mM Anl (Iris-Biotech) and cell lysates were harvested immediately after 30 min. Cell pellets were centrifuged at 4°C and washed with ice-cold LCMS-grade water and frozen at -80°C for downstream lysis and chemical enrichment. All samples were lysed by resuspension in 1% SDS in PBS, boiled at 75°C and sonicated with a microtip probe for 15 seconds at 30% amplification (Qsonica).

Sample preparation for mass spectrometry

For chemical enrichment of BONCAT-labeled proteins from lysates, 2.5 mg of lysates were used for each sample. Lysates were first reduced by dithiothreitol (DTT), alkylated with chloroacetamide and reacted with aza-dibenzocyclooctyne (DBCO) agarose beads (Click Chemistry Tools) via copper-free click chemistry. The reaction was incubated in dark at room temperature overnight, followed by rigorous resin washing with i) 40 mL 0.8% (wt/vol) SDS/PBS; ii) 40 mL 8 M urea in tris hydrochloride (pH = 8.0) and iii) 40 mL 20% (vol/vol) acetonitrile/H_2O to remove nonspecific protein binding. Peptides were detached from DBCO agarose with on-bead digestion with 0.1 µg trypsin and 0.05 µg endoproteinase LysC at 37°C overnight. Supernatant was then collected for further detergent removal (HiPPR column, Thermo Fisher Scientific), and peptides were desalted with C_{18} StageTips.

LC-MS analyses of desalted samples

Peptides were subjected to LC-MS/MS analysis on an EASY-nLC 1200 (Thermo Fisher, San Jose, CA) coupled to a Q Exactive HF Orbitrap mass spectrometer (Thermo Fisher, Bremen, Germany) equipped with a Nanospray Flex ion source. Samples (2 µL out of 10 µL total) were directly loaded onto an Aurora 25 cm x 75 µm ID, 1.6 µm C18 column (Ion Opticks, Victoria, Australia) heated to 50°C. The peptides were separated with a 60 min gradient at a flow rate of 350 nL/min as follows: 2–6% Solvent B (3.5 min), 6-25% B (42 min),

25-40% B (14.5 min), 40-98% B (1 min), and held at 98% B (14 min). Solvent A consisted of 97.8% H2O, 2% ACN, and 0.2% formic acid and solvent B consisted of 19.8% H2O, 80 % ACN, and 0.2% formic acid. The Q Exactive HF was operated in data dependent mode with full scan resolution set to 60,000 at m/z 200 in profile mode, full scan target set to 3×10^6, and a maximum injection time of 15 milliseconds. Full scan mass range was set to 375–1500 m/z. Data dependent MS2 scans were collected for charge state 2-5 precursors in centroid mode using a loop count of 12, AGC target of 1×10^5, an intensity threshold of 1×10^5, and a maximum injection time of 45 milliseconds. Isolation width was set at 1.2 m/z, scan range was 200-2000 m/z, and a fixed first mass of 100 was used. Normalized collision energy was set at 28. Peptide match was set to off, and isotope exclusion was on. Dynamic exclusion was set to exclude after 1 time for 45 seconds.

Proteomics data processing and analysis

Proteomics data analysis was performed in Proteome Discoverer 2.5 (Thermo Scientific) using the SequestHT search algorithm and a nonredundant Uniprot *P. aeruginosa* FASTA file plus common contaminants (CRAPome). Sequest search parameters were as follows: fully tryptic peptides with 6-144 residues and no more than 2 missed cleavages, precursor mass tolerance of 35 ppm and fragment mass tolerance of 0.05 Da, and a maximum of 3 equal modifications. Dynamic modifications were as follows: Cysteine carbamidomethylation, Methionine oxidation, Asparagine and Glutamine deamidation, protein N-terminal acetylation, protein N-terminal Met-loss, and protein N-terminal Met-loss plus acetylation. Percolator FDRs were set at 0.01 (strict) and 0.05 (relaxed). The consensus level peptide and PSM FDR filters were also set at 0.01 (strict) and 0.05 (relaxed). Strict parsimony principle was set to true. Protein quantification was also performed in Proteome Discoverer by summed abundances of the precursor intensities of all high confidence unique and razor peptides.

Raw protein quantification data exported from ProteomeDiscoverer 2.5 was imported into R and analyzed using the romics analysis package (https://jeffsocal.github.io/romics). Once imported the data is filtered for common protein contaminants and normalized between runs using Breiman and Cutler's Random Forests for Classification and Regression (https://cran.r-project.org/web/packages/randomForest) method selected based on best performance in lowering sample replicate variation while maintaining quantitative dynamic range for label free analysis. Protein expression differences between samples were evaluated in the R romics package using the limma algorithm for differential expression (https://bioinf.wehi.edu.au/limma/). Differential expression volcano plots were generated using Prism (GraphPad). For PSM pulse-in proteomics analysis, principal component analysis revealed an outlier for

PSM-treated samples (data not shown). Differential expression analysis performed before (log_2 fold change and raw P-values) and after (log_2 fold change and Benjamini Hochberg FDR adjusted P-values) removal of outlier yielded consistent observations, and the final volcano plots shown represent data analysis post removal of the outlier. Protein set enrichment analysis for significantly up-regulated and down-regulated *P. aeruginosa* proteins was performed using STRING v11 database (Search Tool for Retrieval of Interacting Genes/Proteins) by uploading protein accession codes (PAO1 UniProt) to the server (https://string-db.org/), and results visualized using python libraries matplotlib and networx.

Fluorescence microscopy

To visualize the ClpV1 foci, *P. aeruginosa* PAO1 ClpV1-GFPmut3 was grown in minimal medium (M8 salts supplemented with 0.2% glucose, 1.2% tryptone, and 1 mM $MgSO_4$; M8T) with aeration at 37°C. Cells were sub-cultured in fresh M8T, grown to mid-log phase (OD_{600} of ~0.3 - 0.6), standardized to OD_{600} of 0.3, pelleted, and resuspended in M8T +water (vehicle) or M8T + 8 µg/mL PSMs (4 µg/mL α1 and 4 µg/mL α3). PSMs were sonicated for 5 min prior to use. 0.5 µL of cells were inoculated onto a 4-chamber glass-bottom 35 mm dish (Cellvis, Cat. no. D35C4-30-1.5-N) before placing an agarose pad on top. Agarose pads were made by pipetting 550 µL of M8T with 2% molten agarose (Lonza, Cat. no. 50081) + 0.5 µM propidium iodide into each quadrant of a 4-chamber glass-bottom dish and drying uncovered for ~1 hour 15 min at room temperature, followed by ~1 hour covered with a lid at room temperature, then ~1 hour 15 min at 37°C before transferring the pads onto the inoculated glass-bottom dish. For polymyxin B, since significant cellular toxicity was observed at all concentrations examined, which also increased ClpV1-GFP puncta formation when added at T_0, a final concentration of 4 µg/mL of polymyxin B was added on top of the agarose pad ~2 hours after the cells were inoculated, and then allowed to diffuse for ~40 min. The imaging was performed with an inverted Nikon Ti2 A1R Galvanometer Scanning Confocal Microscope, using a 100x Plan Apo oil objective (1.45 NA). Images were acquired between 2 – 3 hours after the cells were inoculated onto the dish with a 67.69 µm pinhole and 1024 x 1024 pixels. A 488 nm laser was used to excite GFPmut3 and a 561 nm laser to visualize propidium iodide (P.I.). 488 nm imaging acquisition details: laser power 10, offset -5, and HV - gain 65. 561 nm imaging acquisition details: laser power 2, offset -5, and HV - gain 18. Images were saved and analyzed using the Nikon NIS-Elements AR software and the representative images in **Fig. 3** are 644 x 644 pixels. The ClpV1-GFPmut3 puncta were manually quantified and divided by the total cellular area per field of view (FOV). The mean fluorescence intensity (F.I.) was quantified by calculating the average of the mean F.I. of the total cellular area per FOV. A total of three biological replicates with four technical replicates (FOVs) per condition, per biological replicate, were analyzed.

For determination of inner membrane permeability to P.I., *P. aeruginosa* cells harboring P*tac-gfp* on a plasmid were grown in M8T with 250 µg/mL carbenicillin to mid-log phase and prepared as described above except 0.5 µM P.I. was added to the agarose pads and polymyxin B was added directly to the cells at T_0. Phase contrast and epifluorescent images were acquired with an Andor Sona camera. Fluorescent images were taken every 20 min by a Lumencore Sola solid-state white light source at 20% light with a 2-millisecond exposure and Ex. 466/50 nm; Em. 525/50 nm, for GFP, and 18 millisecond exposure and Ex. 562/40 nm; Em. 641/75 nm, for P.I. The rate of P.I. uptake was determined by dividing the total fluorescence intensity of P.I. by the total fluorescence intensity of GFP in each FOV. A total of three biological replicates with two technical replicates (FOVs) per condition, per biological replicate, were analyzed.

TssB fluorescent reporters

P. aeruginosa PAO1 WT and Δ*retS* with and without chromosomal TssB-GFP fusions were grown in M14 at 37°C with aeration to early stationary phase. Cultures were standardized to OD_{600} = 0.5 in a black, clear-bottom 96-well plate with medium alone, polymyxin B, or synthetic PSMα1 and PSMα3. The plate was covered with a gas permeable membrane and OD_{600} and GFP fluorescence (ex: 490 nm; em: 525 nm) measurements were taken at 10 min intervals on a Tecan infinite M200 plate reader. The plate was incubated at 37°C and was shaken for 1 second before each measurement. For each condition, reporter fluorescence was normalized by subtracting GFP/OD_{600} ratios of empty vector controls from GFP/OD_{600} ratios of reporter strains.

Outer membrane permeability

P. aeruginosa cells were grown in M14 at 37°C with aeration to early stationary phase and standardized to OD_{600} = 1.0. Cells were then washed in fresh M14 and incubated with 20 µM 1-N- Phenylnaphthylamine (NPN) and polymyxin B or synthetic PSMα1 and PSMα3 for 15 min. 100 µL from each condition were added to a black, clear-bottom 96 well plate and NPN fluorescence read (excitation: 350 nm, emission: 420 nm) on a Tecan Infinite M200 plate reader. Relative NPN fluorescence was calculated by dividing fluorescence of treated cells by fluorescence of untreated cells.

***P. aeruginosa* growth rate**

P. aeruginosa cells were grown in M14 to mid-log phase, washed in fresh M14, standardized to OD_{600} = 0.05, and added to a clear-bottom 96-well plate with medium alone, polymyxin B, or synthetic PSMα1 and PSMα3.

The plate was covered with a gas permeable membrane and OD_{600} measurements were taken at 10 min intervals on a Tecan infinite M200 plate reader. The plate was incubated at 37°C and was shaken for 1 second before each measurement.

Mammalian cell culture

The human CF bronchial epithelial cell line CFBE41o- (obtained from J. P. Clancy, Cincinnati Children's Hospital) originated from a person with CF that was homozygous for the ΔF508 mutation in CFTR. CFBE41o- cells were routinely cultured in minimal essential media (MEM) supplemented with 10% fetal bovine serum (FBS), 2 mM L-glutamine, 5 U/mL penicillin-5 mg/mL streptomycin, and 0.5 mg/mL plasmocin at 37°C with 5% CO2. CFBE41o- cells were seeded at near confluency on Transwell filters (Costar). After confluency, CFBE41o- cells were differentiated at an air-liquid interface (ALI) for 1-2 weeks before use in experiments. The identity and purity of the CFBE41o- cells were verified by short tandem repeat profiling (University of Arizona Genetics Core). Cells were tested quarterly for mycoplasma using a Southern Biotech mycoplasma detection kit.

Coinfection of CFBE cells

ALI-differentiated CFBE41o- cells were moved to antibiotic-free media by washing with MEM (Gibco) supplemented with 2 mM L-glutamine and replacing basolateral media with MEM supplemented with 10% FBS and 2 mM L-glutamine. *P. aeruginosa* PAO1 and *S. aureus* USA100 were pre-washed in MEM supplemented with 2 mM L-glutamine and inoculated at a 1:1 ratio at an MOI of approximately 250 onto the apical side of polarized CFBE41o- cells. After 2 hours of attachment, non-attached bacteria were removed, and apical media was adjusted to 0.4% L-arginine for a total of 6 hours.

RNA sequencing

RNA was isolated from *P. aeruginosa* PAO1 and *S. aureus* USA100 mono- or 1:1 coculture following 6-hour infection on polarized CFBE41o- cells. RNA was collected by phenol:chloroform extraction using RNA-Bee (AMS Biotechnology) and zirconia/silica beads in a BeadBeater (BioSpec Products) from two independent, biological replicates. RNA was precipitated with isopropanol and linear acrylamide, and RNA pellets were washed by ethanol precipitation. RNA was treated with Turbo DNase (Ambion) and purified by RNA Clean and Concentrator (Zymo Research). DNA removal was confirmed by 260/280 and 260/230 ratios and by PCR for the *P. aeruginosa rplU* gene. RNA integrity was determined by agarose gel electrophoresis and visualization of 5S, 16S, 18S, 23S, and 28S bands.

RNA-seq library preparation and sequencing were performed by the Health Sciences Sequencing Core at Children's Hospital of Pittsburgh (Pittsburgh, PA). RNA concentration and integrity was confirmed by fluorometric quantification (Qubit) and Tapestation analysis (Agilent). RNA was rRNA-depleted using Ribo-Zero Epidemiology, and sequencing libraries were prepared using Truseq stranded Total RNA Kit (Illumina). Single end sequencing was performed on a NextSeq 500. Approximately 75 million 75 bp reads were obtained for each sample. Reads were processed and mapped to the *P. aeruginosa* PAO1 genome and differential expression analysis was performed in CLC Genomics Workbench. Statistically significant changes were considered as $P \leq 0.05$. The *P. aeruginosa* and *S. aureus* co-infection transcriptome sequencing (RNA-seq) data is part of a larger study on the response of *P. aeruginosa* to co-infection. This data has been deposited in the NCBI Sequence Read Archive (BioProject #PRJNA865724).

Supplementary Figures

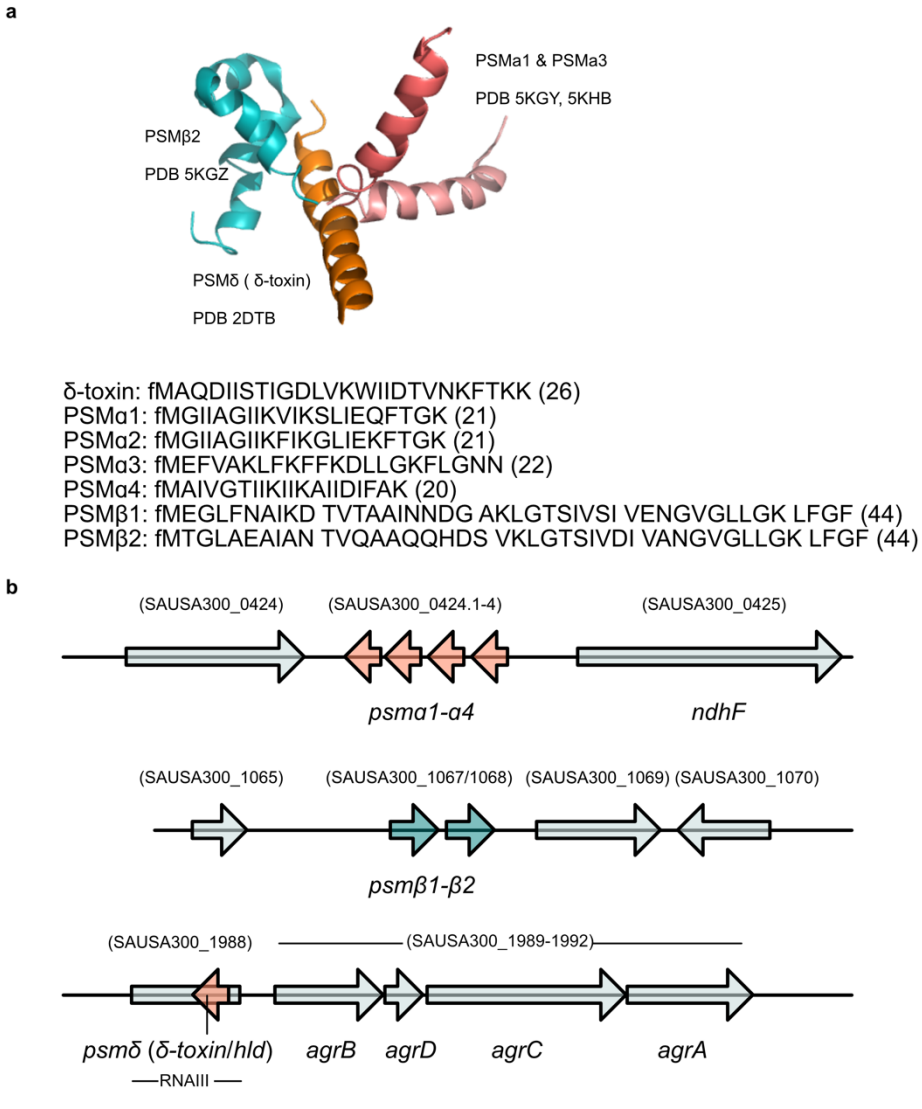

Supplementary Figure 2.1. PSM peptide sequences, structure and genome location.

a. Amino acid sequences for all 7 known peptides in the PSM family of *Staphylococcus aureus* with deposited Protein Data Bank (PDB) structures shown. f=N-formylation. **b.** Regulatory operons and gene locations for PSMs in *S. aureus* (annotations based on strain USA300 LAC). Adapted from[8]. The *psmα1-4* mutant was generated via deletion of the entire *psmα* operon (*psmα1 - α4*). To generate the double *psmαδ* mutant, since *psmδ* is encoded within the coding region of RNAIII, *psmδ* was inactivated through mutation of the start codon from ATG to ATT, as previously described[4].

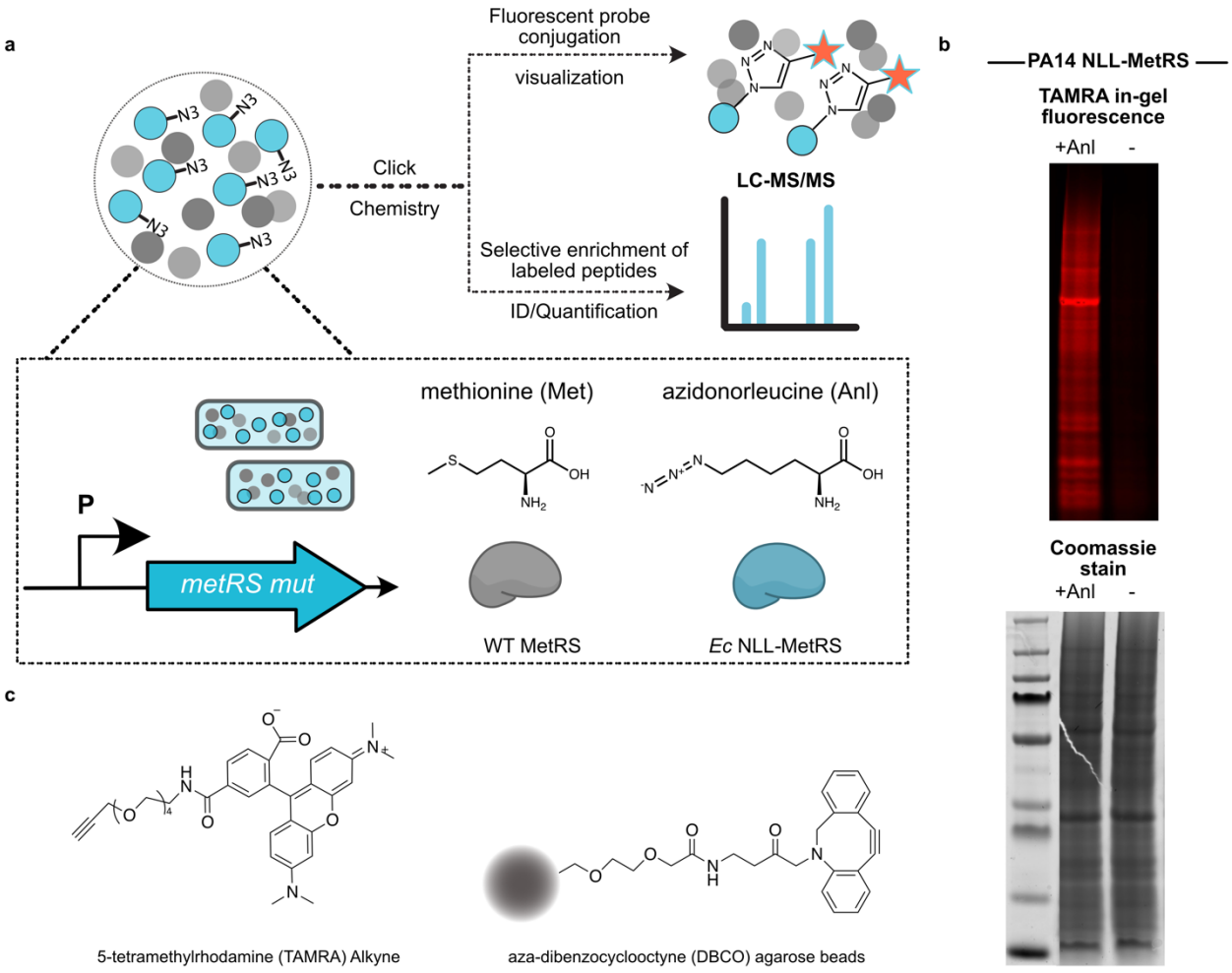

Supplementary Figure 2.2. BONCAT labeling and enrichment of nascent *P. aeruginosa* proteome. a. General scheme of a BONCAT experiment. *P. aeruginosa* cells constitutively expressing NLL-MetRS were treated with 1 mM azidonorleucine (Anl) to initiate protein labeling. Newly synthesized proteins (blue circles) were selectively tagged with azide functional groups on Anl residues and chemically distinct from the pre-existing cellular proteome (grey circles). Labeled proteins were enriched via copper-free azide-alkyne click chemistry onto DBCO-alkyne agarose beads. Enriched proteins were digested and analyzed by LC-MS/MS or visualized via in-gel fluorescence following copper-catalyzed azide-alkyne click chemistry onto TAMRA-alkyne fluorophore (**b**). Anl-labeled proteins in each sample were detected and visualized by TAMRA fluorescence (552 nm ex/ 578 nm em) gel via copper-catalyzed click chemistry as previously described[9]. Briefly, lysates were quantified by the Pierce™ BCA Protein Assay kit (Thermo Fisher Scientific), and samples containing 100 µg protein were incubated with 2.5 µM alkyne-TAMRA (Click Chemistry Tools), 100 µM $CuSO_4$, 500 µM tris (3-hydroxypropyltriazolylmethyl)amine (THPTA ligand; Click Chemistry tools) and 5 mM

aminoguanidine hydrochloride. The click reaction was initiated by addition of 5 mM sodium ascorbate and allowed to proceed for 30 min in the dark at room temperature, followed by methanol/chloroform precipitation. Precipitated proteins in each sample were then washed twice with methanol, resuspended in PBS and SDS loading buffer, and visualized via SDS-PAGE electrophoresis (NuPAGE Novex 4 to 12% Bis-Tris gels; Thermo Fisher Scientific). Imaging was done on a Typhoon gel imager (GE Healthcare) for fluorescence or coomassie (Instant-Blue) signal intensities. **c.** Chemical compounds used for BONCAT in-gel fluorescence and enrichment in this study.

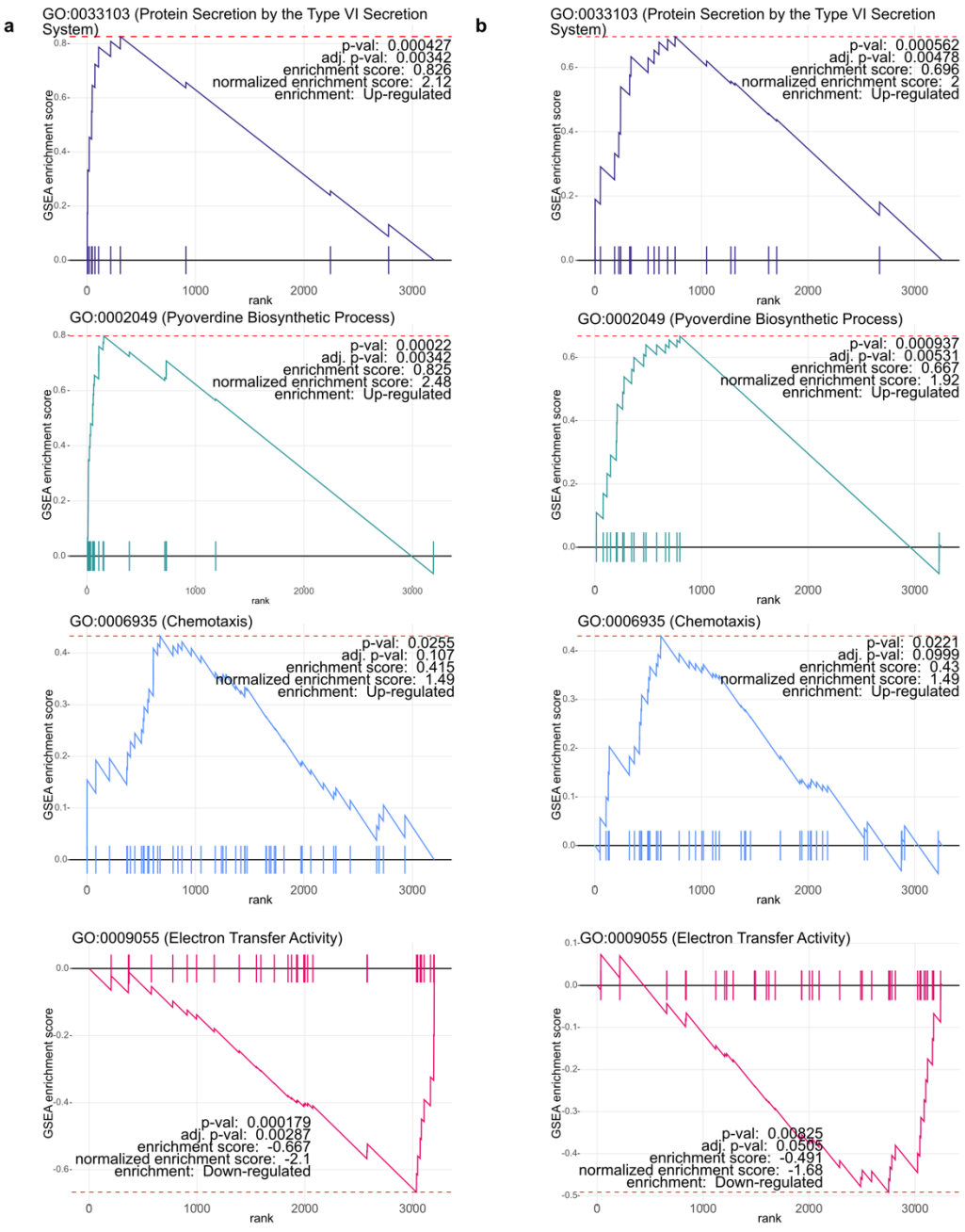

Supplementary Figure 2.3. Enrichment analysis of proteins differentially regulated in response to PSM pulse-in and *S. aureus* coculture.

Gene set enrichment analysis (GSEA)[10] was performed for PSM pulse-in **(a)** and *S. aureus* coculture **(b)** using the fgsea package for R (https://bioconductor.org/packages/release/bioc/html/fgsea). GSEA compares a rank-ordered list of genetic and/or proteomic data to curated annotations. Briefly, proteins with quantified differential expressions were provided as a rank-ordered list by $\log_2$-transformed fold changes with annotations pulled from the *Pseudomonas* Genome Project (pseudocap.gaf) and downloaded UniProtKB

entry annotations for *P. aeruginosa*. Analysis revealed significantly enriched Gene Ontology (GO) terms for cellular components, molecular functions and biological processes with indicated false discovery rate (FDR) adjusted *P* values. The number of permutations was set to 10,000 for *P* value calculation. For complete lists of GSEA output, see **Supplementary Table 2.2** and **2.3**.

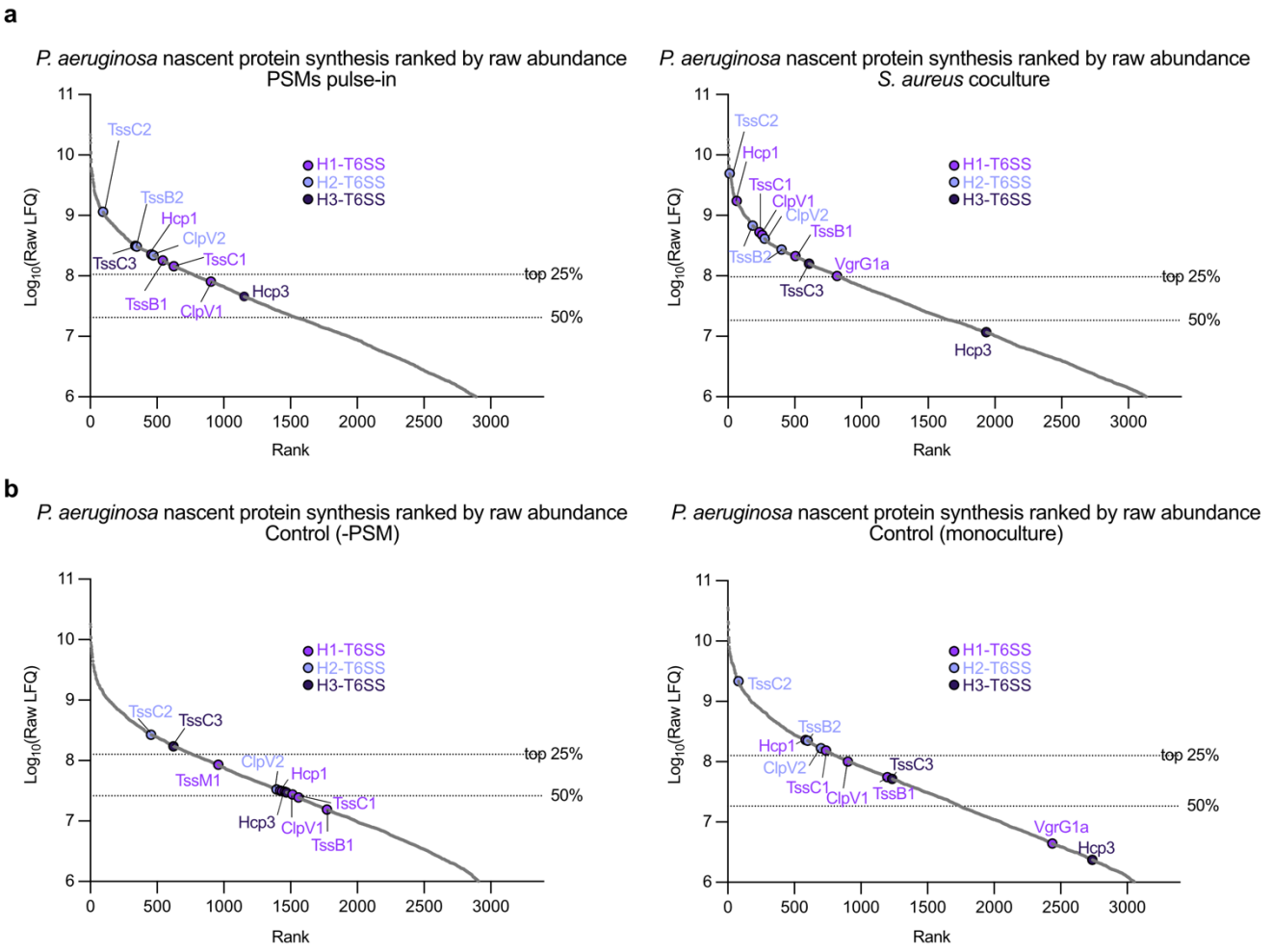

Supplementary Figure 2.4. *P. aeruginosa* proteome ranked by average raw abundances (T6SS core components highlighted).

a. *P. aeruginosa* nascent protein synthesis in response to PSM pulse-in and *S. aureus* coculture during Anl labeling period is ranked by individual protein raw abundance as indicated by Label-Free Quantitation (LFQ) values. **b.** *P. aeruginosa* nascent protein synthesis in control (-PSM and monoculture) samples.

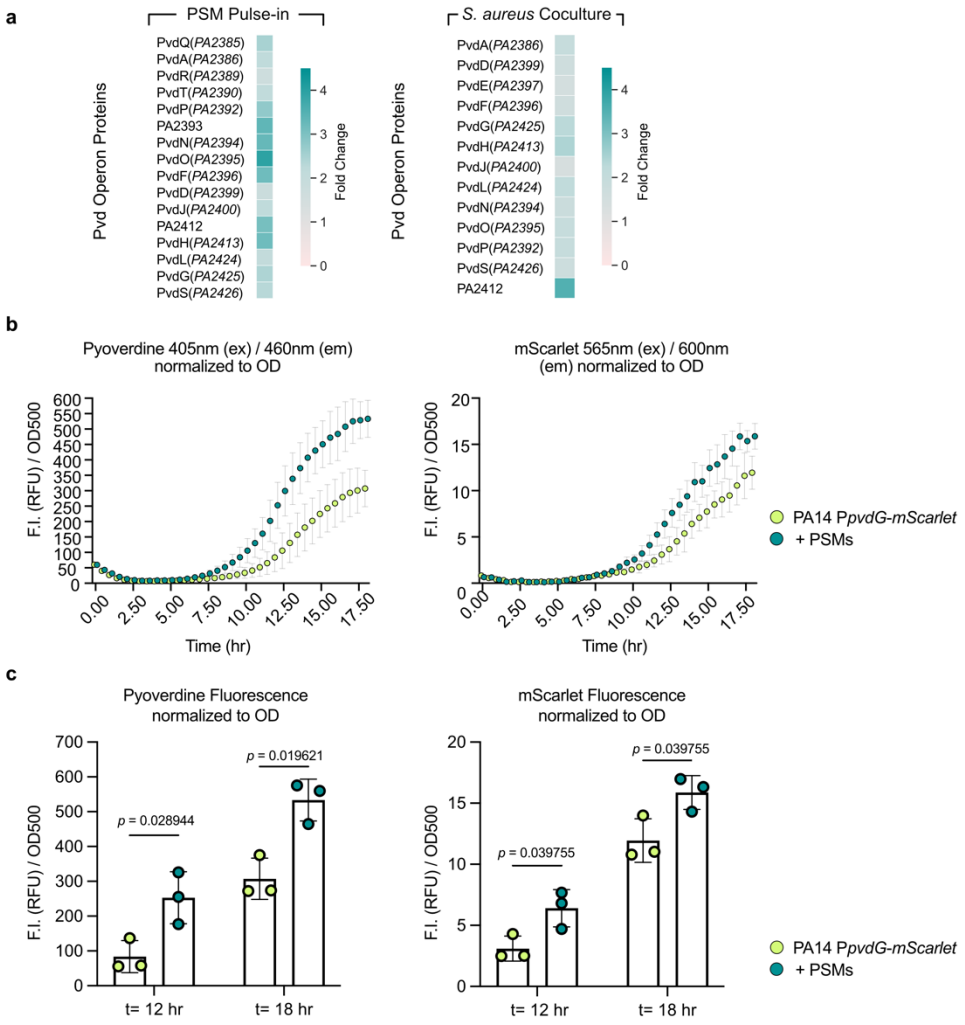

Supplementary Figure 2.5. PSMs induce pyoverdine biosynthesis in *P. aeruginosa*.

a. *P. aeruginosa* induction of pyoverdine biosynthesis protein expression in response to PSM pulse-in and coculture with *S. aureus* cells. Pvd operon proteins with significantly up-regulated fold-changes in response to PSM pulse-in or *S. aureus* coculture are summarized in associated heatmaps. **b.** PSMs induction of P. aeruginosa pyoverdine production and *pvdG* promoter activity. *P. aeruginosa* overnight cultures (PA14 P'*pvdG-mScarlet)* were diluted to OD_{600} of 0.1 in fresh M14 medium. Aliquots (100 µL) of culture were added to 96-well clear, flat-bottom polystyrene plates with or without 10 µg/mL PSMs (5 µg/mL PSMα1 and PSMα3 each), followed by incubation at 37°C with continuous orbital shaking at 1200 rpm using a microplate reader. Fluorescence intensity (mScarlet: 565 nm ex and 600 nm em; pyoverdine: 405 nm ex and 460 nm em) and optical density (UV absorption at 500 nm) measurements were taken every 30 min for 18 hours. Measurements for triplicate wells were averaged, normalized to growth and plotted for raw fluorescence intensity units (**b**) with statistical quantification of end time points (**c**). Data shown represent the mean and

standard deviation of at least three independent replicates. Statistical significance was determined by multiple *t*-test followed by multiple comparisons test for False Discovery Rate adjusted *P*-value.

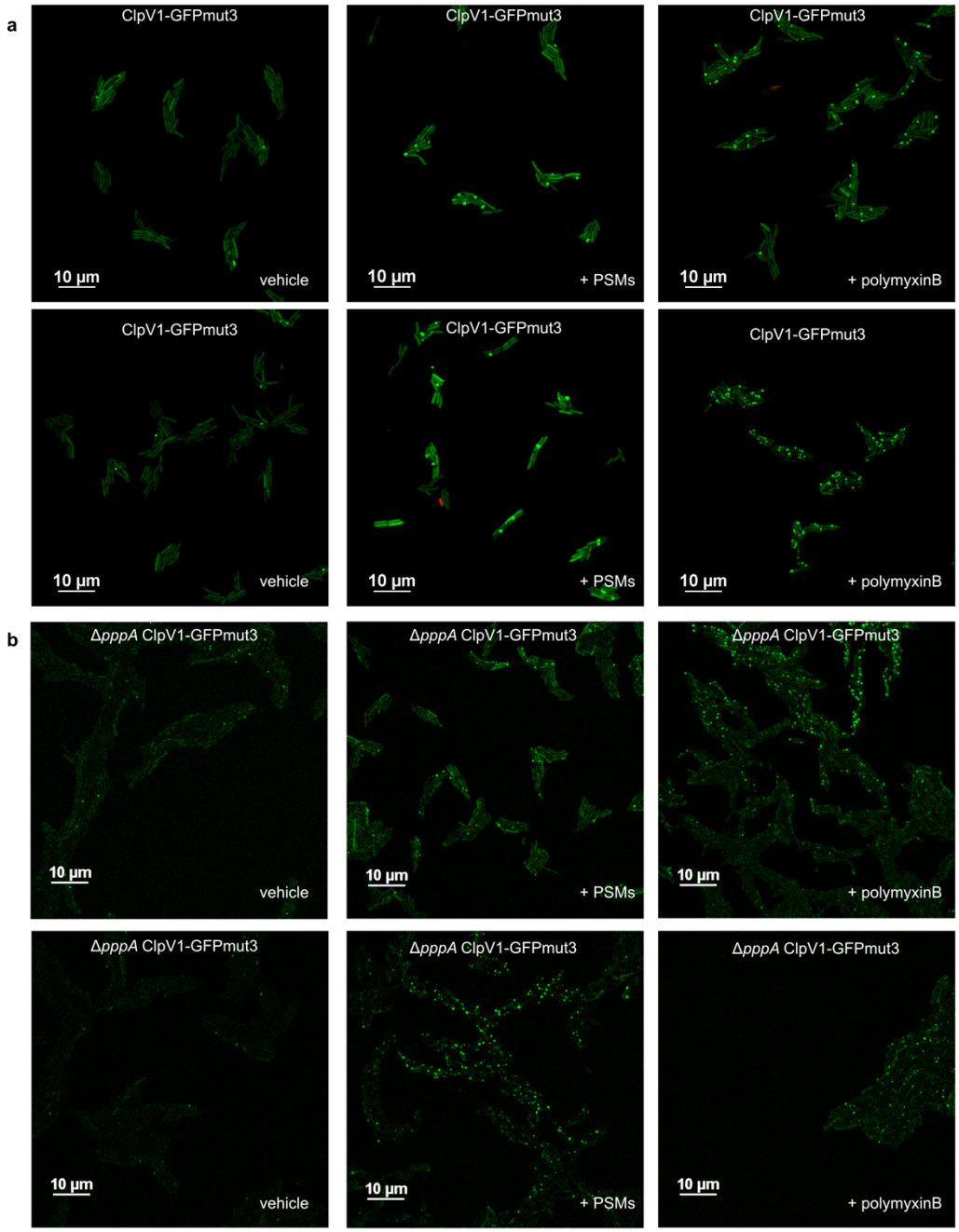

Supplementary Figure 2.6. Additional microscopy images associated with Fig. 3 and **Fig. 4**. *P. aeruginosa* ClpV1-GFP fluorescent puncta formation in WT *P. aeruginosa* (**a**) and *P. aeruginosa* Δ*pppA* mutant (**b**). *P. aeruginosa* ClpV1-GFPmut3 fluorescence was monitored following treatment with vehicle control (water), synthetic PSMs (8 µg/mL) and polymyxin B (4 µg/mL). Two additional microscopy images are shown for each condition: left panel: vehicle; middle panel: synthetic PSMs treatment; right panel: polymyxin B treatment.

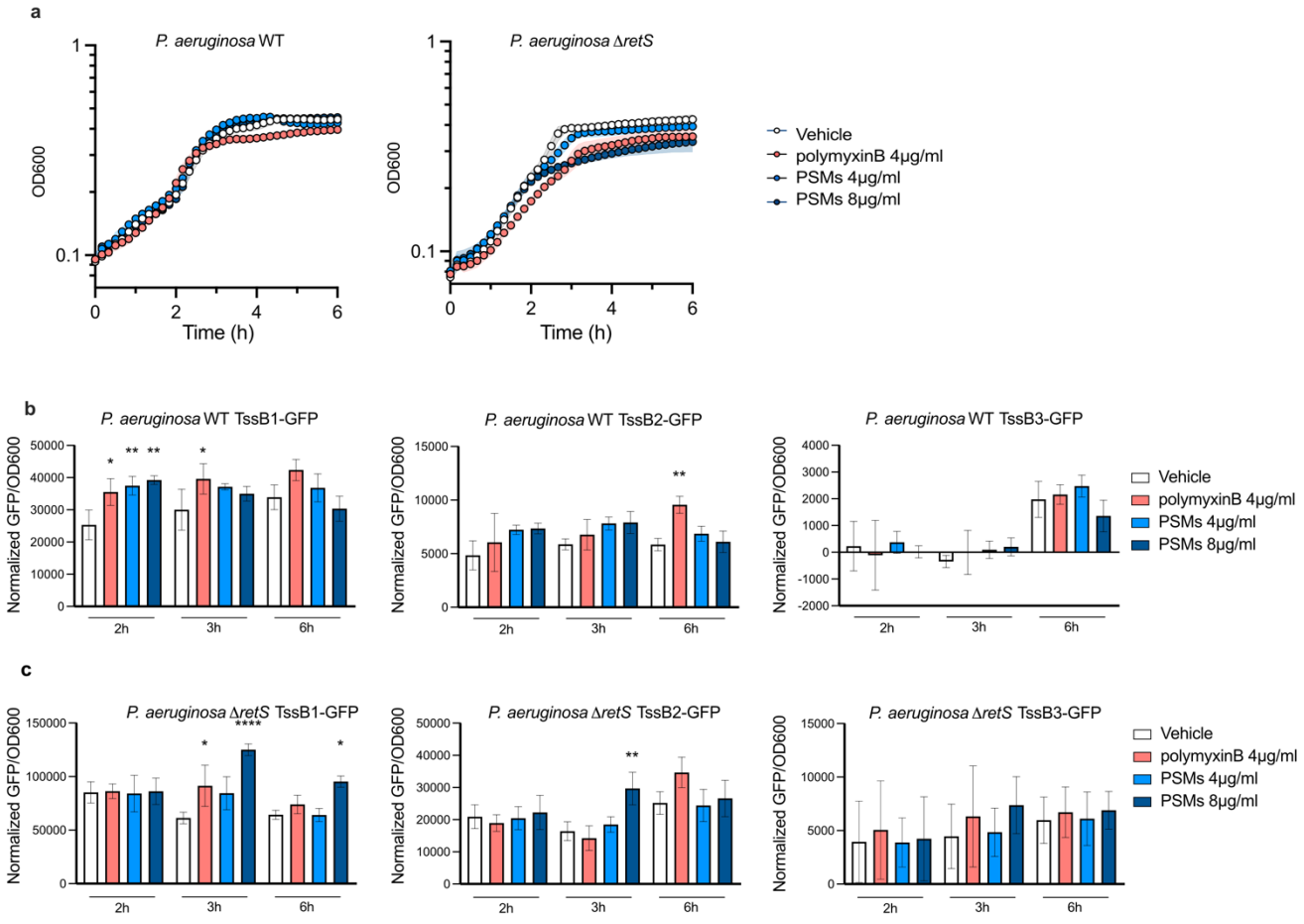

Supplementary Figure 2.7. *P. aeruginosa* Δ*retS* have increased sensitivity to polymyxin B and PSMs. a. *P. aeruginosa* WT (left) and Δ*retS* mutant (right) growth curves following treatment of polymyxin B and PSM peptides. **b.** *P. aeruginosa* WT and Δ*retS* TssB1, TssB2, or TssB3-GFP fusion reporter activities following treatment with PSM peptides and polymyxin B at the indicated concentrations were quantified by subtracting GFP/OD600 ratios of empty vector controls from GFP/OD600 ratios of reporter strains for each condition at the indicated time points. Statistical significance was determined by one-way ANOVA followed by Dunnett's multiple comparisons test. ns, not significant; *, $P \leq 0.05$; **, $P \leq 0.01$; ****, $P \leq 0.0001$. Associated with **Fig. 4**.

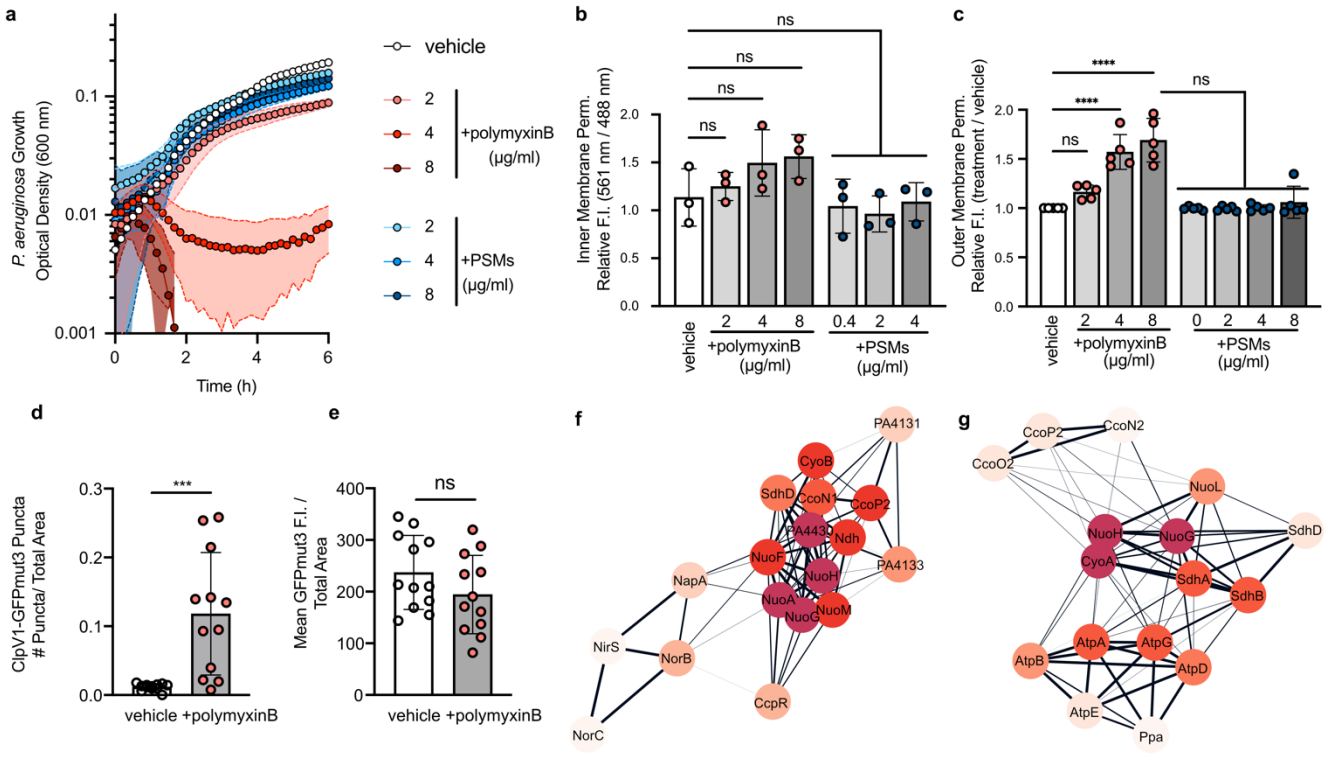

Supplementary Figure 2.8. PSMs may cause transient membrane stress in *P. aeruginosa*.

a. *P. aeruginosa* growth over time monitored by OD_{600} under indicated treatment conditions. **b.** Inner membrane permeability was determined by calculating the ratio of propidium iodide fluorescence to GFP fluorescence of PA14 P*tac-gfp* exposed to the indicated total concentrations of polymyxin B or synthetic PSMα1 and PSMα3. **c.** Outer membrane permeability was determined by measuring NPN fluorescence of *P. aeruginosa* cells incubated with polymyxin B or PSMs. Data shown represent the mean and standard deviation of at least three independent experiments. For **b-c**, statistical significance was determined by one-way ANOVA followed by Dunnett's multiple comparisons test. ***, $P \leq 0.001$; ****, $P \leq 0.0001$. **d.** Quantification of number of ClpV1-GFPmut3 fluorescent puncta per cellular total area following treatment with polymyxin B. **e.** Mean GFPmut3 fluorescence intensity (F.I.) per cellular total area following treatment with polymyxin B. For **d-e**, Data represents a total of three biological replicates with four technical replicates (FOVs) per condition, per biological replicate, analyzed. Statistical significance was determined by unpaired t-test: ns, not significant; ***, $P \leq 0.001$. STRING protein interaction network for ETC proteins with significantly decreased abundances in PSM pulse-in (**f**) and in response to *S. aureus* coculture (**g**). Colors of protein nodes are aesthetic and do not have meaning.

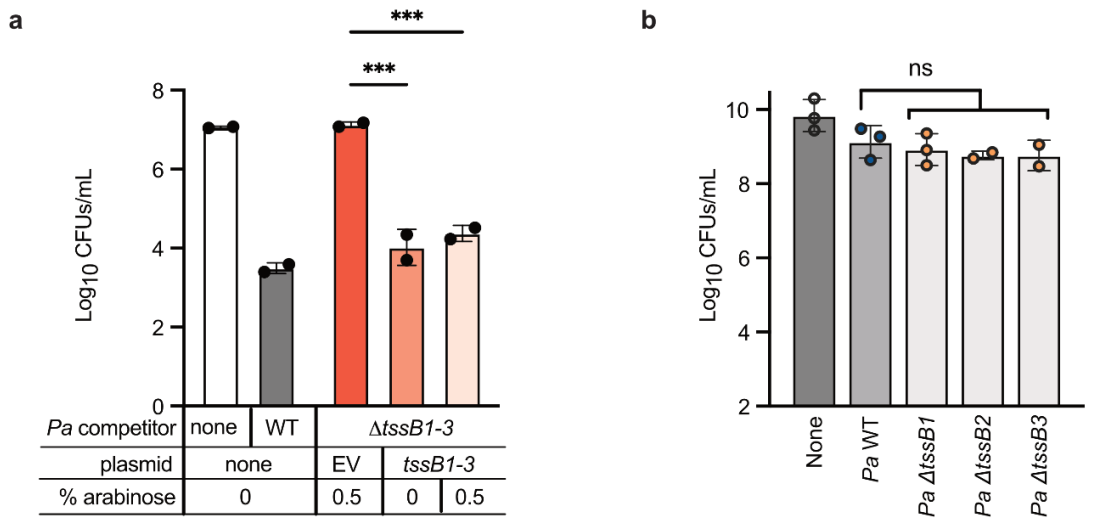

Supplementary Figure 2.9. ***P. aeruginosa*** **T6SS mutants in coculture with *V. cholerae* and *S. aureus in vitro*. a.** Coculture CFU enumeration of *V. cholerae* in coculture with *P. aeruginosa* wild type and Δ*tssB1-3* with or without vector complementation (P*araBAD-tssB*1-3). EV = empty vector. Note: complementation without arabinose is common, due to the known low non-induced expression of the promoter. Data represent two independent biological replicates with the mean and standard deviation indicated. Statistical significance was determined by one-way ANOVA followed by Barlett's test. ***; $P \leq 0.001$. **b.** Coculture CFU enumeration of *S. aureus* with *P. aeruginosa* wild type and indicated single T6SS mutants. Data represent three independent biological replicates with the mean and standard deviation indicated. Statistical significance was determined by one-way ANOVA followed by Dunnett's multiple comparisons test. ns, not significant.

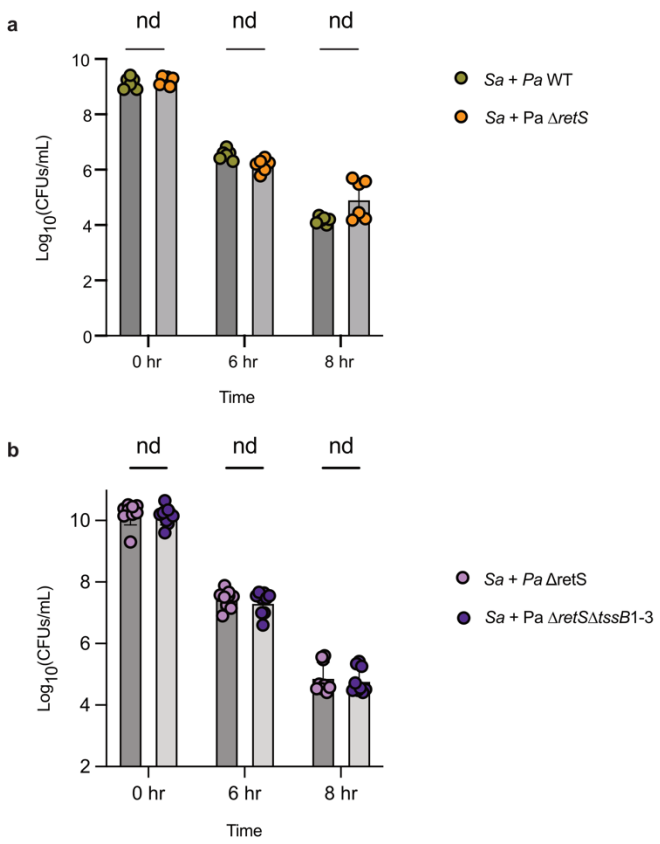

Supplementary Figure 2.10. **Increased *P. aeruginosa* Gac/Rsm does not enhance T6SS-mediated killing of *S. aureus in vitro*. a.** CFU enumeration of *S. aureus* in coculture on an agar surface with *P. aeruginosa* WT and Δ*retS* mutant; Data represent two independent biological replicates each with three technical replicates, with mean and standard deviation indicated. **b.** CFU enumeration of *S. aureus* in coculture on an agar surface with *P. aeruginosa* Δ*retS* and Δ*retS*Δ*tssB1-3* mutant. Data represent three independent biological replicates each with three technical replicates, with mean and standard deviation indicated. Statistical significance was determined by Multiple *t*-test. nd, no discovery.

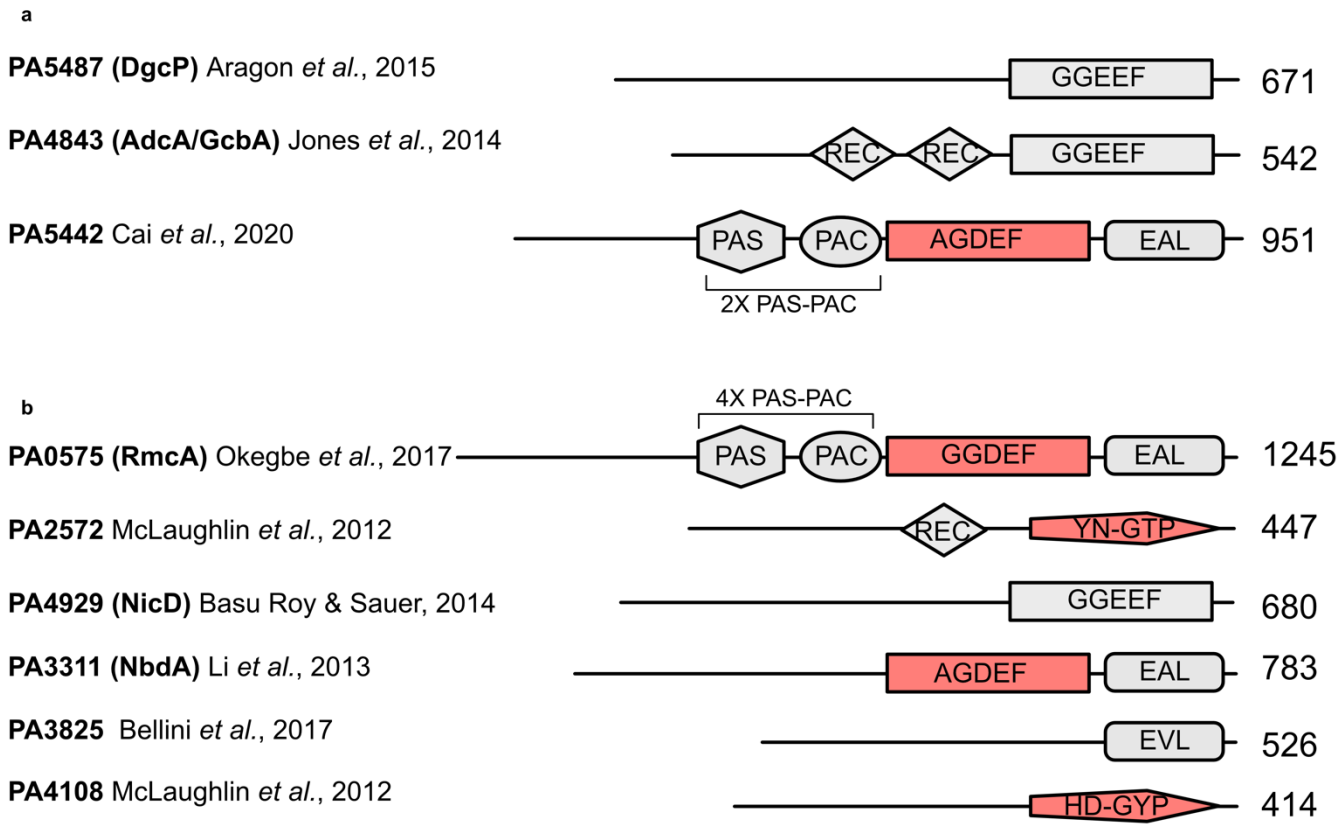

Supplementary Figure 2.11. Diverse c-di-GMP sensing and regulatory enzymes[11] mediate *P. aeruginosa* interspecies response to PSMs and *S. aureus*.

Domain structures of c-di-GMP sensing/regulatory enzymes detected to be significantly up-regulated in response to PSM pulse-in (**a**) and *S. aureus* coculture (**b**). Red color indicates silent domains. GGDEF/AGDEF/GGEEF: diguanylate cyclase (DGC) domain; EAL/EVL: phosphodiesterase (PDE) domain; PAS, PAC, REC are other sensory and/or regulatory domains frequently associated with DGC and PDE domains. For references, see Aragon *et al.*, 2015[12], Jones *et al.*, 2014[13], Cai *et al.*, 2020[14], Okegbe et al., 2017[15], McLaughlin *et al.*, 2012[16], Basu Roy & Sauer, 2014[17], Li *et al.*, 2013[18], Bellini *et al.*, 2017[19].

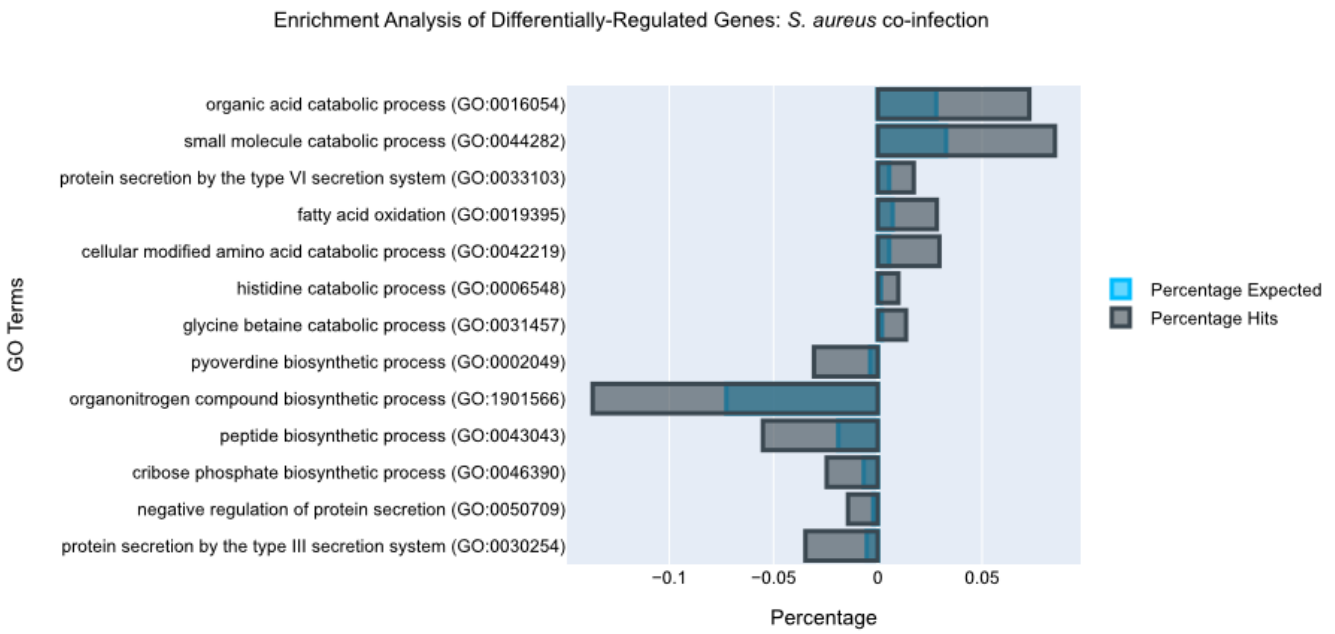

Supplementary Figure 2.12. Functional enrichment analysis of *P. aeruginosa* genes differentially regulated during co-infection with *S. aureus*.

Up-regulated (fold change > 2, *P*<0.05) and down-regulated (fold change < -2, *P* < 0.05) genes from RNA sequencing experiment were analyzed for functional classification using the PANTHER (Protein ANalysis THrough Evolutionary Relationships) Classification System (http://pantherdb.org/about.jsp). Selected functional categories that showed statistically significant enrichment (FDR adjusted P-value <0.05) are plotted. Population total (PT) refer to all protein/genes quantified in each experiment; population hits (PH) refer to all protein/genes annotated as indicated categories in each experiment; list hits (LH) refer to protein/genes annotated as indicated functional categories in subset lists; list total (LT) refer to total number of proteins/genes in each sublist. Percentage expected = PH/PT; Percentage hits = LH/LT.

Table 2.1. Strains and primers used in this study.

Name	Genotype or sequence	Source	Notes
***P. aeruginosa* strains**			
UCBPP-PA14	WT	Laboratory collection	
PA14 NLL-MetRS	attTn7::mini-Tn7T-*Gm*^{R} P_{trc}:*nll-EcmetRS*	Babin *et al.*, 2017[20]	
PA14 *P'pvdG-mScarlet*	*P'pvdG-mScarlet* (pSB175)	Zarrella *et al.*, 2022[21]	
PAO1	WT	Laboratory collection	
PAO1 ClpV1-GFPmut3	Chromosomal fusion of *clpV1*(*PA0090*)-GFP at the native site	Obtained from Joseph Mougous[22]	
PAO1 Δ*pppA* ClpV1-GFPmut3	Chromosomal fusion of *clpV1*(*PA0090*)-GFP at the native site in PAO1 Δ*pppA*	This study	
PAO1 ΔH1-T6SS	Δ*tssB1* (Δ*PA0083*)	This study	
PAO1 ΔH2-T6SS	Δ*tssB2* (Δ*PA1657*)	This study	
PAO1 ΔH3-T6SS	Δ*tssB3* (Δ*PA2365*)	This study	
PAO1 Δ*tssB1-3*	Δ*tssB1*Δ*tssB2*Δ*tssB3*	This study	
PAO1 Δ*tssB1-3* P*araBAD-tssB1-3*	Δ*tssB1*Δ*tssB2*Δ*tssB3* +pJN105::P*araBAD-tssB1-3*	This study	
PAO1 Δ*retS*	Δ*retS* (*PA4856*)	This study	
PAO1 Δ*retS*ΔH123	Δ*retS* (*PA4856*)Δ*tssB1*Δ*tssB2*Δ*tssB3*	This study	
PAO1 TssB1-GFP	stop codon of *tssB1* replaced with *sfgfp* in frame	This study	
PAO1 TssB2-GFP	stop codon of *tssB2* replaced with *sfgfp* in frame	This study	
PAO1 TssB3-GFP	stop codon of *tssB3* replaced with *sfgfp* in frame	This study	

PAO1 Δ*retS* TssB1-GFP	stop codon of *tssB1* replaced with *sfgfp* in frame in PAO1 Δ*retS*	This study	
PAO1 Δ*retS* TssB2-GFP	stop codon of *tssB2* replaced with *sfgfp* in frame in PAO1 Δ*retS*	This study	
PAO1 Δ*retS* TssB3-GFP	stop codon of *tssB3* replaced with *sfgfp* in frame in PAO1 Δ*retS*	This study	
***S. aureus* strains**			
USA100	WT	Laboratory collection	
USA300 LAC	WT	Laboratory collection[23]	
USA300 JE2	USA300 LAC WT cured of plasmids	Obtained from NARSA[24]	
USA300 LAC Δ*psmα*	Δ*psmα*1–4	This study	
USA300 LAC Δ*psmαδ*	Δ*psmα*1–4 *δ*ATG-ATT	Limoli *et al.*, 2019[7]	
***E. coli* strains**			
DH5α	supE44 ΔlacU169(80dlacZΔM15) hsdR17 thi-1 relA1 recA1	Laboratory collection	
S17-1	pro, res− hsdR17 (rK− mK+) recA− with an integrated RP4-2-Tc::Mu-Km::Tn7, Tpr	Laboratory collection	
SM10	KmR, thi-1, thr, leu, tonA, lacY, supE, recA::RP4-2-Tc::Mu, pir	Laboratory collection	
DC10B	*dam*$^+$ Δ*dcm* Δ*hsdRMS endA1 recA1*; Dam methylation only	Monk *et al.*, 2012[3]	
Plasmids			
	pEXG2-Tc::Δ*pppA*	obtained from Joseph Mougous[25]	for allelic exchange to delete *pppA* from *Pa*
	pEXG2::Δ*retS*	obtained from Michael Gebhardt[25]	for allelic exchange to delete *retS* from *Pa*

	pEXG2::TssB1-sfGFP	obtained from Tao Dong[26]	for allelic exchange to replace stop codon of *tssB1* with *sfgfp* in frame in *Pa*
	pEXG2::TssB2-sfGFP	obtained from Tao Dong[26]	for allelic exchange to replace stop codon of *tssB2* with *sfgfp* in frame in *Pa*
	pEXG2::TssB3-sfGFP	obtained from Tao Dong[26]	for allelic exchange to replace stop codon of *tssB3* with *sfgfp* in frame in *Pa*
pDONRPEX18Gm-*tssB1*	pDONRPEX18Gm::Δ*tssB1*(*PA0083*)	This study	for allelic exchange to delete *tssB1* from *Pa*
pDONRPEX18Gm-*tssB2*	pDONRPEX18Gm::Δ*tssB2*(*PA1657*)	This study	for allelic exchange to delete *tssB2* from *Pa*
pDONRPEX18Gm-*tssB3*	pDONRPEX18Gm::Δ*tssB3*(*PA2365*)	This study	for allelic exchange to delete *tssB3* from *Pa*
pJB38	pET194ts oriV, Chl^r Amp^r, pBR322 oriV, $P_{xyl/tetO}$-*secY570*, XhoI site removed, Amp^R/ Cm^R	Bose *et al.*, 2013[27]	
pKAS40	pJB38::Δ*psmα*1-4, Amp^R/ Cm^R	This study	for allelic exchange to delete Δ*psmα*1-4 from *Sa*
pJN105::P*araBAD-tssB1-3*	pJN105::P*araBAD-tssB1, tssB2, tssB3*	This study	Complement ation plasmid for tssB1, 2, 3
Primers			

*PA0083*UpF01-*attB*1	GGG GAC AAG TTT GTA CAA AAA AGC AGG CTA CGT CGC CGA ACG GGT CGG CTC	This study	For PAO1 Δ*tssB1*
*PA0083*UpR01	GGA ATC CTC TTA CGC CTG CGG TCC CAT CTT GTT TCT CCC TCG CG	This study	For PAO1 Δ*tssB1*
*PA0083*DownF01	CCG CAG GCG TAA GAG GAT TCC	This study	For PAO1 Δ*tssB1*
*PA0083*DownR01-*attB*2	GGG GAC CAC TTT GTA CAA GAA AGC TGG GTA GCA GCC ATA GGG CTC GCC G	This study	For PAO1 Δ*tssB1*
*PA0083*F01-SEQ	CAT GCC CTG GCC ATC GAG	This study	For PAO1 Δ*tssB1*
*PA0083*R01-SEQ	GCG GCG ACT GGT CGA AGT	This study	For PAO1 Δ*tssB1*
*PA1657*UpF01-*attB*1	GGG GAC AAG TTT GTA CAA AAA AGC AGG CTA CGG CCA CCC GTG GCT GGA TCA G	This study	For PAO1 Δ*tssB1*
*PA1657*UpR01	GGT GGC TCA GGC GTC CTG GGA CGA GCC TTC TTT GGC CAT GGC	This study	For PAO1 Δ*tssB2*
*PA1657*DownF01	TCC CAG GAC GCC TGA GCC ACC	This study	For PAO1 Δ*tssB2*
*PA1657*DownR01-*attB*2	GGG GAC CAC TTT GTA CAA GAA AGC TGG GTA GAC CGG CTG GCC ACC GAA CTG	This study	For PAO1 Δ*tssB2*
*PA1657*F01-SEQ	CAC GAC GGC AGC GCA TTC	This study	For PAO1 Δ*tssB2*
*PA1657*R01-SEQ	CGG GCG AAC TGG GCG AC	This study	For PAO1 Δ*tssB2*
*PA2365*UpF01-*attB*1	GGG GAC AAG TTT GTA CAA AAA AGC AGG CTA CCC AGC TCC AGG CTC CAT ACC G	This study	For PAO1 Δ*tssB3*

*PA2365*UpR01	GGA AGA GGG TCA GGC CGG CTG GTG CTG CGT ACT CTC GGC CAT	This study	For PAO1 Δ*tssB3*
*PA2365*DownF01	CAG CCG GCC TGA CCC TCT TCC	This study	For PAO1 Δ*tssB3*
*PA2365*DownR01-*attB*2	GGG GAC CAC TTT GTA CAA GAA AGC TGG GTA GCA GGC TGA AGG GGT GTC CGC	This study	For PAO1 Δ*tssB3*
*PA2365*F01-SEQ	CCG ACT CGA TGA ACT GCC C	This study	For PAO1 Δ*tssB3*
*PA2365*R01-SEQ	GCG GAT GGC GAC CGA AGG	This study	For PAO1 Δ*tssB3*
PAO1_*retS*_KO_seq_Fwd	CACGGCCACTTGGCTATAATCCGGC	This study	For PAO1 Δ*retS*
PAO1_*retS*_KO_seq_Rev	GTGCAGCGCCGGAGCACGT	This study	For PAO1 Δ*retS*
KAS214	GTTGTTCTGCAGTAAGATTACCTCCTTT GCTTATGA	This study	For USA300 LAC Δ*psma*1-4
KAS215	GTTGTTGGTACCCGCAGTGAACAATGG AAAG	This study	For USA300 LAC Δ*psma*1-4
KAS216	GTTGTTCTGCAGTTTAAGCGAATTGAATA CTTAAAAT	This study	For USA300 LAC Δ*psma*1-4
KAS217	GTTGTTGTCGACGTATGTCTGAAGCGC AACAA	This study	For USA300 LAC Δ*psma*1-4
KAS169	TGCCACCTGACGTCTAAGAA	Schilcher *et al.*, 2020[28]	For USA300 LAC Δ*psma*1-4
KAS170	CCTCACATTTGTGCCACCTA	Schilcher *et al.*, 2020[28]	For USA300 LAC Δ*psma*1-4
KAS218	AGGCAGTATTTCCCGTCCTT	This study	For USA300 LAC Δ*psma*1-4

KAS219	ATGCATCGCATACACCTGAA	This study	For USA300 LAC Δ*psmα*1-4
KAS220	ACGTGGCACTTTCCAAAAAC	This study	For USA300 LAC Δ*psmα*1-4
KAS221	ACATATGTGCATGGGAGCAC	This study	For USA300 LAC Δ*psmα*1-4
KAS222	TGTGGCGTGTTTTATGTTTGA	This study	For USA300 LAC Δ*psmα*1-4

Supplementary References

1. Hmelo, L. R. *et al*. Precision-engineering the *Pseudomonas aeruginosa* genome with two-step allelic exchange. *Nat. Protoc*. **10**, 1820–1841 (2015).
2. Lofblom, J., *et al*., Optimization of electroporation-mediated transformation: *Staphylococcus carnosus* as model organism. *J Appl Microbiol*. **102**(3): p. 736-47 (2007).
3. Monk, I.R., *et al*., Transforming the untransformable: application of direct transformation to manipulate genetically *Staphylococcus aureus* and *Staphylococcus epidermidis*. *mBio*. **3**(2) (2012).
4. Crosby, H.A., *et al*., The *Staphylococcus aureus* Global Regulator MgrA Modulates Clumping and Virulence by Controlling Surface Protein Expression. *PLoS Pathog*. **12**(5): p. e1005604 (2016).
5. Miller, R. M. *et al*. *Pseudomonas aeruginosa* twitching motility-mediated chemotaxis towards phospholipids and fatty acids: specificity and metabolic requirements. *J. Bacteriol*. **190**, 4038–4049 (2008).
6. Kearns, D. B., Robinson, J. & Shimkets, L. J. *Pseudomonas aeruginosa* exhibits directed twitching motility up phosphatidylethanolamine gradients. *J. Bacteriol*. **183**, 763–767 (2001).
7. Limoli, D. H. *et al*. Interspecies interactions induce exploratory motility in *Pseudomonas aeruginosa*. *elife* **8**, (2019).
8. Cheung, G. Y. C., Joo, H.-S., Chatterjee, S. S. & Otto, M. Phenol-soluble modulins--critical determinants of *Staphylococcal* virulence. *FEMS Microbiol. Rev*. **38**, 698–719 (2014).
9. Presolski, S. I., Hong, V. P. & Finn, M. G. Copper-catalyzed azide-alkyne click chemistry for bioconjugation. *Curr. Protoc. Chem. Biol*. **3**, 153–162 (2011).
10. Subramanian, A. *et al*. Gene set enrichment analysis: a knowledge-based approach for interpreting

genome-wide expression profiles. *Proc. Natl. Acad. Sci.* **43**, 15545-15550 (2005).

11. Banerjee, P. *et al.* Molecular and structural facets of c-di-GMP signaling associated with biofilm formation in *Pseudomonas aeruginosa*. *Mol. Aspects Med.* **81**, 101001 (2021).
12. Aragon, I. M. *et al.* Diguanylate cyclase DgcP is involved in plant and human Pseudomonas spp.infections. *Environ. Microbiol.* 17, 4332–4351 (2015).
13. Jones, C. J. *et al.* ChIP-Seq and RNA-Seq reveal an AmrZ-mediated mechanism for cyclic diGMP synthesis and biofilm development by *Pseudomonas aeruginosa*. *PLoS Pathog.* 10, e1003984 (2014).
14. Cai, Y.-M. *et al.* Differential impact on motility and biofilm dispersal of closely related phosphodiesterases in *Pseudomonas aeruginosa*. *Sci. Rep.* 10, 6232 (2020).
15. Okegbe, C. *et al.* Electron-shuttling antibiotics structure bacterial communities by modulating cellular levels of c-di-GMP. *Proc. Natl. Acad. Sci. U. S. A.* 114, E5236–E5245 (2017).
16. McLaughlin, H. P., Caly, D. L., McCarthy, Y., Ryan, R. P. & Dow, J. M. An orphan chemotaxis sensor regulates virulence and antibiotic tolerance in the human pathogen *Pseudomonas aeruginosa*. *PLoS One*. 7, e42205 (2012).
17. Basu Roy, A. & Sauer, K. Diguanylate cyclase NicD-based signalling mechanism of nutrientinduced dispersion by *Pseudomonas aeruginosa*. *Mol. Microbiol.* 94, 771–793 (2014).
18. Li, Y., Heine, S., Entian, M., Sauer, K. & Frankenberg-Dinkel, N. NO-induced biofilm dispersion in *Pseudomonas aeruginosa* is mediated by an MHYT domain-coupled phosphodiesterase. *J. Bacteriol.* 195, 3531–3542 (2013).
19. Bellini, D. *et al.* Dimerisation induced formation of the active site and the identification of three metal sites in EAL-phosphodiesterases. *Sci. Rep.* 7, 42166 (2017).
20. Babin, B. M. *et al.* Selective proteomic analysis of antibiotic-tolerant cellular subpopulations in *Pseudomonas aeruginosa* Biofilms. *mBio* **8**, e01593-17 (2017).
21. Zarrella, T. M. & Khare, A. Systematic identification of molecular mediators of interspecies sensing in a community of two frequently coinfecting bacterial pathogens. *PLoS Biol.* **20**, e3001679 (2022).
22. Mougous J. D. *et al*. A virulence locus of *Pseudomonas aeruginosa* encodes a protein secretion apparatus. *Science*. 312(5779):1526-1530 (2006).
23. Boles, B. R. *et al*. Identification of genes involved in polysaccharide-independent *Staphylococcus aureus* biofilm formation. *PLoS One*. 5(4): p. e10146 (2010).
24. Yajjala, V. K., Widhelm, T. J., Endres, J. L., Fey, P. D. & Bayles, K. W. Generation of a Transposon Mutant Library in *Staphylococcus aureus* and *Staphylococcus epidermidis* Using *bursa aurealis*. *Methods Mol. Biol.* **1373**, 103–110 (2016)

25. Hood R. D. *et al*. A type VI secretion system of *Pseudomonas aeruginosa* targets a toxin to bacteria. *Cell Host Microbe*. 7(1):25-37 (2010).
26. Wilton, M. *et al.* Chelation of Membrane-Bound Cations by Extracellular DNA Activates the Type VI Secretion System in *Pseudomonas aeruginosa*. *Infect. Immun*. **84**, 2355–2361 (2016).
27. Bose, J. L., Fey, P. D. & Bayles, K. W. Genetic tools to enhance the study of gene function and regulation in *Staphylococcus aureus*. *Appl Environ Microbiol.* **79**(7): p. 2218-24 (2013).
28. Schilcher, K. *et al.* Processing, Export, and Identification of Novel Linear Peptides from *Staphylococcus aureus*. *mBio*, **11**(2) (2020)

Chapter 3. Cell-selective Proteomics Enables Targeted Analysis of a Low-abundance Organism in a Polymicrobial System

Abstract

Mass spectrometry-based proteomics is biased toward the detection and quantification of highly abundant proteins, which presents a significant challenge to the analysis of protein synthesis by low-abundance organisms in complex microbial lysates. Here, cell-selective **b**io**o**rthogonal **n**on-**c**anonical **a**mino acid **t**agging (BONCAT) was employed to target protein synthesis analysis of a low-abundance organism, *Staphylococcus aureus*, in a coculture environment dominated by *Pseudomonas aeruginosa*. *Staphylococcus aureus* accounts for <1% of the total population during late-stage coculture with *Pseudomonas aeruginosa*, and >95% of protein abundances using conventional shotgun proteomics belong to *P. aeruginosa* in late-stage coculture. Engineering *S. aureus* cells to express a mutant methionyl-tRNA synthetase allows for metabolic labeling of newly synthesized proteins by a non-canonical amino acid, enabling cell-selective interrogation of global proteomic dynamics. We demonstrate that chemical enrichment facilitated high-resolution proteomic analysis of *S. aureus* with *P. aeruginosa* and further differential expression analysis results revealed that *S. aureus* upregulates the expression of the repressor of toxins (rot), a global regulator of virulence factors, in the presence of *P. aeruginosa*. This work highlights BONCAT as a unique strategy to address the challenge of studying low-abundance organisms in the field of microbiology.

This chapter is a manuscript to be submitted as:
Wang G.Z., Sánchez Peña A., Lomenick B., Chou T.F., Limoli D.H., Tirrell D.A. Cell-selective proteomics enables targeted analysis of a low-abundance organism in a polymicrobial system.

Introduction

Complex samples with large dynamic ranges in protein abundance such as whole cell lysates are challenging specimens for mass spectrometry (MS)-based proteomic analysis. Highly abundant proteins tend to be over-represented and are identified and quantified with higher confidence[1]. For example, a study using yeast whole cells found that data acquisition using tandem mass spectrometry was biased against low-abundance proteins, yielding only one or two identified peptides compared to 10-fold more on average for abundant proteins[2]. The inherent MS bias towards more abundant analytes presents a distinct challenge to meta-proteomic analysis of complex microbial communities, which often include diverse species compositions of varying abundances.

In the past few decades, advances in metagenomics have illuminated the complexity of microbiota associated with the human body and revealed deterministic links between microbiome composition dynamics and host health[3–5]. To deepen our molecular understanding of microbiome functions, comparative proteomics can be applied to dissect individual contributions by members of a microbiome. Research has shown that microbial networks and interactions within the microbiome are influenced by low-abundance species that contribute to community stability and affect overall microbiome performance[6,7]. In addition, low-abundance bacteria can exhibit high immunogenicity[8] and correlate with advanced cancer disease states[9]. However, low-abundance microorganisms are challenging to characterize using MS-based proteomics approaches, since proteins synthesized by low-abundance species are frequently suppressed by proteins synthesized by the predominant organism(s) in a polymicrobial sample[10].

Here, we took advantage of engineered cell selectivity using **B**io**O**rthogonal **N**on**C**anonical **A**mino acid **T**agging (BONCAT)[11] to perform targeted analysis of protein synthesis by a low-abundance organism in a model polymicrobial system. Chronic respiratory infection is the leading cause of morbidity and mortality in people with cystic fibrosis (CF) and is dominated by the opportunistic pathogens *P. aeruginosa* and *S. aureus*[12–14].

First, we show that *in vitro* coculture of *P. aeruginosa* and *S. aureus* revealed bi-species population dynamics where *P. aeruginosa* outcompetes *S. aureus*, and *S. aureus* becomes the low-abundance organism in the late-stage coculture. *S. aureus* cells constitutively expressing a mutant methionyl-tRNA synthetase in coculture enabled cell-selective enrichment of proteins newly synthesized by *S. aureus*. In this strategy, a non-canonical amino acid (ncAA) acts as a chemical probe metabolically incorporated into

nascent proteins synthesized by cells that express the methionyl-tRNA-synthetase. It is worth noting that several other groups have utilized chemoproteomic tools to study functional proteins in complex microbial lysates (see Parasar *et al.*[16], Jariwala *et al*.[17] and Zhao *et al.*[18]). These studies typically employ designed small molecule probes to pull down interacting protein targets based on enzymatic reactivity or molecular proximity. BONCAT differs from these approaches because it relies on global incorporation of the ncAA with no bias toward protein class or reactivity.

We report significantly improved detection and coverage of proteins synthesized by *S. aureus* in coculture. Approximately 50% of protein hits that showed the highest fold changes in expression during late-stage coculture were not detected in unenriched samples. Ontology enrichment analysis further revealed that *S. aureus* up-regulates DNA damage response pathways and down-regulates quorum sensing and virulence pathways. Finally, we followed up on the Repressor of toxins (Rot), a significantly up-regulated hit with elevated expression in all comparative proteomic experiments and found that Rot mediates *S. aureus* biofilm geography in coculture with *P. aeruginosa*. Overall, cell-selective BONCAT enabled high-confidence and high-resolution profiling and analysis of *S. aureus* protein synthesis in coculture.

Proteins are the ultimate functional biological units and protein abundances can be poorly correlated to transcript levels[15]. Our BONCAT approach can be generally adapted to interrogate genetically tractable microorganisms in complex communities to study their functional dynamics in host-microbe and microbial interspecies interactions.

Results and Discussion

Starting at 1:1 coculture ratio (OD600 = 0.1 at t = 0 h each), both *P. aeruginosa* and *S. aureus* experience lag phase and exponential phase growth to reach high cell density (>10^9 CFUs/mL) in coculture, but the number of *S. aureus* CFUs drastically decreases post-stationary phase (**Fig. 3.1a**). The same trend was observed in coculture even when the starting cell density of *P. aeruginosa* was an order of magnitude lower than that of *S. aureus*—*P. aeruguinosa* still outcompeted *S. aureus* after reaching stationary phase (**Fig. 3.1b**). When starting from an equal ratio, *S. aureus* CFUs dropped several orders of magnitude over the course of a few hours, from accounting for ~50% of the coculture population to less than 1% by the end of 10 h following the inoculation of coculture. This outcompeting phenotype can be replicated in a variety of *S. aureus* strains in coculture with *P. aeruginosa* (**Supplementary Fig. 1**).

To selectively label *S. aureus* proteins in coculture, we introduced a synthetic vector harboring the L13N/Y260L/H301L mutant form of the *Escherichia coli* methionyl-tRNA synthetase[19] codon-optimized for expression in *S. aureus* (designated CoNLL-MetRS) under the control of the hprk/lgt gene (construct designated P_{hprK}-CoNLL-MetRS, **Table 3.1**) via phage transduction into the methicillin-sensitive *S. aureus* (MSSA) strain HG003. The *hprK/lgt* promoter is strongly constitutive and active during infection *in vivo* [20,21]. Azidonorleucine (Anl), a noncanonical amino acid exclusively activated by the NLL-MetRS, was added to coculture medium during early- and late-stage to selectively label proteins synthesized by *S. aureus* in coculture (**Fig. 3.1a**). The incorporation of Anl by NLL-MetRS does not interfere with the incorporation of methionine by the wild-type methionyl-tRNA synthetase (MetRS) since NLL-MetRS exhibits ~1,600-fold lower selectivity toward methionine compared to wild-type MetRS (measured by ratios of Met activation rates in k_{cat}/k_m $M^{-1}s^{-1}$)[22]. Following the tagging of newly synthesized *S. aureus* proteins, we utilized copper-free azide-alkyne click chemistry[23] to conjugate Anl-labeled proteins to aza-dibenzocyclooctyne (DBCO) agarose beads, which facilitated the isolation of *S. aureus* proteins and removal of highly abundant unlabeled *P. aeruginosa* proteins (**Fig. 3.1c**).

In LC-MS/MS-based proteomic analysis of complex biological samples, such as microbial coculture lysates, the competitive process of charging during electrospray ionization (ESI)[24] results in the phenomenon that proteins present at higher concentrations tend to be ionized more easily than those present at lower concentrations. This ionization suppression effect, along with the limited duty cycle of MS in traditional data-dependent acquisition analyses, creates a bias towards more abundant peptides being selected for tandem MS analysis for identification as well as a limited ability to accurately quantify the much lower abundance proteins from the less dominant organisms.

We harvested lysates of Early-stage (annotated “CE”) as well as Late-stage (annotated “CL”, **Fig. 3.2a**) Cocultured *P. aeruginosa* and *S. aureus* to compare the identification and quantification of proteins before and after click chemistry-based enrichment of Anl-labeled *S. aureus* proteins. Note that unlike Stable isotope labeling by amino acids in cell culture (SILAC) or tandem mass tags (TMT) approaches, which use isotopic labeling or isobaric tag-based MS quantification, the label-free quantitation (LFQ) method used here to compare protein abundances employs a workflow identical to that of conventional shotgun proteomics.

Collected MS spectra of coculture lysates before and after BONCAT enrichment were searched against and matched to amino acid sequences of *S. aureus* and *P. aeruginosa* proteomes downloaded from the UniProt

Consortium[25]. The *P. aeruginosa* UCBPP-PA14 strain genome encodes 5,886 total proteins. For *S. aureus*, the MSSA HG003 strain was derived from the reference strain NCTC8325 (with repaired global regulators *rsbU* and *tcaR*)[26], which encodes 2,889 proteins in its genome. Such a difference in proteome size further biases the likelihood of detection toward *P. aeruginosa* proteins.

We examined enrichment results by several measures. First, a Venn diagram summarizing shared protein identification revealed that an additional 831 *S. aureus* proteins were identified after enrichment and that 1,561 *P. aeruginosa* proteins uniquely found in unenriched samples were eliminated by enrichment (**Fig. 3.2a**). Overshadowing of *S. aureus* by *P. aeruginosa* was more pronounced in late stage-coculture, where <5% of total detected protein abundances in coculture lysates belong to *S. aureus (***Fig. 3.2b**)**.** Distribution of protein raw abundances by species was further visualized as empirical cumulative distribution function (ECDF), revealing distinctive shifts when *S. aureus* protein abundances ($\log_{10}$ normalized LFQ values) in unenriched samples are compared to those post-enrichment (**Fig. 3.2c, d**). Note that ECDF curves do not encode population size; for example, although a significant portion of *P. aeruginosa* proteins still appear to surpass *S. aureus* in terms of abundance in late-stage coculture after enrichment (**Fig. 3.2d**), the total number of *P. aeruginosa* proteins is much lower. For additional details on the analysis of LFQs per species, see **Supplementary Fig. 3.2**. Finally, we compared differential abundances of common proteins detected both before and after BONCAT enrichment in late-stage coculture (CL) and found that individual *S. aureus* protein abundances are significantly increased. *P. aeruginosa* proteins generally decreased in raw abundances post-enrichment, with a few exceptions (**Fig. 3.2e**). These observations suggest that enrichment selectively augments the detection and quantification of *S. aureus* proteins over *P. aeruginosa* proteins.

We compared the proteome profiles of *S. aureus* in coculture with *P. aeruginosa* vs. *S. aureus* in monoculture during two distinct time periods, designated “early-state” vs. “late-stage” coculture. During early-stage coculture, both *P. aeruginosa* and *S. aureus* exhibit exponential growth, and each species accounts for roughly 50% of the total coculture population; during late-stage coculture, *S. aureus* was gradually eliminated until it accounted for <1% of the total coculture population during the labeling period (**Fig. 3.1**). Principal component analysis (PCA) revealed that biological replicates under each culture condition clustered within their group (**Fig. 3.3a**). Moreover, PCA showed that while early-stage coculture samples are biologically similar to early-stage monoculture samples, these drastically diverged from the

proteome expression profiles for late-stage coculture vs. monoculture comparisons, which were also quite distinct from each other.

Differential expression analysis was performed by comparing *S. aureus* protein abundances in coculture vs. monoculture using Linear Models for Microarray Data (Limma)[27]. Following multiple testing corrections using the Benjamini-Hochberg procedure[28], proteins with greater than 1.5-fold and statistically significant (adjusted p <0.05) changes in abundance were considered differentially regulated hits. Consistent with the PCA clustering, the late-stage coculture vs. monoculture comparison yielded more hits (~10 times higher) compared to the early-stage coculture vs. monoculture comparison (**Fig. 3.3b**). Therefore, we chose to explore the differential expression analysis results of *S. aureus* proteins further during late-stage coculture.

In the late-stage coculture vs. monoculture comparison, we selected the top 50 hits in each direction (significantly up- or down-regulated) to compare their identification and quantification before and after enrichment. Notably, ~50% of up-regulated hits were not detected in pre-enrichment samples (**Fig. 3.3c**), and ~40% of down-regulated "hits" were not detected in pre-enrichment samples (**Supplementary Fig. 3.3**).

We proceeded with gene set enrichment analysis (GSEA)[29] to examine the functional ontology of differentially regulated *S. aureus* proteins in coculture vs. monoculture samples. GSEA allows flexibility in ranking metrics and customized input of gene/protein annotations, which helps provide a comprehensive view of proteome functional clarifications. We pulled annotations from several knowledge databases to perform GSEA; in addition to the conventional Gene Ontology (GO) terms for biological process, molecular function and cellular location[30] (**Supplementary Fig. 3.4**), we also included annotations from the Kyoto Encyclopedia of Genes and Genomes (KEGG), AureoWiki (the repository of the *S. aureus* research & annotation community) and UniProt "keywords." In these analyses, GSEA adapts a running sum algorithm to walk down a list of proteins ranked by their fold changes in expression to determine whether certain biological terms found in annotation databases are over-represented in up- or down-regulated populations; the "leading-edge" gene (protein) set refers to a subset of genes (proteins) that contribute most significantly to the associated enrichment score of the annotation term, defined by the maximum absolute distance of deviation from zero since the start of the running sum (**Fig. 3.4a-b,** right panels).

In both early-stage and late-stage coculture vs. monoculture comparisons, we detected significantly upregulated expression of proteins involved in DNA repair and pyrimidine biosynthesis pathways (KEGG: sao00240), whereas proteins involved in quorum sensing in *S. aureus* (KEGG: sao02024) and virulence are

significantly enriched in down-regulated populations during both early- and late-stage coculture (**Fig. 3.4a-b, Supplementary Fig. 3.4**).

A global change in virulence factor production usually indicates differential regulation by global activators or repressors of virulence pathways[31,32]. Intriguingly, we found significant changes in expression for several major known regulators of virulence in *S. aureus*. In particular, a helix-turn-helix (HTH)-type transcriptional regulator known as the repressor of toxins (Rot) was observed to be one of the most up-regulated protein hits in both early- and late-stage coculture (**Fig. 3.4c**).

Rot mRNA translation is known to be blocked by SarA, a global regulator of virulence[31], and RNAIII, the primary effector molecule of the Agr quorum sensing system in *S. aureus*[32]. Our observation that Rot's elevated expression in coculture was accompanied by significantly decreased expression of SarA and AgrB (**Fig. 4a-b**) suggests that Rot upregulation may be a result of repression of SarA and RNAIII. Furthermore, several proteins encoded by genes known to be repressed by Rot showed correspondingly significant decreases in expression, including SarZ[32], SaeRS[33], HlgB[34], which belong to the leading-edge protein set in driving the strong negative enrichment score of the "virulence" keyword in late-stage coculture over monoculture (CL/ML) (**Fig. 3.4b**). Simultaneously, proteins encoded by genes positively regulated by Rot, such as clumping factors (ClfA and ClfB), transcriptional regulator SarR, and hemolysin Hla[32–34], showed increased abundance levels in coculture vs monoculture (**Supplementary Table 3.2.4**).

We used the cell-selective BONCAT strategy to perform several additional proteomic experiments further to investigate *S. aureus* protein synthesis in varying coculture conditions (for a summary of all BONCAT experimental designs, see **Supplementary Fig.3.5a**). First, we repeated the long-term coculture experiment during early- and late-stage coculture with a methicillin-resistant *S. aureus* (MRSA) strain, which is more prevalent in clinical CF patients than MSSA[13]. The significant upregulation of Rot was replicated with the MRSA strain (**Supplementary Fig. 3.5b**). We also took advantage of the temporal resolution offered by BONCAT to investigate the immediate response of stationary-phase *S. aureus* being mixed with stationary-phase *P. aeruginosa* cells or physiologically relevant concentrations of a known *S. aureus*-antagonizing *P. aeruginosa* exoproduct, 4-hydroxy-2-heptylquinoline N-oxide (HQNO). Previous literature indicates that HQNO concentration in CF sputum reaches the micromolar range and is ~40μM in stationary *P. aeruginosa* cell culture[35,36]. Treatment with 40 μM HQNO also resulted in up-regulation of Rot within a 30-minute time window, where Anl labeling of *S. aureus* was initiated simultaneously as addition of HQNO (**Fig. 3.4c**, **Supplementary Fig. 3.5a**). HQNO is a secondary metabolite produced by *P. aeruginosa* that inhibits *S.*

aureus cellular respiration[37], which is supported by our observation that enzymes involved in oxidative phosphorylation (**Fig. 3.4a**, KEGG: sao00190) were significantly decreased in abundance with HQNO treatment. Interestingly, Rot was found to be significantly up-regulated in all four experiments: early-stage and late-stage coculture, 30-min immediate coculture, and 30-min HQNO pulse-in (**Fig. 3.4c**).

Rot is a global regulator of virulence in *S. aureus* and is known to positively regulate *S. aureus* biofilm formation[34]. Previous literature shows that an *S. aureus rot* mutant strain exhibits a severe defect in biofilm formation compared to a wild-type strain after 3-day growth in a flow cell[34]. Given that Rot was observed to be up-regulated by *S. aureus* in various coculture conditions, we hypothesized that it has a role in mediating *P. aeruginosa-S. aureus* mixed species biofilm formation.

We used time-lapse fluorescence microscopy to monitor coculture biomass formation in an artificial sputum medium (ASM). ASM mimics the chemical environment of the CF lung, which contains excess extracellular DNA and mucin that contribute to the high viscosity of CF sputum[38]. We employed a *P. aeruginosa* strain constitutively expressing mCherry and *S. aureus* WT and *rot* mutant strains constitutively expressing sGFP to examine the biogeography of mixed species biofilms after 18 h incubation at 37 C.

Interestingly, monoculture *S. aureus* WT or *rot* mutant strains did not yield significant differences in terms of cellular aggregation, biomass organization and thickness (**Supplementary Fig. 3.6**). However, when compared to the biomass surface formed by *S. aureus* WT strain, the *rot* mutant formed a visibly thinner layer in coculture with WT *P. aeruginosa* (**Fig. 3.5a,b**). While the fluorescent volumes of *P. aeruginosa* biomass in coculture did not differ greatly, the total fluorescent volume of *S. aureus* deficient in Rot production diminished significantly compared to that of the WT strain in coculture (**Fig. 3.5c**).

P. aeruginosa is a motile bacterium and can move in all directions using flagella and type-iv pilus motors[39]. In contrast, *S. aureus* cells are nonmotile and can only pile on top of each other. As a result, the mixed species biofilm is overwhelmingly dominated by *P. aeruginosa* on the top, with divided occupation on the bottom (**Fig. 3.5a,b**). As coculture was inoculated on top of a coverslip, the bottom layer of cells competed for adhesion to the surface. Interestingly, previous literature suggests that *P. aeruginosa* can disperse *S. aureus* biofilm and cause *S. aureus* cells to detach from surfaces[37]. Our observation that the *S. aureus rot* mutant is less competitive than WT in coculture with *P. aeruginosa* may point to increased dispersion of the *rot* mutant by *P. aeruginosa*.

Overall, our global comparative proteomics findings synergized with a few previous reports. For example, a

transcriptomic analysis found that *S. aureus* up-regulated genes involved in *de novo* nucleotide synthesis and salvation pathways[40] in coculture with *P. aeruginosa*. In our BONCAT experiments, proteins involved in DNA damage response and pyrimidine biosynthesis in *S. aureus* were found to be up-regulated in coculture (**Fig. 3.4a, b**), with many overlapping hits where the same genes/proteins were detected to be significantly elevated in expression. Reduced virulence in coculture has also been previously reported for both *P. aeruginosa* and *S. aureus*[40–42]. Interestingly, CF clinical isolates of *P. aeruginosa* and *S. aureus* typically exhibit attenuated virulence[43,44]. Our results that virulence pathways are suppressed in *S. aureus* in coculture suggest that bacterial virulence factor production can be altered by interspecies interactions, which can further complicate changes in virulence phenotypes in a host-microbiome environment.

Our findings that *S. aureus* significantly upregulates Rot in coculture and that the *rot* mutant exhibits a survival deficit in mixed-species biofilms compared to wild type suggests that *rot* is important for *S. aureus* competitive fitness against *P. aeruginosa*. Sessile bacterial cells and their secreted extracellular matrix make up biofilm populations[45], which often exhibit high antibiotic tolerance and are protected by physical barriers formed by tightly aggregated monolayers of kin cells[46]. Rot is known to positively regulate biofilm formation via activation of the synthesis of surface adhesion proteins while repressing several extracellular proteases[47]. It is interesting to speculate that *S. aureus* deficient in Rot cannot compete with *P. aeruginosa* for surface adhesion and is more readily displaced than wild-type *S. aureus*. Wild-type cells that successfully initiate the formation of an intact biofilm can enjoy enhanced protection from *P. aeruginosa* toxic exoproducts, potentially accounting for increased viability of *S. aureus* in mixed-species biomass. Rot upregulation was consistently observed in all comparative proteomic experiments, suggesting that such a response is conserved across different *S. aureus* strains and coculture conditions.

Conclusion

Here, we adapted the BONCAT method to perform cell-selective proteomic analysis targeting the outcompeted organism, *S. aureus*, in a coculture environment predominated by *P. aeruginosa*. We demonstrated significantly improved detection and quantification of proteins synthesized by *S. aureus* post-enrichment. Our comparative proteomic experiments yielded high-resolution information on significantly differentially regulated proteins. Many of these, including Rot, have not been previously reported in other global transcriptomic or proteomic studies and can be further pursued to uncover their unique biological roles in mediating coculture dynamics between *P. aeruginosa* and *S. aureus*. Our study highlights the utility of bioorthogonal chemistry in the analysis of complex microbial communities.

References

1. Liu, H., Sadygov, R. G. & Yates, J. R. A Model for Random Sampling and Estimation of Relative Protein Abundance in Shotgun Proteomics. *Anal. Chem.* **76**, 4193–4201 (2004).
2. Nakayasu, E. S. Washburn, M. P., Wolters, D., & Yates, J. R. Large-scale analysis of the yeast proteome by multidimensional protein identification technology. *Nature biotechnology*, ***19***(3), 242–247 (2001).
3. Gilbert, J. A. *et al.* Microbiome-wide association studies link dynamic microbial consortia to disease. *Nature* **535**, 94–103 (2016).
4. Shreiner, A. B., Kao, J. Y. & Young, V. B. The gut microbiome in health and in disease. *Curr. Opin. Gastroenterol.* **31**, 69–75 (2015).
5. Lloyd-Price, J. *et al.* Multi-omics of the gut microbial ecosystem in inflammatory bowel diseases. *Nature* **569**, 655–662 (2019).
6. Coyte, K. Z., Schluter, J. & Foster, K. R. The ecology of the microbiome: Networks, competition, and stability. *Science* **350**(6261), 663–666 (2015).
7. Tom, L. M. *et al.* Low-abundance populations distinguish microbiome performance in plant cell wall deconstruction. *Microbiome* **10**(1), 183 (2022).
8. Han, G., Luong, H. & Vaishnava, S. Low abundance members of the gut microbiome exhibit high immunogenicity. *Gut Microbes* **14**(1), 2104086 (2022).
9. Woerther, P.-L., Antoun, S., Chachaty, E. & Merad, M. Eggerthella lenta bacteremia in solid tumor cancer patients: Pathogen or witness of frailty? *Anaerobe* **47**, 70–72 (2017).
10. Issa Isaac, N., Philippe, D., Nicholas, A., Raoult, D. & Eric, C. Metaproteomics of the human gut microbiota: Challenges and contributions to other OMICS. *Clin. mass Spectrom. (Del Mar, Calif.)* **14 Pt A**, 18–30 (2019).
11. Landgraf, P., Antileo, E. R., Schuman, E. M. & Dieterich, D. C. BONCAT: metabolic labeling, click chemistry, and affinity purification of newly synthesized proteomes. *Methods Mol. Biol.* **1266**, 199–215 (2015).
12. O'Sullivan, B. P. & Freedman, S. D. Cystic fibrosis. *Lancet (London, England)* **373**, 1891–1904 (2009).
13. Fischer, A. J. *et al.* Sustained Coinfections with *Staphylococcus aureus* and *Pseudomonas aeruginosa* in Cystic Fibrosis. *Am. J. Respir. Crit. Care Med.* **203**, 328–338 (2021).
14. Hoiby, N., Ciofu, O. & Bjarnsholt, T. *Pseudomonas aeruginosa* biofilms in cystic fibrosis. *Future Microbiol.* **5**, 1663–1674 (2010).

15. Liu, Y., Beyer, A. & Aebersold, R. On the Dependency of Cellular Protein Levels on mRNA Abundance. *Cell* **165**, 535–550 (2016).
16. Parasar, B. *et al.* Chemoproteomic Profiling of Gut Microbiota-Associated Bile Salt Hydrolase Activity. *ACS Cent. Sci.* **5**, 867–873 (2019).
17. Jariwala, P. B. *et al.* Discovering the Microbial Enzymes Driving Drug Toxicity with Activity-Based Protein Profiling. *ACS Chem. Biol.* **15**, 217–225 (2020).
18. Zhao, X. *et al.* Chemoproteomics reveals microbiota-derived aromatic monoamine agonists for GPRC5A. *Nat. Chem. Biol.* **19**, 1205–1214 (2023).
19. Mahdavi, A. *et al.* Engineered Aminoacyl-tRNA Synthetase for Cell-Selective Analysis of Mammalian Protein Synthesis. *J. Am. Chem. Soc.* **138**, 4278–4281 (2016).
20. Bubeck Wardenburg, J., Williams, W. A. & Missiakas, D. Host defenses against *Staphylococcus aureus* infection require recognition of bacterial lipoproteins. *Proc. Natl. Acad. Sci. U. S. A.* **103**, 13831–13836 (2006).
21. Miller, R. J. *et al.* Development of a *Staphylococcus aureus* reporter strain with click beetle red luciferase for enhanced in vivo imaging of experimental bacteremia and mixed infections. *Sci. Rep.* **9**, 16663 (2019).
22. Tanrikulu, I. C., Schmitt, E., Mechulam, Y., Goddard, W. A. & Tirrell, D. A. Discovery of Escherichia coli methionyl-tRNA synthetase mutants for efficient labeling of proteins with azidonorleucine in vivo. *Proc. Natl. Acad. Sci.* **106**, 15285–15290 (2009).
23. Presolski, S. I., Hong, V. P. & Finn, M. G. Copper-Catalyzed Azide-Alkyne Click Chemistry for Bioconjugation. *Curr. Protoc. Chem. Biol.* **3**, 153–162 (2011).
24. Tang, K., Page, J. S. & Smith, R. D. Charge competition and the linear dynamic range of detection in electrospray ionization mass spectrometry. *J. Am. Soc. Mass Spectrom.* **15**, 1416–1423 (2004).
25. UniProt Consortium (2023). UniProt: the Universal Protein Knowledgebase in 2023. *Nucleic acids research*, ***51***(D1), D523–D531.
26. Sassi, M., Felden, B. & Augagneur, Y. Draft Genome Sequence of *Staphylococcus aureus* subsp. *aureus* Strain HG003, an NCTC8325 Derivative. *Genome Announc.* **2**, (2014).
27. Ritchie, M. E. *et al.* limma powers differential expression analyses for RNA-sequencing and microarray studies. *Nucleic Acids Res.* **43**, e47–e47 (2015).
28. Benjamini, Y. & Yekutieli, D. The Control of the False Discovery Rate in Multiple Testing under Dependency. *Ann. Stat.* **29**, 1165–1188 (2001).

29. Subramanian, A. *et al.* Gene set enrichment analysis: a knowledge-based approach for interpreting genome-wide expression profiles. *Proc. Natl. Acad. Sci. U. S. A.* **102**, 15545–15550 (2005).
30. Thomas, P. D. The Gene Ontology and the Meaning of Biological Function. *Methods Mol. Biol.* **1446**, 15–24 (2017).
31. Gimza, B.D., Larias M.I., Budny. B.G & Shaw L.N. Mapping the Global Network of Extracellular Protease Regulation in *Staphylococcus aureus*. *mSphere* **4**(5), 10.1128/msphere.00676-19 (2019).
32. Christian, J. & Horswill, A.R. Regulation of *Staphylococcus aureus* Virulence. *Microbiol. Spectr.* **7**, 10.1128/microbiolspec.gpp3-0031–2018 (2019).
33. Cheung, A. L., Bayer, A. S., Zhang, G., Gresham, H. & Xiong, Y.-Q. Regulation of virulence determinants *in vitro* and *in vivo* in *Staphylococcus aureus*. *FEMS Immunol. Med. Microbiol.* **40**, 1–9 (2004).
34. Said-Salim, B. *et al.* Global Regulation of *Staphylococcus aureus* Genes by Rot. *J. Bacteriol.* **185**, 610–619 (2003).
35. Déziel, E. *et al.* Analysis of *Pseudomonas aeruginosa* 4-hydroxy-2-alkylquinolines (HAQs) reveals a role for 4-hydroxy-2-heptylquinoline in cell-to-cell communication. *Proc. Natl. Acad. Sci.* **101**, 1339–1344 (2004).
36. Raba, D. A. *et al.* Characterization of the Pseudomonas aeruginosa NQR complex, a bacterial proton pump with roles in autopoisoning resistance. *J. Biol. Chem.* **293**, 15664–15677 (2018).
37. Filkins, L. M. *et al.* Coculture of *Staphylococcus aureus* with *Pseudomonas aeruginosa* Drives S. aureus towards Fermentative Metabolism and Reduced Viability in a Cystic Fibrosis Model. *J. Bacteriol.* **197**, 2252 LP – 2264 (2015).
38. Rouil, K.R., Kissner, W.J., Markovetz. M.R. & Hill, D.B. Effects of Mucin and DNA Concentrations in Airway Mucus on *Pseudomonas aeruginosa* Biofilm Recalcitrance. *mSphere* **7**, e00291-22 (2022).
39. Gibiansky, M.L. *et al.* Bacteria Use Type IV Pili to Walk Upright and Detach from Surfaces. *Science* **330**(6001), 197 (2010).
40. Tognon, M., Köhler, T., Luscher, A. & van Delden, C. Transcriptional profiling of *Pseudomonas aeruginosa* and *Staphylococcus aureus* during in vitro co-culture. *BMC Genomics* **20**, 30 (2019).
41. Baldan, R. *et al.* Adaptation of *Pseudomonas aeruginosa* in Cystic Fibrosis airways influences

virulence of *Staphylococcus aureus* in vitro and murine models of co-infection. *PLoS One* **9**, e89614 (2014).

42. Briaud, P. *et al.* Coexistence with *Pseudomonas aeruginosa* alters *Staphylococcus aureus* transcriptome, antibiotic resistance and internalization into epithelial cells. *Sci. Rep.* **9**, 16564 (2019).
43. Rumpf, C., Lange, J., Schwartbeck, B. & Kahl, B. C. *Staphylococcus aureus* and Cystic Fibrosis-A Close Relationship. What Can We Learn from Sequencing Studies? *Pathogens. (Basel, Switzerland)* **10**(9), 1177 (2021).
44. Smith, E. E. *et al.* Genetic adaptation by *Pseudomonas aeruginosa* to the airways of cystic fibrosis patients. *Proc. Natl. Acad. Sci. U. S. A.* **103**, 8487–8492 (2006).
45. Jefferson, K. K. What drives bacteria to produce a biofilm? *FEMS Microbiol. Lett.* **236**, 163–173 (2004).
46. Vestby, L. K., Grønseth, T., Simm, R. & Nesse, L. L. Bacterial Biofilm and its Role in the Pathogenesis of Disease. *Antibiot. (Basel, Switzerland)* **9**(2), 59 (2020).
47. Mootz, J. M. *et al.* (2015). Rot is a key regulator of Staphylococcus aureus biofilm formation. *Molecular microbiology*, ***96***(2), 388–404.

Figures

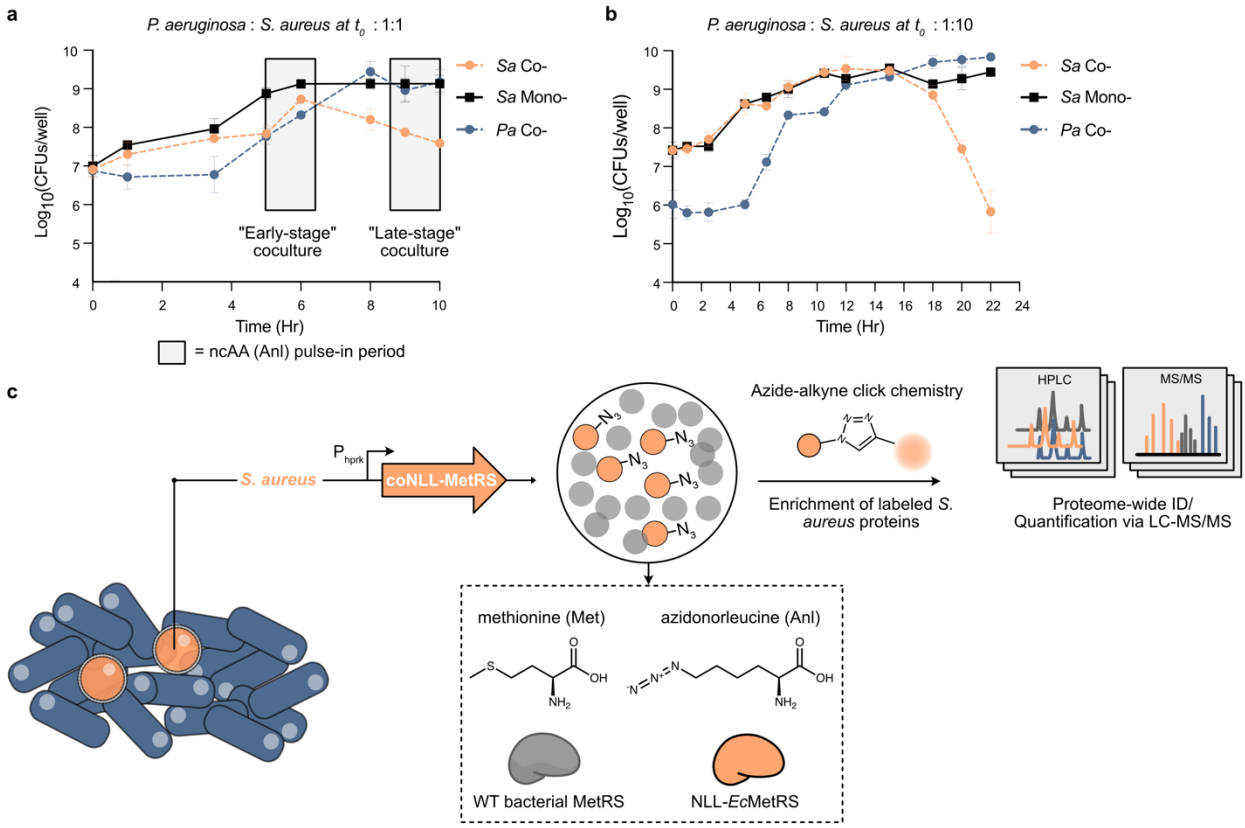

Figure 3.1. Cell-selective BONCAT experimental design. *P. aeruginosa* and *S. aureus* coculture colony-forming units (CFUs) vs time for starting population ratio (*P. aeruginosa* : *S. aureus*) = 1:1 (**a**) and starting population ratio (*P. aeruginosa* : *S. aureus*) = 1: 10 (**b**). **c.** Scheme of cell-selective BONCAT labeling and proteomic analysis.

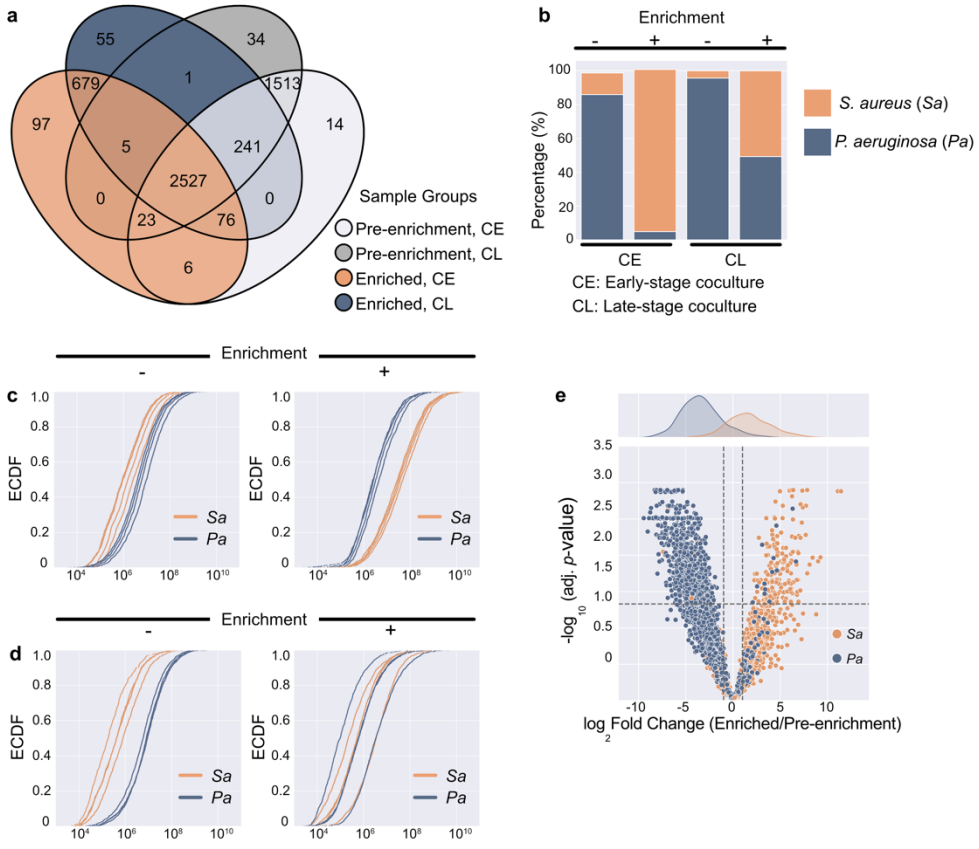

Figure 3.2. Summary of cell-selective BONCAT enrichment results. a. Venn diagram of all proteins identified in each sample condition. White: Pre-enrichment, CE, where CE is **E**arly-stage **C**o-culture; Grey: Pre-enrichment, CL, where CL is **L**ate-stage **C**o-culture; Orange: enriched, CE; Blue: Enriched, CL. **b.** Percentage contribution of protein abundances (LFQ values, LFQ = Label-free quantification) by species (*P. aeruginosa* and *S. aureus*). **c-d**: ECDF plots for *P. aeruginosa* (blue) and *S. aureus* (orange) protein abundances distribution in pre-enrichment (left panel) vs. enriched (right panel) samples for early-stage coculture (CE, **c**) and late-stage coculture (CL, **d**). **e.** Volcano plot comparing differential protein abundances for common proteins found in enriched vs. pre-enrichment CL samples (right), colored by *P. aeruginosa* (blue) and *S. aureus* (orange). Note that many *S. aureus* proteins were uniquely found in enriched samples, and therefore could not be quantified for fold changes in expression, the same for *P. aeruginosa* proteins only present in unenriched samples.

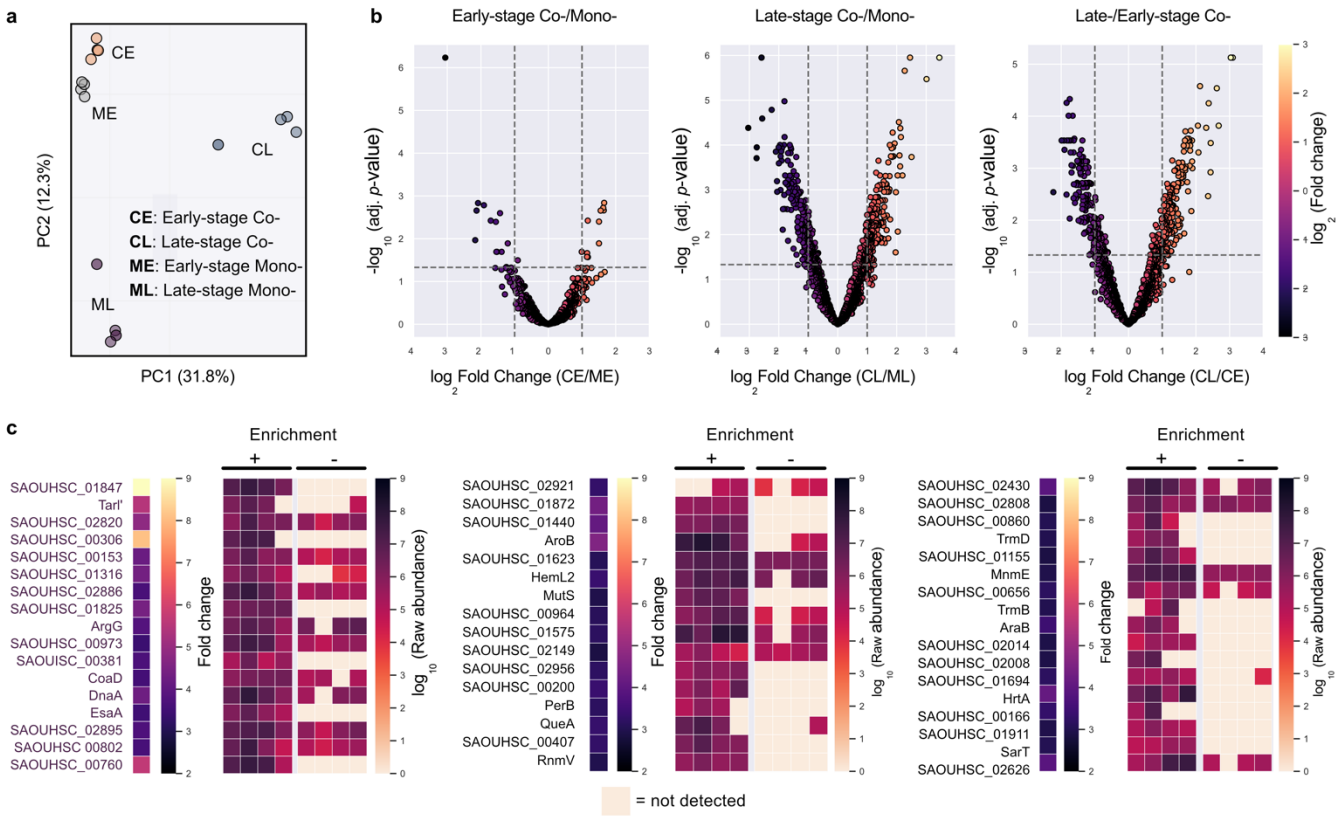

Figure 3.3. BONCAT enables high-confidence and high-resolution proteomic analysis of differentially regulated *S. aureus* proteins in coculture with *P. aeruginosa*. a. Principal component analysis (PCA) of protein abundances; each data point represents an individual biological replicate (total n=4 biological replicates per condition). **b.** Volcano plots showing comparative proteomic results for annotated comparisons: early-stage coculture/monoculture *S. aureus* (CE/ME, left); late-stage coculture/monoculture *S. aureus* (CL/ML, middle); late-stage / early-stage coculture *S. aureus* (CL/CE, right). **c.** Top 50 proteins with the most up-regulated expression levels in late-stage coculture/monoculture comparison and associated raw abundances before and after enrichment summarized in a heatmap.

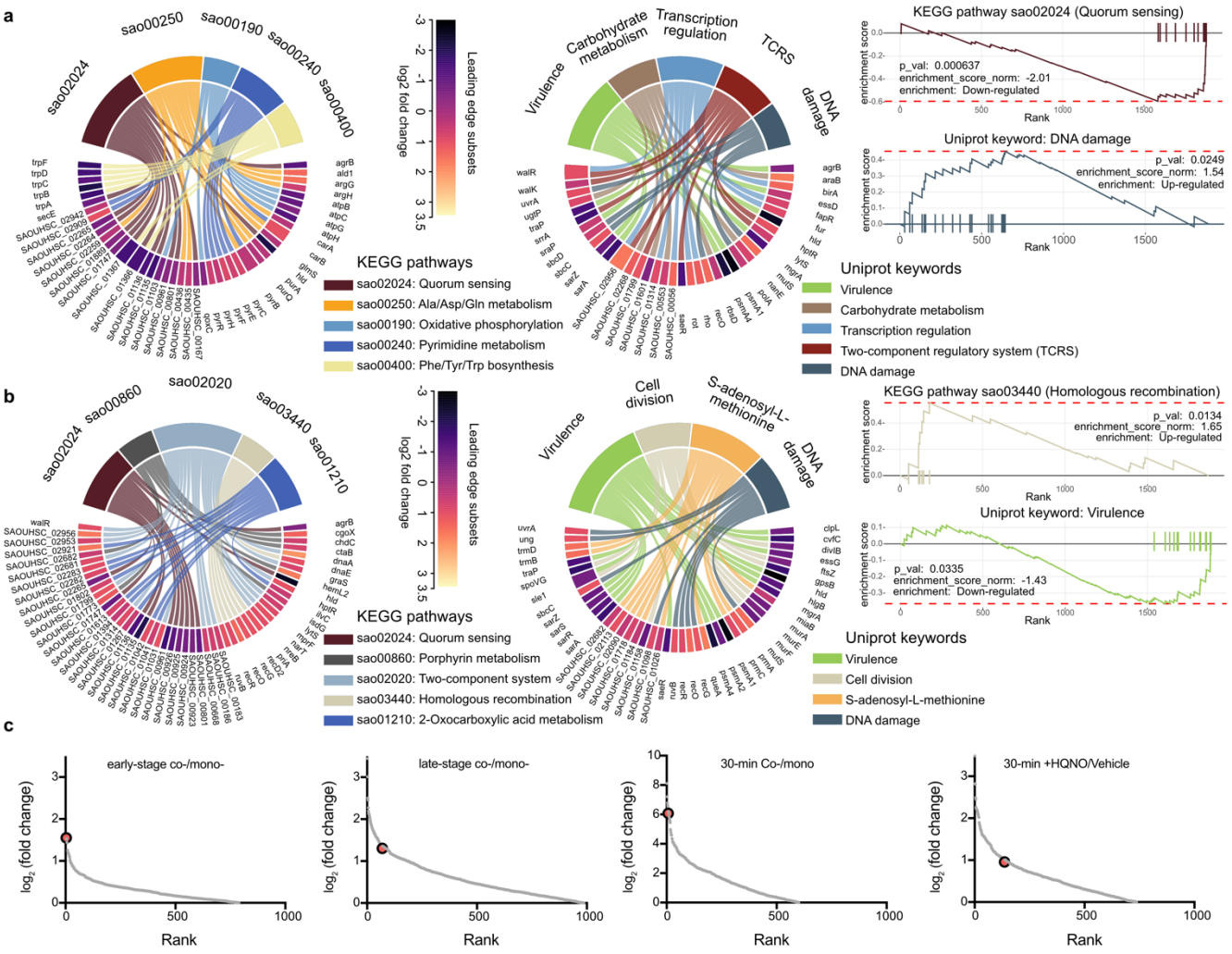

Figure 3.4. *S. aureus* proteome signature in coculture with *P. aeruginosa* indicates DNA damage, quorum quenching and repressed virulence. a-b: Chord diagram showing enriched biological terms found in KEGG and UniProt knowledge databases revealed by GSEA and their selected leading-edge gene (protein) sets. Proteins are color-coded by their fold change values in differential expression analysis in early-stage coculture/monoculture comparison (**a**) and late-stage coculture/monoculture comparison (**b**). Representative enrichment plots for selected biological terms are shown with the leading-edge gene (protein) sets as tick marks. **c.** Scatter plots show all proteins quantified for differential expression for the indicated comparisons ranked by their fold-change values. Rot is highlighted on each plot to indicate it is a top up-regulated hit in all experiments (for results for early-stage and late-stage coculture/monoculture proteomic experiments performed using MRSA, see **Supplementary Fig. 5b**).

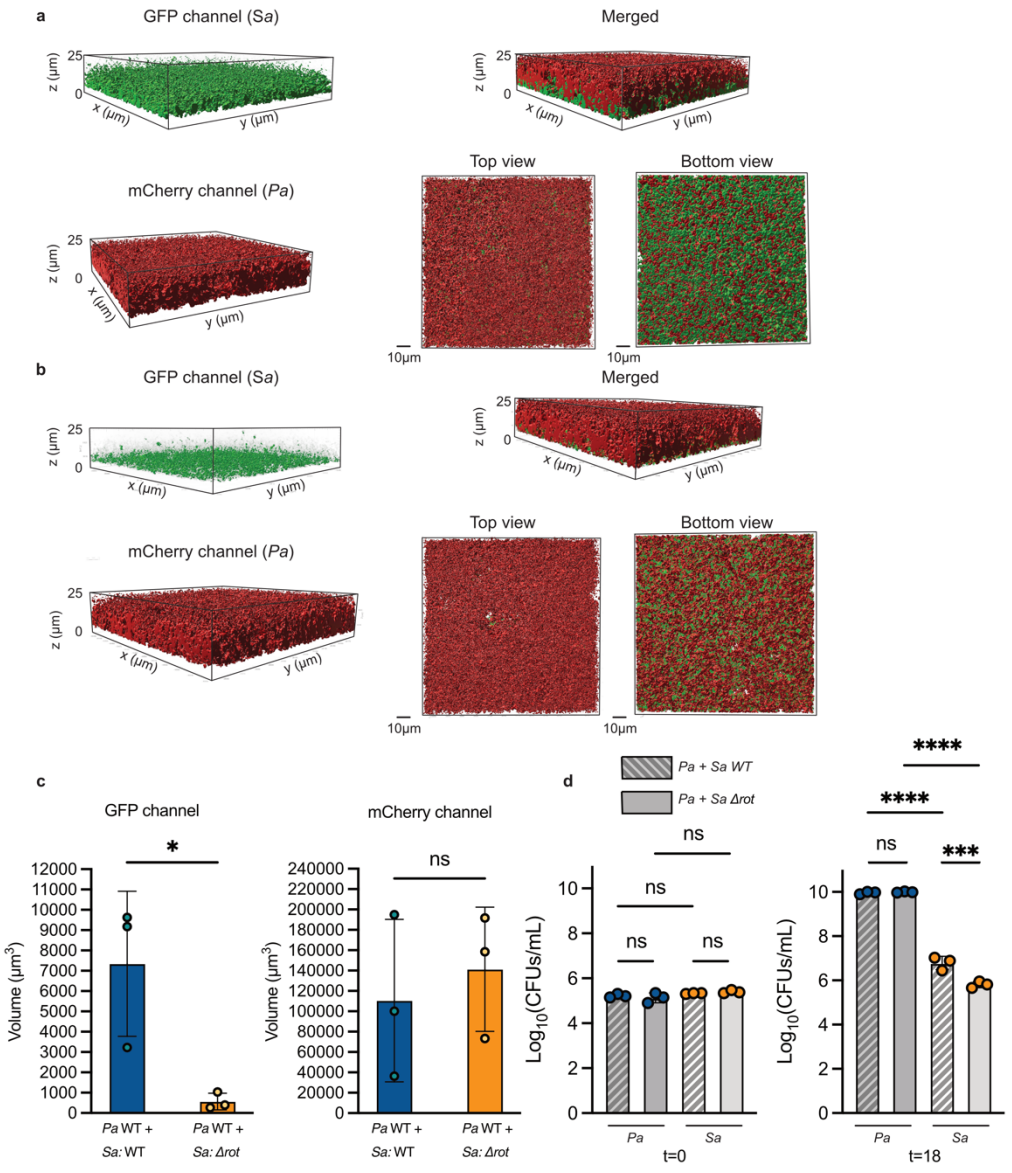

Figure 3.5. Rot is important for *S. aureus* fitness in mixed species biomass with *P. aeruginosa* in artificial sputum medium (ASM). Representative microscopy images show 3D- as well as sectional views of 18 h *P. aeruginosa*-*S. aureus* coculture biomass in ASM in the following coculture conditions: *P. aeruginosa* wildtype + *S. aureus* wildtype (**a**) and *P. aeruginosa* wildtype + *S. aureus* Δ*rot* (**b**); **c.** 3D volume quantification per fluorescence channel (GFP & mCherry); Data represent three biological replicates with the mean and standard deviation indicated. Statistical significance was determined by student t-test. ns, not significant; *, $P < 0.05$ **d.** CFU enumeration per species. Data represent three biological replicates with the mean and standard deviation indicated. Statistical significance was determined by one-way ANOVA followed by Tukey's multiple comparisons test. ns, not significant; ***, $P < 0.001$; ****, $P < 0.0001$.

Supplementary Information

Materials and Methods

Bacterial strains, plasmids and culture conditions

P. aeruginosa was routinely cultured in lysogeny broth (LB; 1% tryptone, 0.5% yeast extract, 1% sodium chloride) and *S. aureus* in tryptic soy broth (TSB, Becton Dickinson), unless otherwise indicated, with aeration at 37ºC. All strains used in this study can be found in **Table 3.1**.

Bacterial competition assay

Liquid competition. *P. aeruginosa* and *S. aureus* overnight cultures were diluted to OD_{600} = 0.1 in fresh M14 medium (M9 salts supplemented with 10 mM glucose, 10 mg/mL casamino acids, 1 mM $MgSO_4$, 2 μg/mL thiamine (vitamin B1), 2 μg/mL niacin (vitamin B3), 2 μg/mL calcium pantothenate (vitamin B5), 0.1 μg/mL biotin (vitamin B9)), mixed at 1:1 or 1: 10 ratio by species in M14 and grown at 37ºC. Coculture was harvested at indicated time points, and selective plating (Mannitol salt agar for *S. aureus* and *Pseudomonas* isolation agar for *P. aeruginosa*) was used for CFU enumeration.

Artificial Sputum Media Competition Assay**.** *P. aeruginosa* and *S. aureus* strains were grown overnight in M8T, rotating at 37°C for 14 to 16 h. The P*rpoB-sgfp* (pCM29 backbone) plasmid in *S. aureus* was maintained with 7.5 μg/mL of chloramphenicol. The overnight liquid cultures were subcultured in M8T (no antibiotic selection) and grown rotating until the mid-exponential phase. Cultures were normalized to an OD_{600} of 0.2 in M8T and then washed 1X in PBS. Prior to starting the experiment, 2X ASM and 10 mg/mL mucin (Table S4) were mixed at a 1:1 ratio. The washed cultures were then inoculated into ASM+mucin at an OD_{600} of 0.025 in mono- or coculture in a total volume of 500 μL in a 1.5 mL microcentrifuge tube. The tubes were mixed by vortexing, and then 200 μL were inoculated into each quadrant of a 4-chamber glass-bottom 35 mm dish (Cellvis, Cat. no. D35C4-30-1.5-N). To harvest the bacteria from the microscopy dishes at ~24 h, 0.2 % Triton X-100 was added to the cultures and incubated at room temperature from 10 - 20 min. Then, the bacteria were scraped with a pipette tip and all the volume per quadrant was transferred to a 1.5 mL centrifuge tube. The tubes were thoroughly mixed by vortexing before performing the serial dilutions.

BONCAT labeling of *S. aureus*

For *P. aeruginosa* coculture proteomics experiments, *S. aureus* HG003 coNLL-MetRS cells and P. aeruginosa PA14 WT were diluted to OD_{600}~0.1 in defined M14 medium, mixed at 1:1 ratio, and plated into 6-well plates. Labeling was initiated by the addition of 1 mM Anl (Iris-Biotech) during indicated periods and cell lysates were harvested immediately after. Cell pellets were centrifuged at 4ºC and washed with ice-cold

LCMS-grade water and frozen at -80°C for downstream lysis and chemical enrichment. All samples were lysed by resuspension in LCMS water, treated with 5µg/mL lysostaphin for 30 min, SDS to 1%, boiled at 75°C and sonicated with a microtip probe for 15 seconds at 30% amplification (Qsonica).

Sample preparation for mass spectrometry

For chemical enrichment of BONCAT-labeled proteins from lysates, 2.5 mg of lysates were used for each sample. Lysates were first reduced by 1mM dithiothreitol (DTT), alkylated with 600mM chloroacetamide and reacted with aza-dibenzocyclooctyne (DBCO) agarose beads (Click Chemistry Tools) via copper-free click chemistry. The reaction was incubated in the dark at room temperature overnight, followed by rigorous resin washing with i) 40 mL 0.8% (wt/vol) SDS/PBS; ii) 40 mL 8 M urea in tris hydrochloride (pH = 8.0) and iii) 40 mL 20% (vol/vol) acetonitrile/H_2O to remove nonspecific protein binding. Peptides were detached from DBCO agarose with on-bead digestion with 0.1 µg trypsin and 0.05 µg endoproteinase LysC at 37°C overnight. Supernatant was then collected for further detergent removal (HiPPR column, Thermo Fisher Scientific), and peptides were desalted with C_{18} StageTips.

LC-MS analyses

Peptides were subjected to LC-MS/MS analysis on an EASY-nLC 1200 (Thermo Fisher, San Jose, CA) coupled to a Q Exactive HF Orbitrap mass spectrometer (Thermo Fisher, Bremen, Germany) equipped with a Nanospray Flex ion source. Samples (2 µL out of 10 µL total) were directly loaded onto an Aurora 25 cm x 75 µm ID, 1.6 µm C18 column (Ion Opticks, Victoria, Australia) heated to 50°C. The peptides were separated with a 60 min gradient at a flow rate of 350 nL/min as follows: 2–6% Solvent B (3.5 min), 6-25% B (42 min), 25-40% B (14.5 min), 40-98% B (1 min), and held at 98% B (14 min). Solvent A consisted of 97.8% H_2O, 2% ACN, and 0.2% formic acid and solvent B consisted of 19.8% H_2O, 80 % ACN, and 0.2% formic acid. The Q Exactive HF was operated in data dependent mode with full scan resolution set to 60,000 at m/z 200 in profile mode, full scan target set to 3×10^6, and a maximum injection time of 15 milliseconds. Full scan mass range was set to 375−1500 m/z. Data dependent MS2 scans were collected for charge state 2-5 precursors in centroid mode using a loop count of 12, AGC target of 1×10^5, an intensity threshold of 1×10^5, and a maximum injection time of 45 milliseconds. Isolation width was set at 1.2 m/z, scan range was 200-2000 m/z, and a fixed first mass of 100 was used. Normalized collision energy was set at 28. Peptide match was set to off, and isotope exclusion was on. Dynamic exclusion was set to exclude after 1 time for 45 seconds.

Proteomics data processing and analysis

Proteomics data analysis was performed in Proteome Discoverer 2.5 (Thermo Scientific) using the SequestHT search algorithm and nonredundant Uniprot *S. aureus* and *P. aeruginosa* FASTA files plus common contaminants (CRAPome). Sequest search parameters were as follows: fully tryptic peptides with 6-144 residues and no more than 2 missed cleavages, precursor mass tolerance of 35 ppm and fragment mass tolerance of 0.05 Da, and a maximum of 3 equal modifications. Dynamic modifications were as follows: Cysteine carbamidomethylation, methionine oxidation, asparagine and glutamine deamidation, protein N-terminal acetylation, protein N-terminal Met-loss, and protein N-terminal Met-loss plus acetylation. Percolator FDRs were set at 0.01 (strict) and 0.05 (relaxed). The consensus level peptide and PSM FDR filters were also set at 0.01 (strict) and 0.05 (relaxed). Strict parsimony principle was set to true. Protein quantification was also performed in Proteome Discoverer by summed abundances of the precursor intensities of all high confidence unique and razor peptides.

Raw protein quantification data exported from ProteomeDiscoverer 2.5 was imported into R and analyzed using the romics analysis package (https://jeffsocal.github.io/romics). Once imported, the data are filtered for common protein contaminants and normalized between runs using Breiman and Cutler's Random Forests for Classification and Regression (https://cran.r-project.org/web/packages/randomForest) method selected based on the best performance in lowering sample replicate variation while maintaining quantitative dynamic range for label-free analysis. Protein expression differences between samples were evaluated in the R romics package using the limma algorithm for differential expression (https://bioinf.wehi.edu.au/limma/). Differential expression volcano plots were generated using Prism (GraphPad). Protein set enrichment analysis for significantly up-regulated and down-regulated *S. aureus* proteins was performed using Gene set enrichment analysis (GSEA) via the fgsea package for R (https://bioconductor.org/packages/release/bioc/html/fgsea). The number of permutations was set to 10,000 for *P* value calculation.

Time-lapse fluorescence microscopy

The bacteria were grown statically for ~ 24 h inside the microscope's incubation chamber at 37°C with 90% relative humidity controlled by the Okolab Humidity Controller. At ~24 h, two 50 μm Z-stacks per condition were acquired with an inverted Nikon Eclipse Ti2 A1R Resonant Scanning Confocal Microscope, using a CFI SR HP Plan Apochromat Lambda S 100XC Sil objective (1.35 NA) with a 56.19 μm pinhole and 1024 x 1024 pixels. A 488 nm laser (laser power 5, offset -10, and HV – gain 10) was used to excite the sGFP in *S. aureus* cells, and a 561 nm laser (laser power 7, offset -10, and HV – gain 40) to excite the mCherry in *P. aeruginosa*

strains. The images were saved and analyzed with the Nikon NIS-Elements AR Software. *S. aureus* and *P. aeruginosa* growth was assessed at 0 h (inoculum) and at ~24 h by plating the serial dilutions on selective media (Mannitol Salt Agar (MSA) and *Pseudomonas* Isolation Agar (PIA), respectively).

Supplementary figures

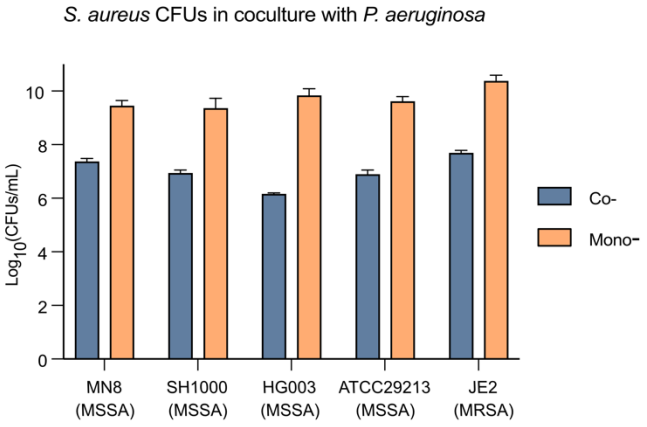

Supplementary Figure 3.1. *P. aeruginosa* outcompeting *S. aureus* is conserved across various strains of *S. aureus*. MSSA: methicillin-sensitive *S. aureus*; MRSA: methicillin-resistant *S. aureus*. Data represent mean and standard deviations for at least three biological replicates in each condition. Coculture growth was inoculated in the defined M14 medium at OD_{600} = 0.1 at 1:1 species ratio, incubated at 37°C and plated on selective agars (*Pseudomonas* isolation agar for *P. aeruginosa* isolation and Mannitol salt agar for *S. aureus* isolation) after 18 h for CFU enumeration.

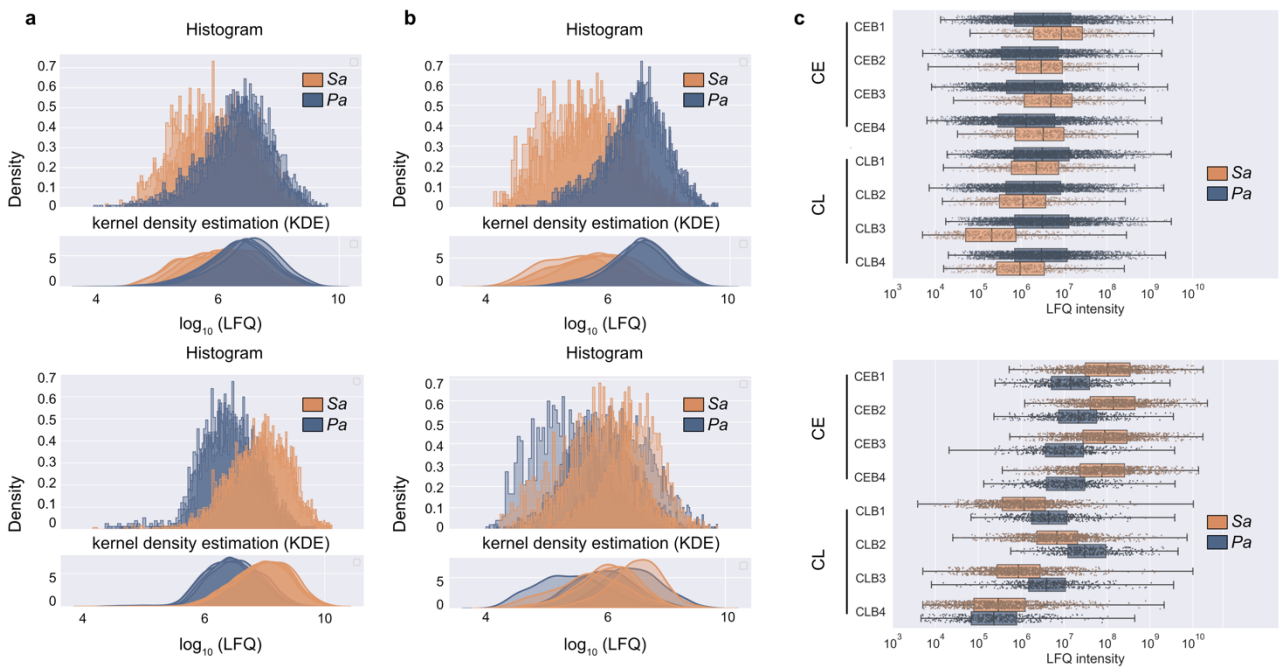

Supplementary Figure 3.2. Coculture protein abundance analysis per species before and after enrichment. **a.** Histograms and kernel density estimation (KDE) show the distribution of *S. aureus* (*Sa*, orange) and *P. aeruginosa* (*Pa*, blue) proteins before (top) and after (bottom) BONCAT enrichment for early-stage coculture samples (CE). **b.** Distribution of *S. aureus* and *P. aeruginosa* proteins before (top) and after (bottom) enrichment for late-stage coculture samples (CL). **c.** Scatter plots highlight Individual protein abundances per species and are overlaid with box plots summarizing the median and range in each indicated condition before (top panel) and after (bottom panel) enrichment.

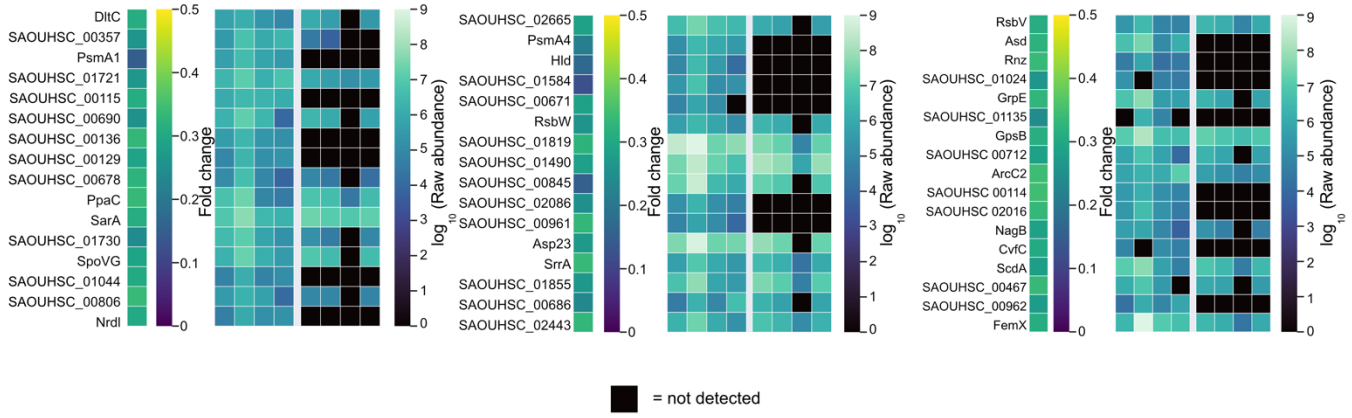

Supplementary Figure 3.3. 40% of down-regulated "hits" were not detected in pre-enrichment samples. Heatmaps display the 50 proteins with the largest decreases in abundance in late-stage coculture/monoculture (CL/ML) proteomics comparison, with their associated fold changes and raw abundances before and after enrichment encoded in respective colormaps. 20/50 of these hits were not detected in any pre-enrichment samples.

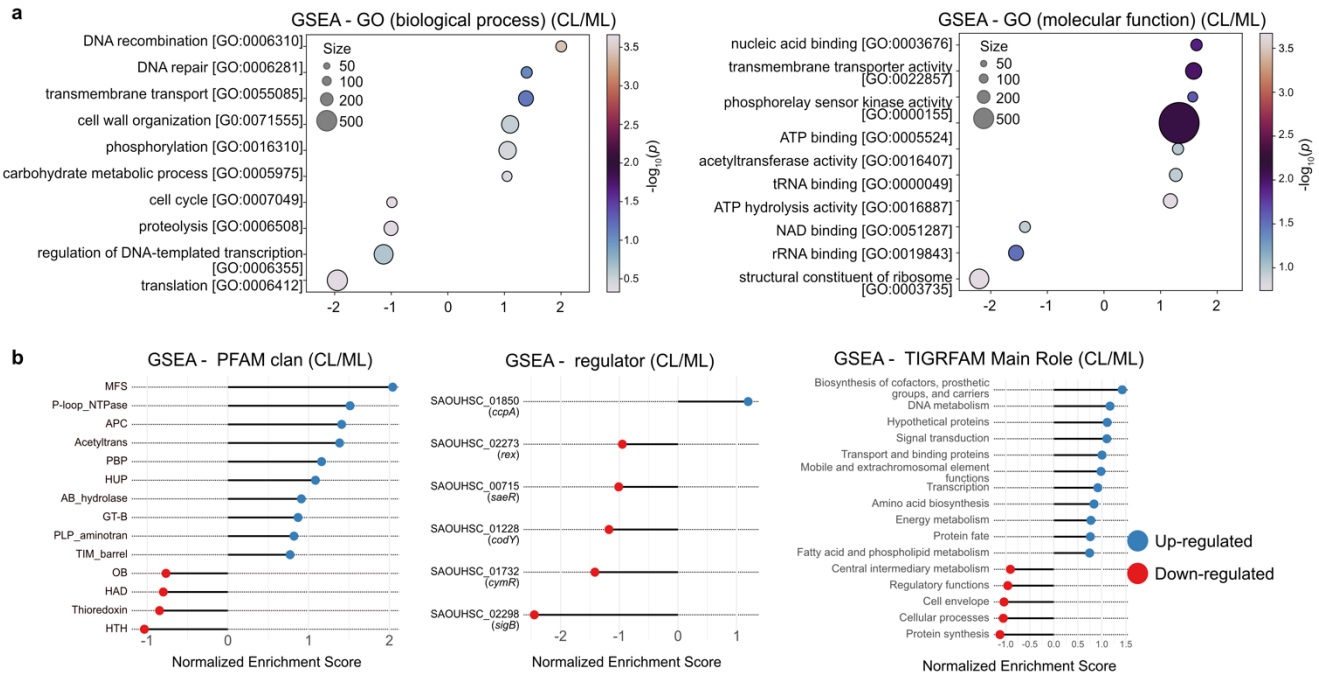

Supplementary Figure 3.4. Summary of GSEA results for late-stage coculture vs. monoculture proteomics comparison (CL/ML). GSEA was performed using the fgsea package for R (https://bioconductor.org/packages/release/bioc/html/fgsea). **a.** Gene ontology (GO) annotations were assigned by Proteome Discoverer (PD); **b.** Annotations from protein families (PFAM), the Institute for Genomic Research (TIGRFAM), and known regulators were downloaded from AureoWiki (aureowiki.med.uni-greifswald.de). For all GSEA *P* value calculations, the number of permutations was set to 10,000. For complete GSEA output with all biological pathways and associated leading-edge subset proteins, see **Supplementary Table 3.3.** The PFAM categories presented in **b** are as follows: MFS: Major Facilitator Superfamily; P-loop_NTPase: Phosphate-loop Nucleoside Triphosphate Hydrolase; APC: Amino acid-Polyamine-Organocation; PBP: Penicillin-Binding Protein; Hup: Helix-turn-helix Uptake Permease; AB-hydrolase: α/β-hydrolase; GT-B: Glycosyltransferase Family B; PLP-aminotran: Pyridoxal phosphate-dependent Aminotransferase; TIM Barrel: Triosephosphate Isomerase (TIM) Barrel; OB: Oligonucleotide/oligosaccharide-binding; HAD: Haloacid Dehalogenase; HTH: Helix-turn-helix.

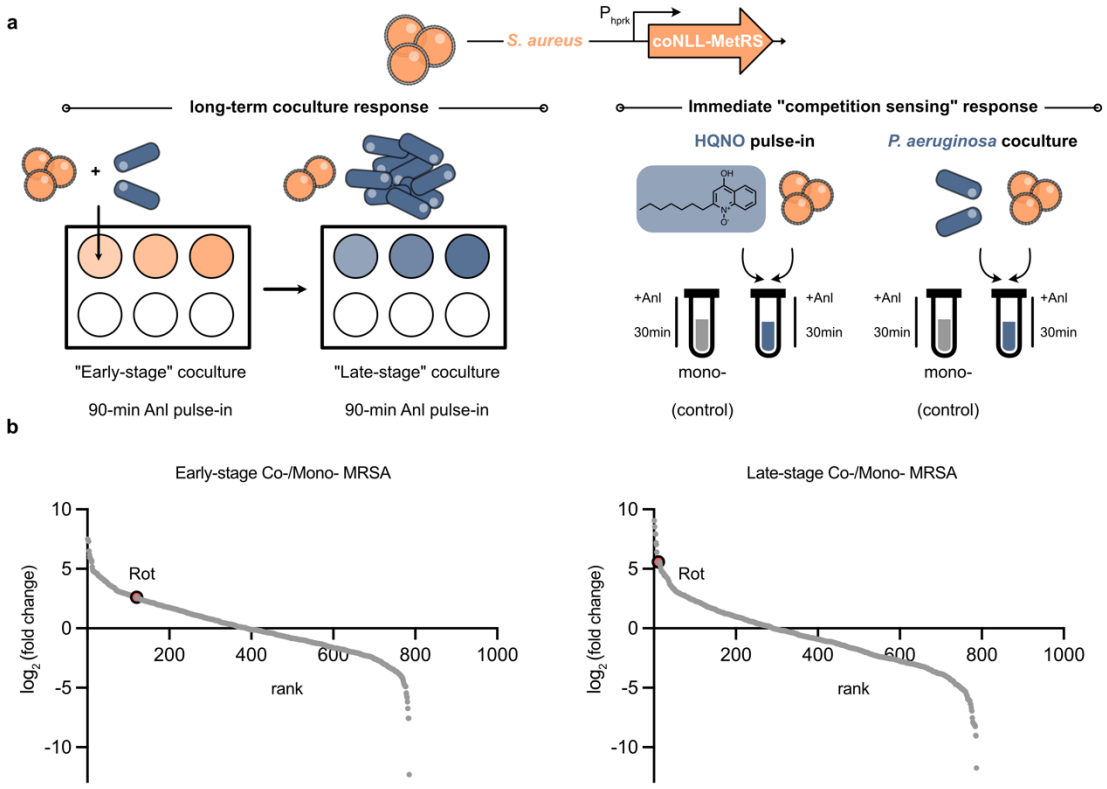

Supplementary Figure 3.5. Summary of BONCAT experimental design and additional fold-change rank plots for comparative proteomics using an MRSA strain. a. In long-term coculture response analysis, *S. aureus* coNLL-MetRS coculture with *P. aeruginosa* was inoculated in 6-well plates at starting OD_{600}=0.1 for each species and labeled for 90-min with Anl during early-stage (CE) and late-stage coculture (CL). For immediate "competition sensing" experiments, a 30-min Anl labeling window was used for 40 µM HQNO pulse-in and mixing of stationary-phase (OD_{600}>1.5) *S. aureus* and *P. aeruginosa* coculture. **b.** All proteins quantified for differential expression for the indicated comparisons ranked by their fold-change values. Rot is highlighted on each plot to indicate it is a top up-regulated hit in early-stage and late-stage coculture/monoculture proteomic experiments performed using MRSA.

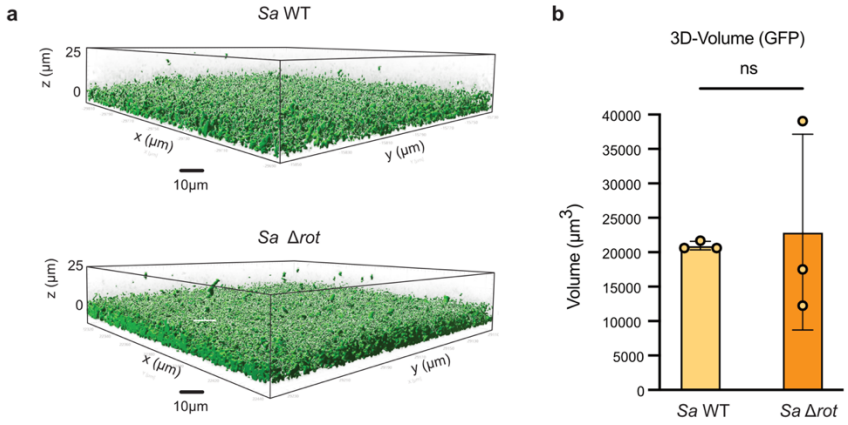

Supplementary Figure 3.6. Time-lapse fluorescence microscopy monoculture control. a. Representative microscopy images show 3D-views of 18 h wild-type *S. aureus* (top) and Δ*rot* monoculture biomass in ASM (bottom). **b.** Quantification of 3D-volume of all GFP pixels that pass a threshold for absolute fluorescence intensity. Data represent three biological replicates with the mean and standard deviation indicated after 18 h growth at 37°C in an artificial sputum medium (ASM). Statistical significance was determined by an unpaired t-test. ns, not significant.

Table 3.1. Strains and plasmids used in this study.

Name	Genotype or sequence	Source	Notes
***S. aureus* strains**			
HG003 wild type (WT)	NCTC-8325 reference strain with repaired global regulators *rsbU* and *tcaR*; methicillin-sensitive *S. aureus* (MSSA)	Obtained from Marvin Whiteley (Emory University)	
HG003 coNLL-MetRS	pSS20 P_{hprK}:*nll-EcmetRS*	This study	
JE2 wild type (WT)	USA300 methicillin-resistant *S. aureus* (MRSA)	Laboratory collection	
JE2 coNLL-MetRS	pSS20 P_{hprK}:*nll-EcmetRS*	Laboratory collection	
JE2 *rot*::TnMar	*rot*::TnMar	Nebraska transposon mutant library	
JE2 WT sGFP	pASP03 P*rpoB-sgfp*	Laboratory collection	SADHL193
JE2 *rot*::TnMar sGFP	pASP03 P*rpoB-sgfp*	Laboratory collection	SADHL202
MN8 wild type (WT)	methicillin-sensitive *S. aureus* (MSSA)	Obtained from Dianne Newman (Caltech)	
SH1000 wild type (WT)	methicillin-sensitive *S. aureus* (MSSA)	Obtained from Ambrose Cheung (Dartmouth)	
ATCC29213 wild type (WT)	methicillin-sensitive *S. aureus* (MSSA)	ATCC	

***P. aeruginosa* strains**			
UCBPP-PA14 wild type (WT)		Laboratory collection	
PA14mCherry	*attB*::mini-Tn7T2.1-Gm-GW:PA1/04/03-mCherry	Laboratory collection	PADHL441
Plasmids			
pSS20	P_{hprK}:*nll-EcmetRS*	Laboratory collection	
pASP03	P*rpoB-sgfp* (pCM29 backbone)	Laboratory collection	
pCM29		Obtained from Ken Bayles (University of Nebraska)	
pBT277		Obtained from Boo Shan Tseng (University of Nevada)	Used to construct PA14mCherry

Supplementary Datasets

All proteins identified by LC-MS/MS associated with the results presented in **Chapters 2** and **3** are uploaded as CSV files.

Table 2.1.1 Protein raw abundances and differential expressions for PSM pulse-in

Table 2.1.2. Protein raw abundances and differential expressions for S. aureus coculture

Table 2.1.3. All GSEA output associated with data presented in Chapter 2

Table 3.2.1 Protein raw abundances pre-enrichment

Table 3.2.2 Protein raw abundances after enrichment

Table 3.2.3 Differential expression tables (CE/ME; CL/ML; CL/CE)

Table 3.2.4 Differential expression tables (MRSA CE/ME; MRSA CL/ML; HQNO pulse-in; 30-min coculture)

Table 3.3 All GSEA output associated with data presented in Chapter 3